Università degli Studi di Napoli
"Federico II"

Tesi di Dottorato di Ricerca in
Tecnologie Innovative per Materiali, Sensori ed Imaging
XVII Ciclo

MINIATURIZED SUPERCONDUCTING PLANAR FILTERS FOR TELECOMMUNICATION APPLICATIONS

Mario Barra

Coordinatore di Dottorato
Prof. Ruggero Vaglio

Naples, December 2004

CONTENTS

INTRODUCTION

In present wireless communication scenario, the development of new network signal processing algorithms and innovative hardware devices is fundamental to support the rapidly growing expansion of new and sophisticated services. In particular, modern microwave architectures have to satisfy more and more stringent requirements concerning their performances, together with a general criterion of compactness and easy integration with other systems. In the field of the microwave pass-band filters, which play a fundamental role in many applications, the aforementioned technological trend can be fully satisfied by the use of thin-film high temperature superconductors (HTS) in the fabrication of microstrip filters. Indeed, despite the reduced dimensions, HTS microstrip resonators present very high quality factors ($>10^4$ at T=77K and in the full microwave range) and consequently make possible the fabrication of compact filters with improved performances in terms of very low insertion in-band losses and stepper skirts for out-of-band rejection (high selectivity). These very special features are substantially due to the fact that HTS thin films, grown epitaxially on both sides of low microwave loss single-crystal substrates, exhibit very low surface resistance values (two or three orders lower than traditional metals) at cryogenic temperatures. Moreover, the possibility to integrate the HTS filters with cryogenic low noise amplifiers (LNAs) gives rise to a new class of receiver systems with reduced noise figure and consequently improved sensitivity performances. Within the last 10 years, many research projects have experimentally confirmed all these potentialities and great efforts have been carried out to develop compact and low cost cryogenic systems which could favor the wide scale expansion of this emerging technology. Presently, as a result of these activities, HTS filters are very close to a commercial application, especially for mobile communication systems of 2nd and 3rd generation, where a large variety of HTS systems is offered.

Since the early developments, one of the fundamental issues in HTS filters design has been the miniaturization of these devices, in order to reduce the costs related to the necessary superconducting area, also relaxing the cryogenic

burden for the cryo-coolers. To this end, owing to the development of powerful electromagnetic simulators, a wide series of new and highly compact microstrip resonators, mainly based on particular geometric shapes, has been proposed. A contribution to this research effort is given in this thesis work, developed at University of Naples "Federico II", INFM Coherentia Labs, where new compact resonators have been designed and experimentally investigated.

A part of the work concerned the miniaturization performances of fractal curves provided of special "space filling" properties and has been carried out in collaboration with the Universitat Politecnica de Catalunya of Barcelona (Spain). The performances of all the considered resonators have been investigated by different simulators based on the method of moment: Ensemble 4.2 and 7.0 from Ansoft, IE3D from Zeland software and ADS-Momentum from Agilent technologies. The derived HTS filters have been fabricated by standard photolithographic processes on commercial double sided films and tested both in cryogenic liquids and in commercial cryo-coolers.

A second part was devoted to the analysis of a new dual mode resonator (cross slotted patch), miniaturized by the application of surface cuts which, increasing the current path length, produce a decreasing of the resonance frequency without changing the external dimensions. This new resonator topology allows obtaining a good trade-off between miniaturization and maximum power handling. Indeed, due to the non linear nature of the surface impedance of superconductors, the signal power at the input of a HTS filter has not to exceed a maximum value to preserve the filter performances. Usually, due to the presence of crowding surface currents near the edge of resonators, the power handling decreases if the filter miniaturization increases, such that a compromise has to be found for every application.

This work is summarized in four chapters. The first chapter gives a description of the HTS filter basics, introducing the main steps of the design procedure. Furthermore, the most common miniaturization techniques are discussed and a little review of the most recent miniaturized resonators is provided. The next chapter discusses the impact of HTS filter performances on some modern

telecommunication systems, with particular attention to mobile communications of 2nd and 3rd generation, satellite applications and more recent realizations in radio astronomy field. The third chapter deals with highly miniaturized HTS filters based on fractal layouts. In particular, Koch-Minkowski and Hilbert space filling curves have been investigated in terms of achievable miniaturization levels and corresponding quality factors. Several prototype four pole filters, with Chebychev and quasi elliptic responses, have been designed and fabricated both for potential UMTS and radio astronomy applications. The experimental measurements are here reported

In the last chapter, the novel miniaturized cross slotted patch resonators are introduced. The miniaturization principle is illustrated by many examples of two and four pole filters, designed and tested in L, C and Ku band. A very compact four pole filter configuration, with both pseudo Chebychev and quasi elliptic responses is obtained by combining cross slotted and stepped impedance resonators. The introduction of transmission zeroes does not require extra coupling structures and their position can be partially controlled by rearranging the feed lines. An L band 4 pole filter, based on this configuration, has been integrated in a metallic packaging with a LNA amplifier designed at University of Rome "Tor Vergata". Test measurements on scattering parameters and noise figure are presented at the chapter end. Final remarks are reported in the conclusions.

CHAPTER 1

HTS FILTER BASICS

This chapter introduces the main features of HTS planar microwave filters, comparing them with those of filters based on conventional materials. After a general description of the filter design principles, particular attention has been dedicated to introduce the concepts of unloaded quality factor and maximum power handling for the superconducting microstrip resonators. Furthermore, main techniques for the miniaturization of HTS planar filters have been discussed and a short review of the miniaturized resonators recently proposed is provided.

1.6 Filter basics

An analog band-pass filter is a two ports network (fig.1.1) which works by allowing signals in a specific band of frequencies to pass, while signals at all other frequencies are stopped. Basically, a filter is realized by a set of resonators electromagnetically coupled each other and coupled to an external feed circuit. The number and the type of the couplings between the resonators determine the overall performances of the device [1,2].

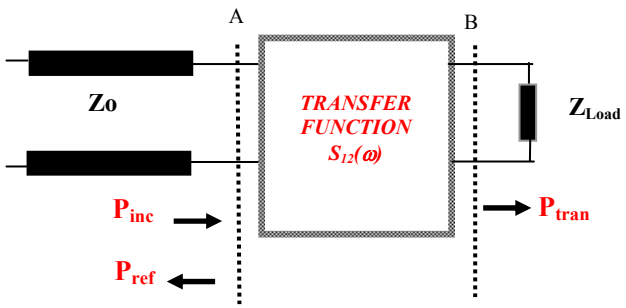

Fig.1.1 Filter as a two ports network

The filter response is defined by its transfer function which, in the microwave range, is used to provide a desired expression to the transmission coefficient $S_{12} = |S_{12}|e^{-j\Phi_{12}}$. An important parameter describing the filter characteristics is the group delay $\tau_D = \frac{d\Phi_{12}}{d\omega} = \frac{1}{2\pi}\frac{d\Phi_{12}}{df}$, which represents the overall delay of a signal due to filtering. However, in many practical applications, the filter specifications are mainly referred to the amplitude function $|S_{12}|$ which describes how the magnitude of the response varies with frequency. This is also done by the so called "insertion loss" response, defined as [1,2]:

$$IL(\omega)|_{dB} = 10\log\left(\frac{P_{inc}}{P_{tran}}\right) = 10\log\left(\frac{1}{|S_{12}|^2}\right) = -|S_{12}|_{dB} \qquad (1.1).$$

In the ideal case, a filter presents a perfectly rectangular amplitude response, where $|S_{12}|_{dB}$ is zero within of the pass-band and -∞ elsewhere (fig.1.2a). Moreover, the phase response would be linear as a function of the frequency, implying a constant group delay. Provided these conditions, the input spectral components, contained in the pass-band, would be perfectly replicated in the output signal, while the spectral content outside of the pass-band would be completely reflected.

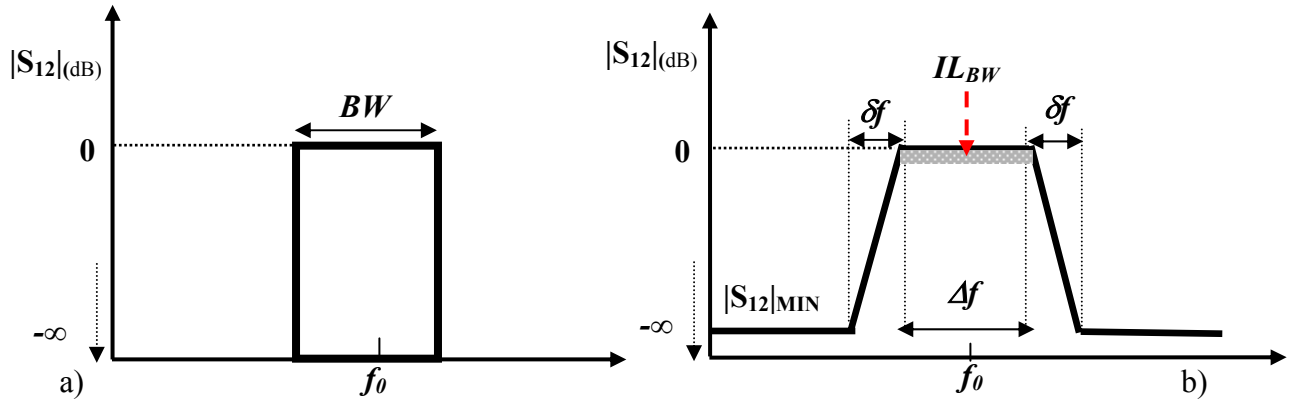

Fig.1.2 a) Ideal and b) real filter amplitude response

Since such an ideal filter cannot be realized, in real cases a small but finite pass-band insertion loss IL_{BW} is always found (fig.1.2b). Furthermore, there is

a transition region δf between the pass-band and the stop-band ($|S_{12}|_{dB} = |S_{12}|_{MIN}$), which determines the so called filter selectivity. As we will show in detail in the following sections, a key objective in telecommunication systems is usually to keep δf as small as possible, in order to make the filter able to reject the interference of strong signals operating in the adjacent bands. In the design of practical filters, the ideal rectangular amplitude response is approximated by using some specific polynomials, presenting different features concerning the steepness of the filter skirts and also implying different internal structures. Usually, $|S_{12}|^2$ is expressed as:

$$|S_{12}(j\Omega)|^2 = \frac{1}{1 + k^2 F_N^2(\Omega)} \qquad (1.2),$$

where $\Omega = \frac{f_0}{Bw}\left(\frac{\omega}{\omega_0} - \frac{\omega_0}{\omega}\right)$, f_0 is the center frequency and BW the filter bandwidth. The degree N of the polynomial (F_N) represents the number of the resonators and the roots of $[1 + k^2 F_N^2(\Omega)]$ are also called "poles" of the filter.

In the modern applications, three types of polynomials are really considered: Chebychev, Cauer (elliptic) and quasi elliptic.

	$F_N(\Omega)$
Chebychev	$\cos[N\cos^{-1}(\Omega)] \quad \lvert\Omega\rvert \le 1$ $\cosh[N\cosh^{-1}(\Omega)] \quad \lvert\Omega\rvert \ge 1$
Quasi - Elliptic	$\cosh\left\{(N-2)\cosh^{-1}(\Omega) + \cosh^{-1}\left(\frac{\Omega_a\Omega - 1}{\Omega_a - \Omega}\right) + \cosh^{-1}\left(\frac{\Omega_a\Omega + 1}{\Omega_a + \Omega}\right)\right\}$
Cauer - Elliptic	$M\frac{\prod_{i=1}^{n/2}(\Omega_i^2 - \Omega^2)}{\prod_{i=1}^{n/2}\left(\frac{\Omega_s^2}{\Omega_i^2} - \Omega^2\right)}$ for N even $N\frac{\Omega\prod_{i=1}^{(n-1)/2}(\Omega_i^2 - \Omega^2)}{\prod_{i=1}^{(n-1)/2}\left(\frac{\Omega_s^2}{\Omega_i^2} - \Omega^2\right)}$ for N odd and ≥3

Table 1.1 Polynomials for filter responses

Table 1.1 summarizes the expressions of $F_N(\Omega)$ in these three cases and fig.1.3 reports their typical exemplary responses.

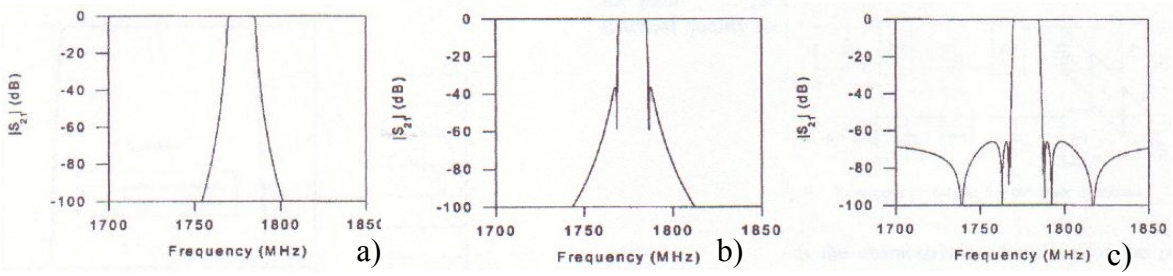

Fig.1.3 a) Chebychev, b) quasi elliptic and c) elliptic responses

In the quasi elliptic and elliptic cases, $|S_{12}|$ is characterized by the presence of transmissions zeroes (respectively 2 and N-1), which can be opportunely positioned very close to the band edges, improving the selectivity performances in comparison with a Chebychev filter with same N. Indeed, it is easy to show that for every type of response, the degree N of the polynomials affects directly the desired selectivity δf , as shown in fig.1.4 for a Chebychev filter.

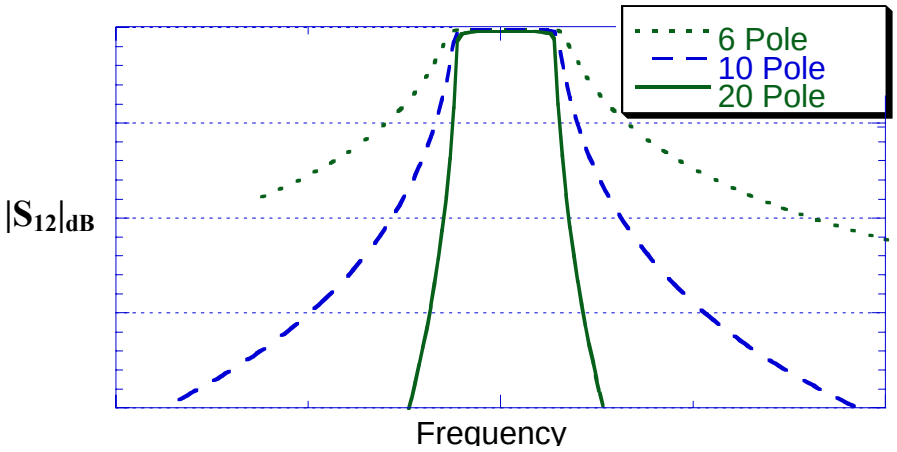

Fig.1.4 Chebychev filter response as a function of the number of poles (N)

For Chebychev filters, it is approximately valid the expression $N_{Cheby} \approx 0.5 + 3\sqrt{\frac{BW}{\delta f}}$ [3]. Instead, for the same δf , the elliptic response requires $N_{Cauer} \approx \frac{1}{3} N_{Cheby}$, while for the quasi elliptic case it results

$N_{Cauer} < N_{quasielliptical} < N_{Cheby}$. The reduction of N for a desired selectivity allows a reduction of the number of the resonators and this fully justifies the great interest for these response typologies. On the other hand, the quasi elliptic and elliptic responses imply a more complicated internal structure for the filter, which in many practical cases makes them difficult to obtain.

As stated above, the building blocks of a filter are the coupled resonators. Once fixed a desired filter response, it is possible to deduce a matrix [k] of real numbers, where the generic k_{ij} (coupling coefficient) represents the coupling between the i^{th} and j^{th} resonators.

A general expression for the coupling coefficient k_{ij} of two coupled microwave resonators can be given considering the ratio between the coupled energy and the stored energy [1]:

$$k_{ij} = \frac{\iiint \varepsilon E_1 . E_2 dv}{\sqrt{\iiint \varepsilon |E_1|^2 dv * \iiint \varepsilon |E_2|^2 dv}} + \frac{\iiint \mu H_1 . H_2 dv}{\sqrt{\iiint \mu |H_1|^2 dv * \iiint \mu |H_2|^2 dv}} \qquad (1.3),$$

where E and H are the electric and magnetic fields, respectively, evaluated at the resonance frequency. As shown, the overall coupling is composed by two terms, representing separately the electric and the magnetic couplings. It is to note that the coupling can have either positive or negative sign. In particular, a positive sign implies that the coupling enhances the stored energy of uncoupled resonators, whereas a negative sign implies a reduction. So, the electric and magnetic couplings could either have the same effect, if they have the same sign, or have the opposite effect, if their signs are opposite. Beyond the couplings between the resonators, it is also necessary to define the coupling strength of the input and output resonators with the feed circuit. To this end, for these resonators, one can introduce the external quality factor:

$$Q_{ext} = \frac{\omega_0 W}{P_{EST}} \qquad (1.4),$$

where W is the overall stored electromagnetic energy and P_{EST} is the power flowing out of the corresponding port. Usually, in all practical cases, the desired responses require the same value of P_{EST} for every port. In the following sections, we will shortly introduce the filter design procedure,

describing how to get the coupling k_{ij} and Q_{ext} from the desired $|S_{12}|$ expression. Here, it is worth to remember that in the Chebychev case, considering all resonators having same resonant frequencies (synchronously tuned), only the ($k_{j,j+1}=k_{j+1,j}$) elements of the coupling matrix [k] have non zero values. This means that a Chebychev response can be obtained by a simple ladder network with only sequential couplings, as shown in fig.1.5 for a four pole filter.

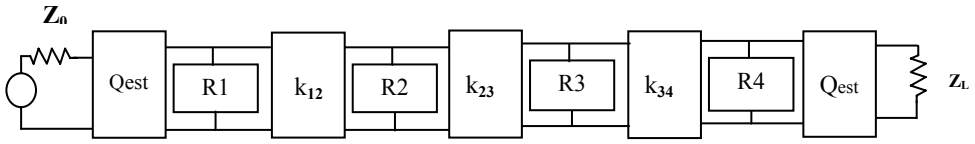

Fig.1.5 Four pole Chebychev network

On the contrary, the elliptic filters, which offer the best performances in terms of selectivity, require also a very high number of couplings and result practically unrealizable in many cases. To this regard, a very good trade-off is provided by the quasi elliptic model. Indeed, this can be realized starting from the Chebychev model, by adding only one cross coupling of opposite sign respect to that of the sequential couplings (fig.1.6).

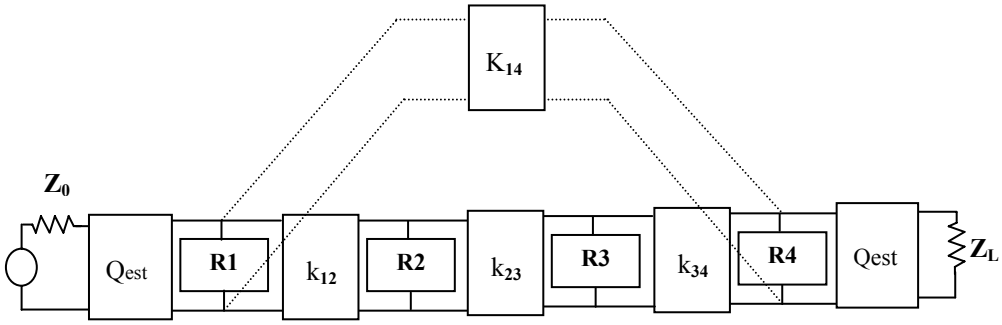

Fig.1.6 Four pole quasi elliptic network

1.2 Unloaded quality factor Q

The working principle of the microwave resonators is based on the capability to storage the electromagnetic field energy which is periodically converted

between electric and magnetic energy. Consequently, any resonator has to constrain the field to a finite volume and, in principle, all structures composed of conducting and/or dielectric materials able to satisfy this requirement can serve as a resonator.

However, in the choice of the resonator type for a filter realization, it is necessary to take into account a fundamental parameter, which directly affects the performances of the final device: the unloaded quality factor Q_0. In an ideal resonator, with no dissipative loss mechanisms, the eigen oscillations of the electromagnetic energy would be undamped. On the contrary, in a real resonator, where different loss sources are present, these oscillations decay with a time constant t_D which is related to Q_0 by the expression:

$$Q_0 = \pi f_0 t_D \tag{1.5}$$

Hence, Q_0 is the parameter which takes into account all the dissipative losses within the resonator and, in accordance with (1.5), can be defined as:

$$Q_0 = \frac{\omega_0 W}{P_{diss}} \tag{1.6}$$

where P_{diss} is the dissipated power and $\omega_0 W$ is also named as "oscillating power" [3]. The unloaded quality factor Q_0 has a direct impact on the final filter performances in terms of the in-band maximum insertion loss IL_{BW} and maximum obtainable selectivity. In particular, for IL_{BW} it is roughly valid the expression $IL_{BW} \propto \frac{1}{Q_0}\frac{f_0}{BW} g(N)$, where g(N) is an increasing function of N. This expression makes clear that the in-band insertion losses can be reduced if resonators with high quality factors are considered and, observing the dependence on BW and N, this is especially true if filters with narrow bandwidths and high number of resonators (poles) are desired (fig.1.7).

Similar considerations can be repeated for δf. In this case, if a dissipative loss of about 1dB is taken as the maximally tolerable degradation, the smallest realizable transition width $\delta f_{\min}$ for a given quality factor is determined by $\delta f_{\min} \approx 8\pi\beta_0 \frac{f_0}{Q_0}$, where β_0 is dependent on the type of response. In particular, β_0 is 0.75 and 0.25 for Chebychev and elliptic responses,

respectively, confirming that the transmission zeroes tend to guarantee higher selectivity levels [3].

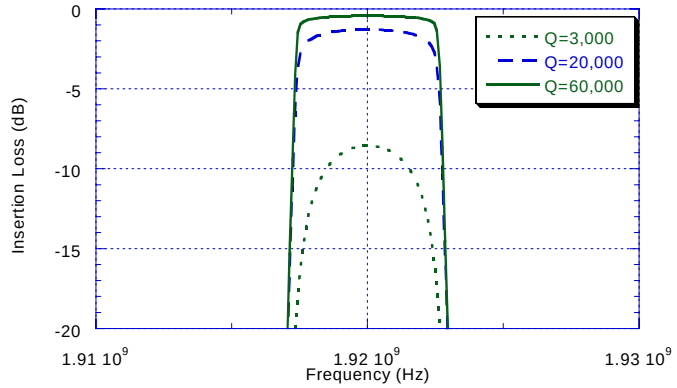

Fig.1.7 Simulated transmission response of a 10 pole 5 MHz bandwidth Chebychev filter as a function of the quality factor of each resonator

In general, the loss mechanisms (*i*) present in a resonator are substantially independent from each other, such that, considering $P_{diss} = \sum_i P_{diss,i}$, it is possible to rearrange (1.6) as:

$$\frac{1}{Q_0} = \sum_i \frac{1}{Q_i} \qquad (1.7).$$

Practically, in the microwave resonators based on conventional materials, the losses related to the presence of conducting parts $P_{diss,c}$ largely dominate and it results that $Q_0 \approx Q_c$. This condition has important consequences, since it introduces the necessity, by using the conventional technologies, to consider resonators with larger size in order to have high quality factors. This can be made clear analyzing in detail the expression of Q_c. At microwave frequencies, the conducting losses in a given material can be approximately described by the surface resistance R_s, defined as the real part of the surface impedance Z_s. On its turn, Z_s is defined as the intrinsic impedance encountered by a plane wave which, coming from the free space, is perpendicularly incident on an infinite half plane of the considered material. Z_s is related to the material conductivity σ by the expression:

$$Z_S = R_S + jX_S = \sqrt{\frac{j\omega\mu}{\sigma}} \qquad (1.8)\ [4].$$

Once defined R_s, the dissipative power in the conducting parts of a resonator is given by:

$$P_{diss,c} = \frac{1}{2} R_S \int_{Sc} \left| H_t^{\,2} \right| dS \qquad (1.9),$$

where S_c is the overall conductor surface and H_t is the related tangential component of the magnetic field. Similarly, the stored electromagnetic energy can be written by:

$$W = \frac{1}{2} \mu \int_V |\mathbf{H}|^2 \, dV \qquad (1.10),$$

where V represents the overall resonator volume. In this way, the quality factor Q_c results:

$$Q_c = \frac{\omega\mu}{R_s} \frac{\int_V |\mathbf{H}|^2 \, dV}{\int_{Sc} |\mathbf{H}|^2 \, dS} = \frac{\Gamma}{R_s} \qquad (1.11),$$

where Γ is a parameter, with the dimensions of a resistance, representing the ratio between an effective volume of the resonator (a volume weighted with the field) and the corresponding effective surface of the conducting parts. In many cases, this expression is differently rearranged by the introduction of the length $l_C = \frac{2\int_V |\mathbf{H}|^2 \, dV}{\int_{Sc} |\mathbf{H}|^2 \, dS}$ and (1.11) becomes:

$$Q_c = \frac{\pi Z_0}{\lambda_0 R_s} l_C \qquad (1.12),$$

where $Z_0 = \sqrt{\frac{\mu_0}{\varepsilon_0}} = 377 Ohm$ and λ_0 are respectively the free space intrinsic impedance and the corresponding wavelength at the resonant frequency. It is easy to show that both l_c and Γ increase when resonators with higher ratios between V and S_C are considered. By using conventional metals (i.e. gold or copper), with R_S of the order of mΩ in frequencies range of (1-10GHz),

unloaded quality factors of about $1\text{-}2*10^4$ ($l_c=2\text{-}4*10^2$mm) can be easily obtained only with bulky resonators such as metallic cavities or wave guides.

1.3 Microstrip technology

The microstrip resonators are composed by two conducting planes separated by a dielectric layer with a permittivity ε_r and a thickness h (fig.1.8).

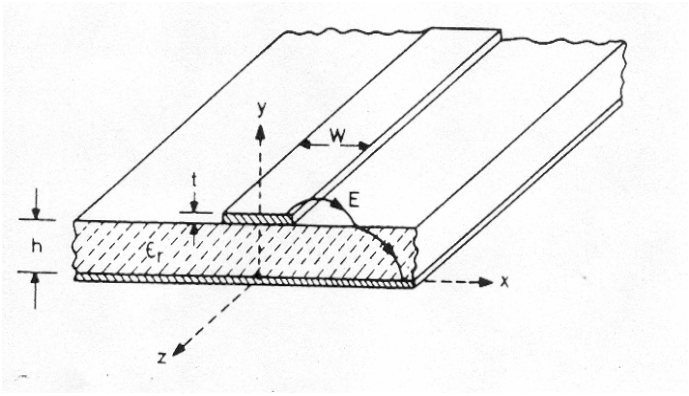

Fig.1.8 Microstrip transmission line

While one of the two conducting planes is used as ground plane, the other one can be patterned by photolithographic processes, giving rise to different resonator types. The microstrip technology is very interesting since it offers a very easy way to fabricate frequency selective devices which, owing to their low size and weight, can be largely integrated with other devices and systems. However, by using conventional metals, the microstrip filters present very poor performances (high insertion losses and poor selectivity) and are inadequate to satisfy the needs of the modern telecommunication systems. Indeed, in a microstrip resonator, the ratio between the "resonant" volume and the conducting surface is very low, with a magnitude order comparable with the substrate thickness h. This means that Γ (l_c) for the microstrip resonators are about two orders of magnitude lower than those of the bulky resonators and Q_0 is limited to few hundreds.

Before discussing how the superconducting technology overcomes the problem, it is useful to report some basic microstrip filter configurations, introducing the basic design steps.

The simplest way to realize a microstrip resonator is to consider a straight line with open-circuit ends (fig.1.9a). According to the elementary transmission line model, if the microstrip line has length L, the modes resonate at the frequencies at which:

$$L = n\frac{\lambda_g}{2} = \frac{n}{2f_0\sqrt{\varepsilon_0\mu_0\varepsilon_{r,eff}}} \qquad (1.13),$$

where λ_g is the wavelength in the considered dielectric substrate (basic $\lambda_g/2$ resonator) and $\varepsilon_{r,eff}$ is the effective permittivity which takes into account the fringing fields and depends on ε_r, h and also on the microstrip width w.

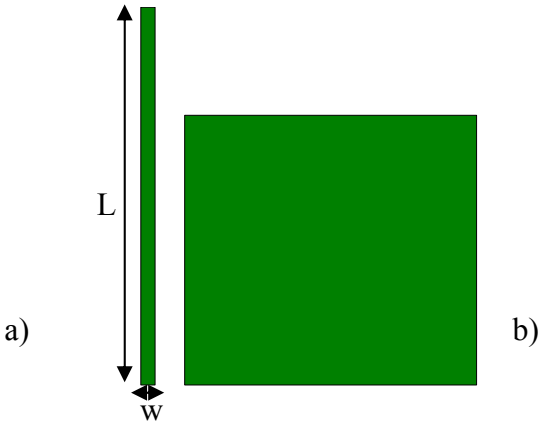

Fig.1.9 Basic planar resonators

Another type of basic planar resonator can be realized by enlarging the transverse dimension w, in order to obtain structures, also called patch resonators, which posses a two dimensional set of modes with two mode numbers (n,m). A typical example is a square resonator (fig.1.9b). In this case, as it will be discussed in detail in the chapter 4, the symmetrical geometry provides also the possibility to generate two modes at the same frequency, thus having a two pole filter with only one patch (dual mode resonator). In the realization of a microstrip filter, the resonators are placed next to each other in specified distances d and are coupled simply by the fringing fields. Considering the basic $\lambda_g/2$ resonator, fig.1.10 shows some typical Chebychev configurations, where the resonators have been coupled magnetically, putting

close their long sides in the backward and forward configurations (fig.1.10a and fig.1.10b, respectively) or electrically through the edge-coupled configuration (fig.1.10c)[5].

Fig.1.10 Basic microstrip filter layouts: a) Backward coupling, b) Forward coupling and c) Edge coupling

Similarly, different approaches can be followed for the feed line configuration. Usually, the 50Ohm microstrip feed lines are coupled to the external resonators by a capacitive gap H (fig.1.11a) or by a direct connection (tapped line configuration in fig.1.11b).

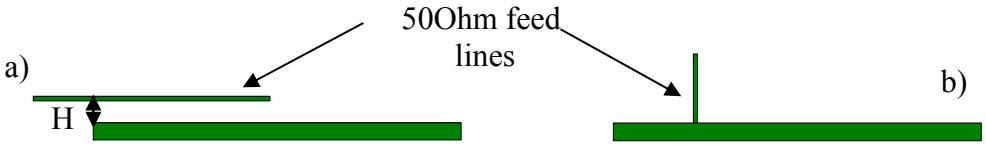

Fig.1.11 a) Feed line configurations: a) capacitive gap and b) direct connection

1.3.1. Filter design basics

For a desired filter response, the coupling matrix and the external quality factors may be obtained using the synthesis procedure developed in [6,7]. In general, the coupling elements and the scattering parameter S_{12} are related by the expression:

$$S_{12} = 2\frac{1}{\sqrt{q_{e1}.q_{en}}}[A]^{-1}_{n1} \qquad (1.14),$$

with $[A]=[q]+p[U]-j[k]$, where p is $p=j\frac{f_0}{Bw}(\frac{f}{f_0}-\frac{f_0}{f})$, $[U]$ is the NxN identity matrix, $[k]$ is the general coupling matrix. Finally, $[q]$ is a NxN matrix with all entries zero except for $q_{11}=\frac{1}{q_{e1}}$ and $q_{nn}=\frac{1}{q_{e2}}$, where q_{e1} and q_{e2} are the scaled external factors given by $q_{ei}=\frac{Bw}{f_0}Q_{ext,i}$, for $i=1,2$ [1]. For Chebychev and quasi elliptic responses, this general approach has been widely developed and their synthesis is possible by analytical or numerical formulas. In particular, the specifications of a Chebychev filter are given by: the number N of poles, the centre frequency f_0, the in-band ripple r_p and the equi-ripple bandwidth BW. Provided these values, the coupling coefficients between resonators and Q_{ext} can be evaluated, for i from 1 to N-1, by:

$$k_{i,i+1}=\frac{1}{\sqrt{g_i g_{i+1}}}\frac{BW}{f_0} \text{ and } Q_{ext}=g_1\frac{f_0}{BW} \qquad (1.15),$$

where g_i is the generic parameter of the low-pass prototype filter, reproducing the desired response, but with f_0=0 and *BW/2*=1. The g_i parameters depend only on N and r_p and can be evaluated by analytical formulas [8]. Some tables for fixed r_p values are shown in fig.1.12. The approach to quasi elliptic responses, where the zeroes position with respect to the band edges have also to be indicated in the specifications, is theoretically more complex, since an exact analytical formulation does not exist. However, even in this case, tables and approximated expressions are present in literature for the low-pass parameters of some basic quasi elliptic filter configurations with 4, 6 and 8 poles [1, 9].

Once known k_{ij} and Q_{ext} for a desired response, the design of a microstrip filter is realized by the use of electromagnetic simulators which, given the substrate characteristics, allow fixing all the geometric parameters concerning the resonator dimensions, the distances between them and the considered feed line configurations.

Value of n	g_1	g_2	g_3	g_4	g_5	g_6	g_7	g_8	g_9	g_{10}	g_{11}
N					0.01-*dB Ripple*						
1	0.0960	1.0000									
2	0.4488	0.4077	1.1007								
3	0.6291	0.9702	0.6291	1.0000							
4	0.7128	1.2003	1.3212	0.5476	1.1007						
5	0.7563	1.3049	1.5773	1.3049	0.7563	1.0000					
6	0.7813	1.3600	1.6896	1.5350	1.4970	0.7098	1.1007				
7	0.7969	1.3924	1.7481	1.6331	1.7481	1.3924	0.7969	1.0000			
8	0.8072	1.4130	1.7824	1.6833	1.8529	1.6193	1.5554	0.7333	1.1007		
9	0.8144	1.4270	1.8043	1.7125	1.9057	1.7125	1.8043	1.4270	0.8144	1.0000	
10	0.8196	1.4369	1.8192	1.7311	1.9362	1.7590	1.9055	1.6527	1.5817	0.7446	1.1007
					0.1-*dB Ripple*						
1	0.3052	1.0000									
2	0.8430	0.6220	1.3554								
3	1.0315	1.1474	1.0315	1.0000							
4	1.1088	1.3061	1.7703	0.8180	1.3554						
5	1.1468	1.3712	1.9750	1.3712	1.1468	1.0000					
6	1.1681	1.4039	2.0562	1.5170	1.9029	0.8618	1.3554				
7	1.1811	1.4228	2.0966	1.5733	2.0966	1.4228	1.1811	1.0000			
8	1.1897	1.4346	2.1199	1.6010	2.1699	1.5640	1.9444	0.8778	1.3554		
9	1.1956	1.4425	2.1345	1.6167	2.2053	1.6167	2.1345	1.4425	1.1956	1.0000	
10	1.1999	1.4481	2.1444	1.6265	2.2253	1.6418	2.2046	1.5821	1.9628	0.8853	1.3554

Fig.1.12 Exemplary parameters of Chebychev low pass prototype filters

Most of these simulators are based on the method of moment [10], such that they evaluate the filter response by dividing first the resonators in small regions (mesh), less or more fitted according to the desired accuracy, and then solving a set of linear equations derived from an integral equation, whose unknown is the surface current density J_s. A typical mesh for a 4 pole filter analyzed in chapter 4 is depicted in fig.1.13.

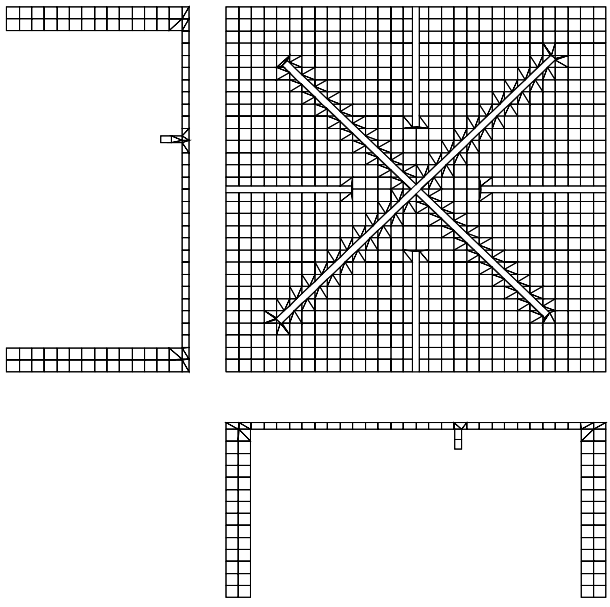

Fig.1.13 Typical mesh for a 4 pole filter (see chapter 4)

Once defined the shape and the dimensions of the resonators, for a given coupling configuration, the coefficient k_{ij} as a function of the spacing d can be determined by analyzing the transmission response of two resonators, when they are weakly coupled to the external feed lines. Indeed, provided this fundamental condition, it is possible to show that the corresponding $|S_{12}|$ presents two characteristic peaks at frequency f_1 and f_2 (fig.1.14), symmetrically centered on f_0. The coupling coefficient will be given by:

$$k_{12} = \frac{2(f_2 - f_1)}{(f_2 + f_1)} \qquad (1.16)\ [1,11].$$

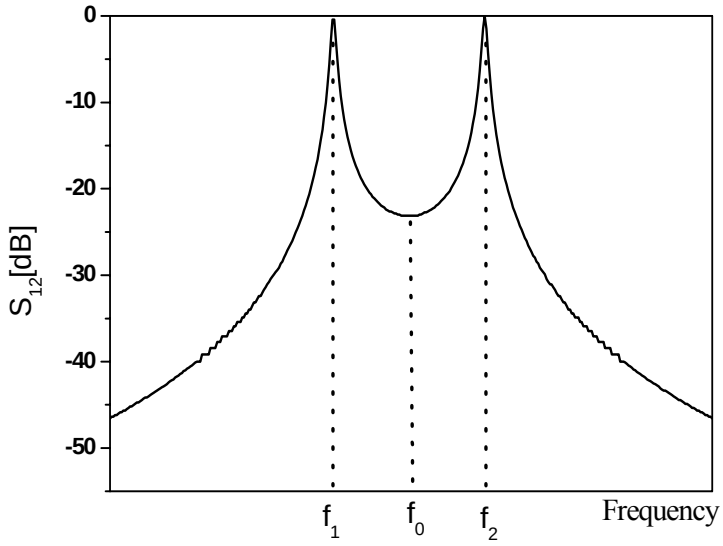

Fig.1.14 Typical transmission response of two coupled resonators

A similar procedure can be followed for Q_{ext}. In this case, a single resonator is coupled to the feed lines in the chosen configuration and its frequency response in analyzed as a function of a geometric parameter, for example the gap H or the distance between the tap point and the resonator center.

The resonator can be coupled only to an input port (singly loaded resonator) or to both input/output ports (doubly loaded resonator) [1]. In the former case, Q_{ext} can be extracted from the phase response S_{11} by using the relation:

$$Q_{ext} = \frac{f_{(0°)}}{f_{(-90°)} - f_{(+90°)}} \qquad (1.17)\ (\text{fig.1.15a}).$$

In the latter case, the resonator is used as one pole filter and Q_{ext} can be derived from 3-dB bandwidth transmission peak:

$$Q_{ext} = \frac{2 f_0}{BW_{3dB}} \qquad (1.18)\ (\text{fig.1.15b}).$$

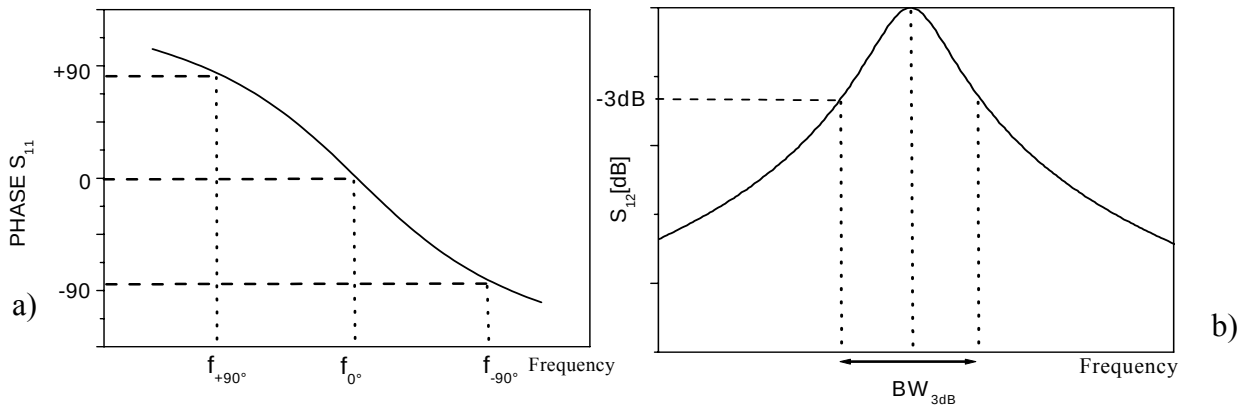

Fig.1.15a) Q_{ext} calculation for (a) singly and (b) doubly loaded resonators

1.4 HTS microstrip filters

The Q_o limitation for the conventional microstrip resonators can be overcome by utilizing HTS (High Temperature Superconductors) films, for the realization of the conducting planes. Indeed, the surface resistance of HTS films, discovered in 1986 by Bednorz and Muller, is about two or three order of magnitude lower than that of normal metals up to 20GHz.

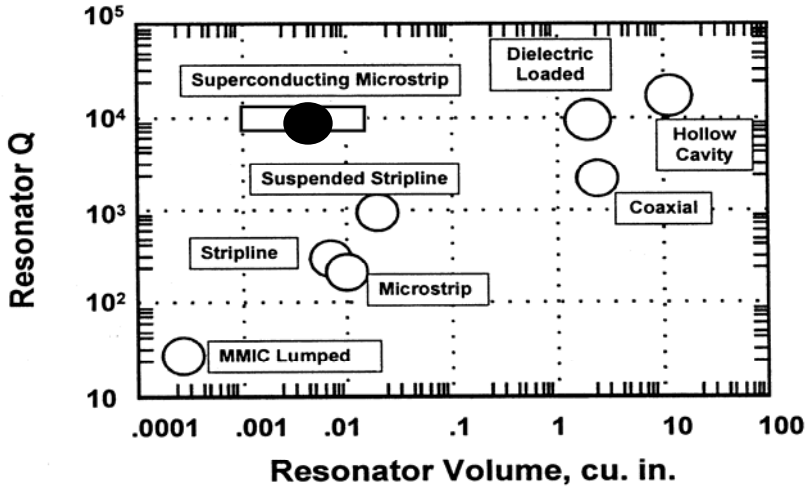

Fig. 1.16 Quality factors vs volume size for conventional and HTS resonators

This guarantees the possibility to obtain a very good trade-off between the compactness of the planar technology and the high quality factors (10^4-10^5), necessary to satisfy the filtering specifications of the modern applications. This situation is clearly evidenced in fig.1.16, where the unloaded quality factors and the volume size of some conventional resonators are compared with those of the HTS planar resonators.

1.4.1 HTS Films

Although the conduction mechanism in the HTS materials is still not deeply understood, here we will adopt the phenomenological two fluids model, in order to give a short introduction of their basic properties at microwave frequencies. This model is based on a local description of the electromagnetic response which, in most situations, is well applicable to HTS materials. According to this theory, in a superconductor the charge carries are of two different types: super-carriers (also called "Cooper pairs"), with density n_s, which do not produce any energy dissipation, and normal carriers (density n_n), which give rise to a normal conduction with energy dissipation due to scattering phenomena. Both n_n and n_s are strongly dependent on the temperature below T_c. This double nature of the carriers is translated into a complex conductivity $\sigma = \sigma_{1TF} - j\sigma_{2TF}$, whose real and imaginary parts are related to n_n and n_s, respectively. If a sinusoidal time dependence is assumed for the fields, σ_{1TF} and σ_{2TF} can be expressed by:

$$\sigma_{1TF} = \frac{n_n e^2 \tau}{m(1+\omega^2\tau^2)} \text{ and } \sigma_{2TF} = \frac{n_S e^2}{\omega m} + \frac{\omega n_n e^2 \tau^2}{m(1+\omega^2\tau^2)} \qquad (1.19),$$

where τ is the scattering time. Usually, since $(\omega\tau)^2 << 1$, (1.19) can be approximated as:

$$\sigma_{1TF} = \frac{n_n e^2 \tau}{m} \text{ and } \sigma_{2TF} = \frac{n_S e^2}{\omega m} \qquad (1.20).$$

By introducing the complex conductivity in (1.8), it is possible to rearrange the expression of the surface resistance R_s and the surface reactance X_s. By using

some approximations valid when the temperature is not very close to T_c, this procedure leads to:

$$R_S = \frac{\sigma_{1TF}}{2\sigma_{2TF}}\sqrt{\frac{\omega\mu}{\sigma_{2TF}}} = \frac{\omega^2\mu^2\sigma_{1TF}\lambda_L^3}{2} \text{ and } X_S = \sqrt{\frac{\omega\mu}{\sigma_{2TF}}} = \omega\mu\lambda_L \qquad (1.21),$$

where λ_L is the penetration depth. The surface reactance X_s represents the kinetic energy of super-carriers which are confined into a surface layer with thickness λ_L. This last term is a characteristic length of the material, frequency indipendent but strongly dependent on the temperature, as it can be roughly described by the Goter and Casimir formulas:

$$\lambda_L(T) = \frac{\lambda_L(0)}{\sqrt{1-(\frac{T}{T_C})^4}} \qquad (1.22).$$

As shown, the surface resistance R_s of the superconductors varies with ω^2, while in normal metals it depends on $\sqrt{\omega}$. This means that in a superconductor R_s increases more rapidly with frequency and, for this reason, there will be a crossover frequency, above which the superconductor performances are no longer better than convention metals. For example, at 77K the crossover frequency between HTS films and copper occurs at about 100GHz (fig.1.17). The HTS films are usually deposited on large area dielectric substrates, which have diameters up to 2 or 3 inches and thicknesses of about 0.2 inches (0.508mm). Films with thickness between 300 and 1000nm can be grown by many techniques (laser ablation, sputtering, molecular beam epitaxy, evaporation), characterized by different costs, production rate and obtainable quality films [12]. Presently, $YBa_2Cu_3O_7$ (YBCO, T_c=92K), $Tl_2Ba_2CaCu_2O_8$ (Tl-2212, T_c=110K) and $Tl_2Ba_2Ca_2Cu_3O_8$ (Tl-2223, T_c=125K) are the most interesting for microwave applications. At microwave frequencies, R_s is in the range 5-500μΩ and λ_L is between 150 and 200nm at temperature close 0K.YBCO is mostly used since it can be grown with high structural quality. However, over the past years, an increasing interest has been dedicated to Tl compounds, owing to its highest T_c and the consequent possibility to relax the cooling requirements and to strongly increase the competitiveness of the superconducting planar devices.

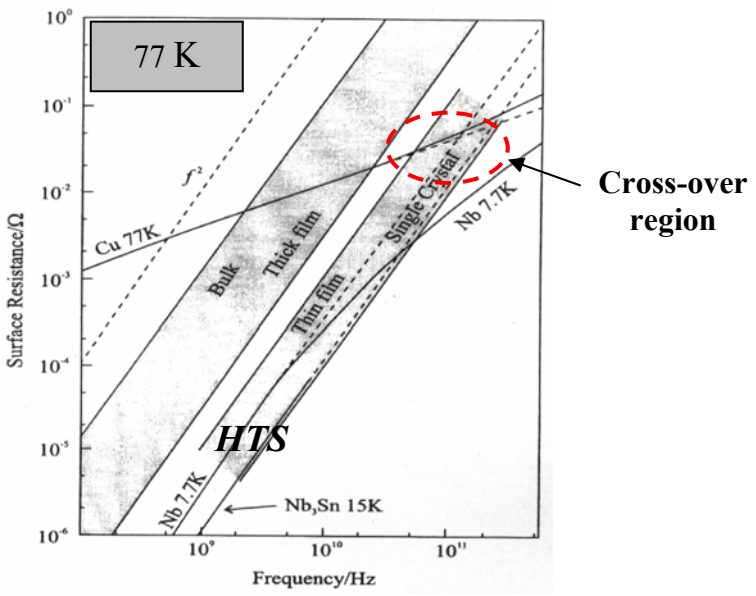

Fig.1.17 Comparison at 77K of R_s of HTS thin films with copper and other bulk superconducting materials

1.4.2 R_s power dependence

When HTS materials are used in the fabrication of microwave devices, it is essential to take into account their peculiar non linear characteristics. Indeed, the surface impedance Z_s is magnetic field H_{rf} dependent and, when this is increased to exceed a certain value, a strong non linear behavior takes place. A typical $Z_s(H_{rf})$ plot, measured for a planar resonator, is reported in fig.1.18.

The non linear response of HTS films is caused by many different phenomena. At low power levels, granularity effects (Josephson-junction-like defects in the crystalline structure) usually imply a quadratic dependence of R_s on H_{rf}. Above a critical field strength H_{c1}, strongly dependent on temperature, non linearity is mainly influenced by the hysteretic vortex penetration and breakdown of the superconducting state can occur with a strong degradation of the surface resistance R_s [13].

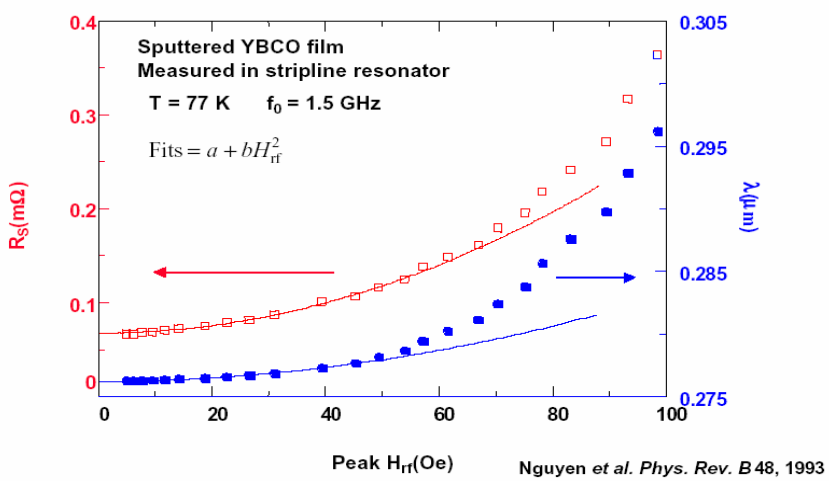

Fig.1.18 R_s and λ as a function of H_{rf}(Oe) for a stripline resonator

This dependence on H_{rf} produces a limitation of the maximum current density J_S which can flow in a HTS film. Furthermore, in a device J_S is not uniform and so the critical values can be exceeded first in some selected areas. For example, in a basic $\lambda_g/2$ resonator, much higher current density occurs at the strip edges [5]. Consequently, for every HTS filter, it is necessary to define a maximum acceptable input power (power handling), which does not degrade the overall performances. Above this value, the in-band insertion losses rapidly increase and the shape of the filter response is strongly distorted. It is important to note that the power handling of a filter depends on many parameters: the quality of the films, the type and the number of resonators, the bandwidth and the operating temperature.

In first place, for a given filter configuration and incident power P_{inc}, it is possible to estimate the oscillating power (ωW) for every resonator simply via:

$$(\omega W)_n = \frac{f_0}{BW}\varsigma_n(f')P_{inc} \qquad (1.23),$$

where $f' = \frac{(f - f_0)}{BW}$. As shown, narrower bandwidths require higher oscillating powers, since in this case the current density on the resonators tends to increase. The factor $\varsigma_n(f')$ depends on the frequency within the pass-band, on the filter type (Chebychev, quasi-elliptic, etc.) and on the position of the resonator in the filter structure. Usually, $\varsigma_n(f')$ is maximum for frequencies

close to the band edges and for n=2 resonator. To this regard, fig.1.19 shows the current distribution, as a function of the frequency, for the resonators of a four pole filter [14].

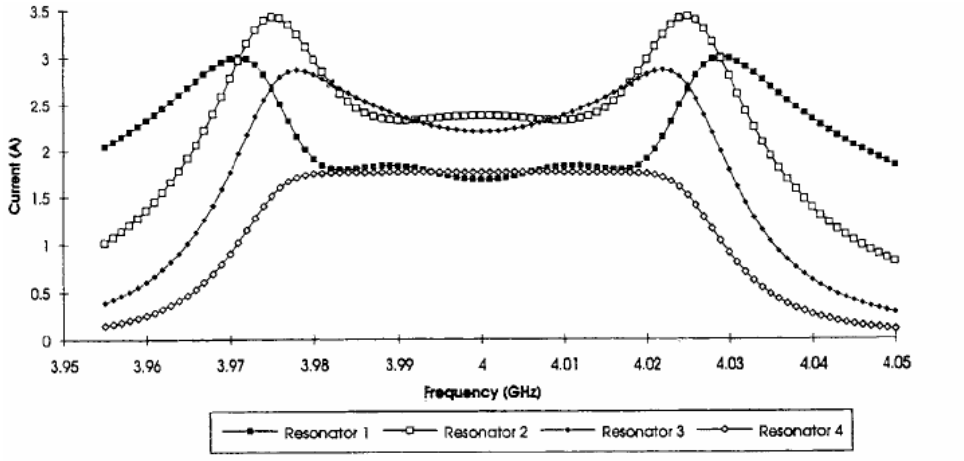

Fig.1.19 Current distribution on the resonators of a four pole filter with f_0=4GHz

Practically, for a filter with a 1% fractional bandwidth, the maximum $\varsigma_n(f')$ is in the range (2-4) and this means that every resonator should manage an oscillating power of 10-20kW, if an incident power of 50 W is considered [15]. On the other hand, the maximum oscillating power which can be handled by a HTS microstrip resonator, beyond the quality film, is strictly related to its shape and corresponding current density. According to what stated above, it is simple to show that the inhomogeneity of the current density, because of peaks which easily exceed the critical values, tends to lower the maximum P_{circ}. In particular, considering the basic microstrip $\lambda_g/2$ resonator, $P_{circ,max}$ is proportional to the strip width w and typical values, with w up to 3 mm, are in the range of 100-200W at T=77K. So, it is possible to conclude that, according to (1.23), a HTS pass-band filter based on these resonators and with 1% fractional bandwidth is limited to an incident power lower than 1W. This value is even reduced if miniaturized resonators (see section 1.5) with lower strip width are considered. This condition implies that, at present, HTS filters can be utilized only in the receiving channels of modern telecommunication systems, where the input signals are of few milliwatts.

A power handling improvement can be realized if patch resonators are considered, since in this case the current is spread over a larger area. However, this improvement results to be slight for all the modes which are characterized by the existence of currents flowing along the edges, with the consequent "peaked" density distribution. In the context of HTS microstrip technology, the only key to overcome this limitation is represented by the utilization of circular disks and ring resonators, operating in TM_{0n0}. These modes are the only ones in the planar structures which are free from edge parallel currents, since the current flows only in a radial direction (fig.1.20). Based on the TM_{010} disk resonator, some prototype filters for possible applications in output transmitter channels of telecommunication systems have been realized, showing no appreciable degradations of response up to incident power of 50-100W (oscillating power ranging from 10 to 100kW) [16,17]. In this way, an improvement of factor close 500 can be obtained in comparison with the basic $\lambda_g/2$ resonators.

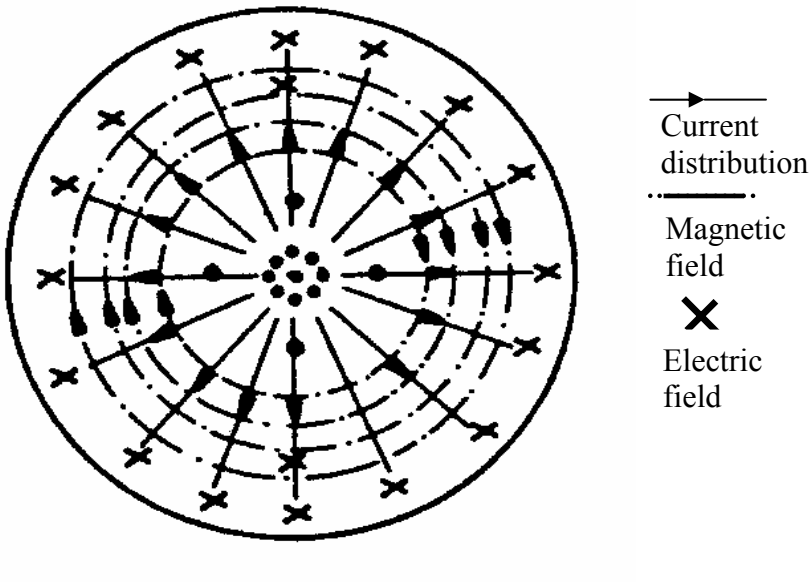

Fig.1.20 TM_{010} mode configuration in a disk resonator

Beyond the increase of the insertion losses, another important effect due to the non linearity of HTS filters is the generation of spurious harmonics by the transfer of energy from the fundamental input signal. This phenomenon can produce a distortion of the input signal, caused by the harmonic signal mixing down in the frequency back into the pass-band. For example, if we consider

two frequencies f_1 and f_2 fairly close together in the filter band, the non linearity will generate the corresponding harmonics $n*f_1$ and $n*f_2$. By mixing the third harmonics with the fundamental ones, two signals with frequencies $(2f_1-f_2)$ and $(2f_2-f_1)$ are also produced and, since they are close to f_1 and f_2, can generate strong distortion in the filter working [4].

According to this scenario, the non linear behavior of a HTS filter can be tested by a standard two tone method. Usually, the signals f_1 and f_2 are synthesized by two microwave generators and are given to the under test filter through a power combiner. Then, the output power P_{out} of the fundamentals tones and the third order intermodulation products (IMP), $2f_1-f_2$ and $2f_2-f_1$ are determined as a function of the input power P_{in}. A simple theoretical model, under the assumption to neglect the saturation effects, suggests that, while the slope of P_{out} for f_1 and f_2 is one, it is three for the IMP. In this way, these two curves can theoretically intersect and the intersection point is usually called third order intercept (TOI). In practice, this intercept can never be measured due the saturation effects, which at high P_{in} distort the linear curves.

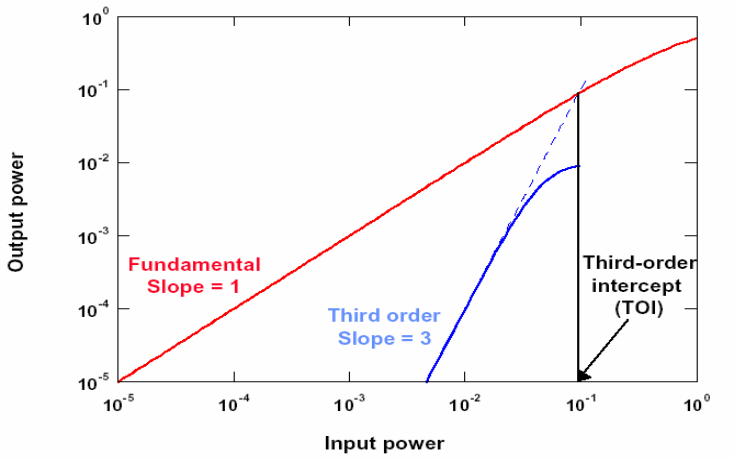

Fig.1.21 Third Order Intercept (TOI) definition

However, TOI can be derived by plotting first the levels of the fundamental tones and IMP at lower power levels and then using linear extrapolation (fig.1.21). Once the intercept point is found, it is possible to know the signal to intermodulation level for every given input power. Indeed, it is valid the expression (in dB):

$$P_{IMD} = 3P_{IN} - 2TOI \qquad (1.24).$$

It should be also mentioned that the definition of TOI is also related to the position of f_1 and f_2 within the band. Indeed, it has been largely demonstrated that when the two tones are close to the band edges, the IMP are higher due to the higher oscillating power (higher current density) and consequently a lower TOI is found [18]. Recently, an alternative technique for the non linearity investigation in HTS filters has been discussed in [19]. This new approach is based on a three tone measurement and can guarantee a better accuracy in the analysis of the intermodulation effects, produced by strong interference signals adjacent to the filter band.

1.4.3 Dielectric and housing losses

In HTS microstrip resonators, given the high Q_c, it is necessary to take into account any other loss contribution which could degrade the overall unloaded Q factor. Firstly, for the dielectric losses related to the substrate, according to (1.7), the specific Q_d can be expressed by:

$$Q_d \approx \frac{1}{\beta_d \tan(\delta)} \qquad (1.25),$$

where $\tan(\delta)$ is the dielectric loss tangent and $\beta_d \leq 1$ is a geometric factor, depending on the resonator type, on ε_r and h. For ε_r higher than 10, β_d can be considered to be 1. Beyond low values of $\tan(\delta)$, other important features that the dielectric substrate should have, are: high permittivity, in order to miniaturize the resonators, a reproducible value of ε_r from batch to batch, a low dispersion in the device band, a good stability with the temperature and a good lattice matching with the superconducting film, able to guarantee a good epitaxial growth. Clearly, all these requirements imply that only few dielectrics can be used to produce high quality HTS films. Probably, the most widely used substrate is Lanthanum Alluminate ($LaAlO_3$), with ε_r close to 24 and $\tan(\delta)$ below $1*10^{-5}$ at T=77K. Unfortunately, $LaAlO_3$ exhibits crystalline defects

with the formation of twinned structures. This phenomenon results in an average dielectric constant with a uniformity of approximately 1%, which can strongly affect the possibility to set the center frequency in narrow band devices. Another commonly used substrate for HTS films is Magnesium Oxide (MgO), with ε_r=9.7 and tan(δ) similar to that of $LaAlO_3$. MgO does not suffer twinning problems and the uniformity of ε_r is close to 0.1%. A third possible choice is given by sapphire substrates ($\varepsilon_r \cong 10$), with various buffer layers to provide an appropriate lattice matching to HTS films. However, in this case, the surface resistance R_s values are inferior to films on $LaAlO_3$ and MgO.

Finally, it should be remembered that the microstrip resonators are open structures such that radiation losses have also to be considered. However, in the practical applications, for reasons of shielding, the HTS filters are mounted in closed metallic boxes and this changes the boundary conditions, preventing the resonators from radiating a far field pattern. On the other hand, a near field is still present and this can induce currents on the metallic walls of the housing, producing a $P_{diss,h}$ and a related Q_h (Q housing). $P_{diss,h}$ can be written as (1.9), considering the R_s of the metallic box. In this way, it depends on the size and the material of the box, but also on the resonator shape. In particular, as evidenced in detail in [18], miniaturized resonators, with a strongly meandered current density J_s, tend to reduce the $P_{diss,h}$ thus improving Q_h.

1.5 Miniaturization principles of HTS planar filters

In the early years after the discovery of HTS, many planar filters based on the layouts of fig.1.10 have been designed and investigated for practical applications. Despite the simplicity of this approach, for which a wide series of analytical expressions and numerical tools have been developed, it is evident that the use of the basic resonator does not optimize the space occupied by the

superconducting filters. To this regard, recently, also owing to the development of powerful electromagnetic simulators, great efforts have been carried out to propose alternative and miniaturized planar resonators. For a given application, the miniaturization of a HTS filter is very important since it reduces the costs, relaxes the cryogenic requirements and favors the integration with other systems. On the other hand, it is clear that the reduction of the superconducting area in the miniaturization process involves an increase of current density, with the consequent Q_c and power handling degradation. For example, for a basic $\lambda_g/2$ resonator, the geometric parameter l_c tends to be equal to w, when w is much lower than h and, according to (1.12), this means that the reduction of Q_c is directly proportional to the w reduction [3]. Hence, assigned the desired specifications for every single application, a particular attention has to be dedicated to find a good trade-off between miniaturization and high performances, in terms of Q_0 and power handling. Many methods for the miniaturization of planar filters have been proposed and in [4] they are summarized in five main categories:

1. Use of high dielectric constant substrates
2. Use of increased internal inductance
3. Use of slow wave transmission lines
4. Meandering and cooling of transmission lines
5. Use of lumped element components

According to the entry (1), the most intuitive miniaturization method is related to the choice of dielectric substrates with high ε_r. Indeed, this produces a reduction of the wave propagation velocity on the transmission line and the consequent reduction of the wavelength for a given frequency. However, as discussed above, in order to be used as substrate for HTS films, a dielectric material has to satisfy very stringent requirements, such that, presently, only $LaAlO_3$ and MgO are really used in the filter design. It is clear that $LaAlO_3$ offers the best miniaturization perspectives but, in many practical applications, its low ε_r uniformity makes more reliable the use of MgO.

Also the internal inductance method is based on the reduction of the wave velocity on a transmission line. This velocity v_T can be also expressed by:

$$v_T = \frac{1}{\sqrt{LC}} \qquad (1.26),$$

where L and C are the equivalent inductance and capacitance for unit length, respectively. For a microstrip line, they are mainly related to h and $\varepsilon_{r,eff}$. The internal inductance of a HTS transmission line is given by $L_I = \mu\lambda_L$, representing the kinetic energy of the super-carriers and, in (1.26), it can be added to L in order to produce an equivalent reduction of v_T. However, the internal inductance contribution is significant only if comparable with the external L and, for a microstrip filter, this implies the necessity to use very thin substrates, with thickness comparable to the penetration depth (hundreds of nanometers). By this technique, velocity reduction up to a factor 100 is possible [20,21], but it presents significant drawbacks. Indeed, the choice of ultra-thin substrates degrades considerably the quality factors up to some orders of magnitude. Furthermore, due to (1.22), the filter response would be extremely dependent on the temperature, thus making very difficult to control the f_0 stability. In conclusion, this approach is not of real interest for commercial applications.

Slow wave resonators are generally realized by loading basic transmission lines by a large number of planar inductances and/or capacitances, with very small dimensions. In this way, periodic structures are obtained, where the wave propagation constant is strictly dependent on the frequency (high dispersion). Usually, they present also an increasing spacing between harmonics with an improved out-of-band rejection for the filter response. A typical slow wave resonator is reported in fig.1.22. In this case, the inner region of a basic $\lambda_g/2$ resonator is removed and loaded by a series of capacitive fingers, which increase the equivalent capacitance C. The consequent reduction of the velocity v_T is strictly dependent on the number and dimensions of the fingers. By this technique, a resonant frequency reduction between 20-30% can be obtained, even if the smaller dimensions of the loading elements (in same cases around

few tens of microns) can make the design particularly sensitive to the photolithography process quality.

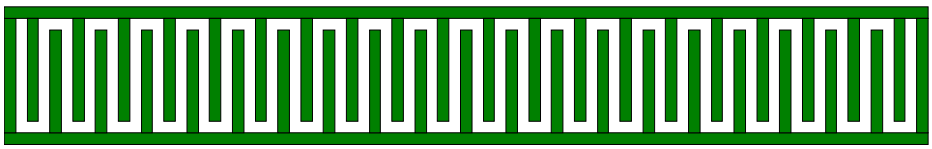

Fig.1.22 Slow wave resonator loaded by capacitive fingers

Certainly, the entry (4) of the above list represents the most commonly used miniaturization technique. In last years, many geometries as loops, hairpins, spirals and fractals have been utilized to fold the elementary basic resonator in very sophisticated ways, in order to put it in an area as little as possible [22,23,24,25,26]. These geometries have been extensively investigated and, a part from the miniaturization level, have revealed to differ for many characteristics: the capability to realize couplings with different signs, the dependence on the tolerances of physical parameters as the substrate thickness and permittivity, the tuning performance, the capability to provide reduced coupling coefficients between adjacent resonators even if the distances are very short. All these features are strictly dependent on the resonator shape and on the consequent field distribution, which is strongly affected by the coupling between the neighboring sections.

As far as the microstrip lumped elements are concerned, they can be considered as the result of an extreme application of the meandering technique. In these structures, similarly to what happens in a LC couple, the resonator parts, where the magnetic field is stored, are separated from the parts where the electric field is stored. A typical example, where the inductive and the capacitive regions are evidenced, is shown in fig.1.23.

The use of quasi lumped elements leads to a significant size reduction of a filter and is very interesting above all for applications in UHF range (lower than 1GHz). However, due to the presence of extremely miniaturized sections, the reduction of the quality factor can be significant, with values in some cases lower than 10^4 [27].

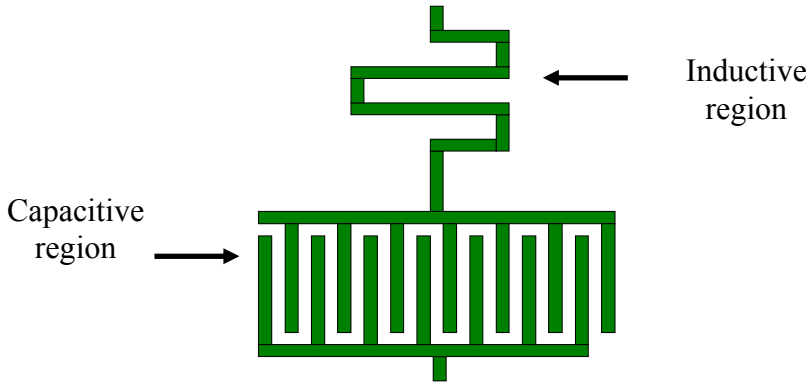

Fig.1.23 A microstrip lumped element

Another miniaturization technique, not reported in the previous list, is based on the dual mode principle. In this case, as mentioned above, the geometrical symmetry of some patch resonators (squares, disks, rings) implies the presence of degenerate modes and provides the possibility to obtain two resonances with only one structure. The size advantage is clear but, in multi-poles filter, it is limited by the necessity to couple the modes of different patches. In particular, for narrow bandwidths, this obliges to place the resonators far apart with a considerable increase of the occupied space. On the other hand, the use of patch resonators can improve the power handling, so that the dual mode filters are usually considered as the best candidates to offer a good trade-off between miniaturization and power handling. In our work (see chapter 4), this approach has been followed and developed with the introduction of new dual mode resonators, miniaturized by the presence of cuts on the surface patch.

1.5.1 Miniaturized HTS resonators

This section provides a little review of HTS miniaturized planar resonators, recently proposed by different international research groups working on HTS filter development. All these resonators are based on meandering geometries and, when indicated in the corresponding references, we will summarize schematically their dimensions and the measured unloaded Q_0 factors. In order

to compare the different miniaturization levels, since the considered resonators have different fundamental frequencies, their dimensions will be expressed as fractions of the wavelength λ_g for a 50Ohm basic microstrip resonator, at the corresponding centre frequency and on the corresponding substrate. As far as the filters realized in this work thesis are concerned, the corresponding details will be adequately discussed in chapter 3 and 4.

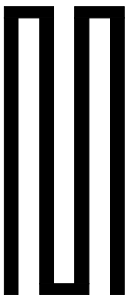

Meander resonator proposed in [22].
Size: [$0.077\lambda_g$ x $0.124\lambda_g$], realized on $LaAlO_3$.
Q factor =about 50000 at T=77K and f_0=1.8GHz.
Fabricated filters: A 8 pole quasi elliptic filter with overall size [39x12]mm^2, BW=15MHz and IL=0.3dB.

Open loop meander resonator proposed in [23].
Size: not indicated
Q factor=25400 at T=77K and f_0=1.738GHz.
Fabricated filters: A 8 pole quasi elliptic filter with overall size [39x22.5]mm^2 on a MgO substrate, BW=15MHz and IL about 1 dB.

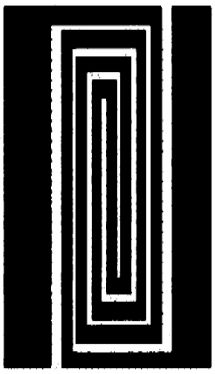

Spiral Meander line resonator proposed in [25].
Size: [$0.083\lambda_g$ x $0.057\lambda_g$], on $LaAlO_3$.
Q factor= not indicated.
Fabricated filters: A 8 pole Chebychev filter with overall size [5x32]mm^2, f_0=1.76GHz, BW=17MHz, and IL=0.4dB at T=65K. The resonator is based on the same principle of the spiral in spiral out developed at Superconductor technologies (see chapter 2).

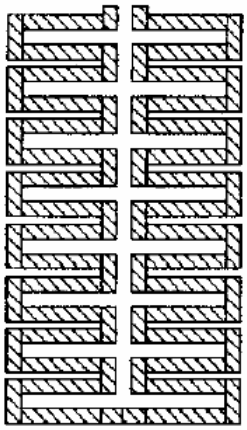

Zig Zag Hairpin Comb resonator proposed in [26].

Size: [0.0584 λ_g x 0.0803 λ_g] on MgO.

Q factor= about 40000 at T=77K and f_0 of about 2GHz.

Fabricated filters: A 4 pole Chebychev filter with overall size [15.36x4.8]mm^2, f_0=1.986.6MHz and BW=15.3MHz. (IL not indicated). A slightly modified version of this resonator has been proposed to realize tunable filters with constant bandwidth

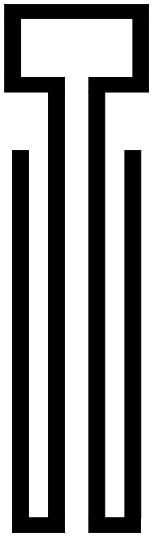

Clip form resonator: proposed in [28].

Size: [0.0354λ_g x 0.158λ_g] on MgO.

Q factor= about 100000 at T=70K and f_0=1.95GHz.

Fabricated filters: A 22 pole quasi elliptic filter with 10 transmission zeroes fabricated on a 2 inches diameter wafer, f_0=1.950MHz, BW=20MHz and IL=0.2dB at center frequency. The selectivity performances of this filter were demonstrated to surpass those of a 50 pole Chebychev filter.

Doubly symmetric hairpin resonator proposed in [18].

Size: [0.144λ_g x 0.144λ_g] on $LaAlO_3$.

Q factor= 60000 at T=70K and f_0=1.95GHz.

Fabricated filters: A 4 pole quasi elliptic filter with overall size [20x20]mm^2, f_0=1.97GHz, BW=5MHz and minimum IL=0.3dB at T=77K. Two 9 pole quasi elliptic filters with overall size [39x14.5]mm^2, BW_1=15MHz (f_{01}=1.775GHz) and BW_2=10.5MHz (f_{02}=1.715GHz). Minimum IL=0.2-0.3dB at T=60K (see chapter 2).

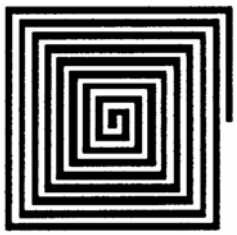

Single spiral resonator proposed in [24].

Size: [0.0251λ_g x 0.0251λ_g] on MgO.

Q factor= about 25000 at T=77K and f_0=1.75GHz.

Fabricated filters: A 4 pole Chebychev filter with overall size [14x1.7]mm^2, f_0=1.75GHz, BW=15MHz and IL=0.35dB at T=77K. A 8 pole quasi elliptic filter with overall size [32x18]mm^2, f_0=408MHz, BW=15MHz and IL=0.38dB at T=39K (see chapter 2).

Dual spiral resonator proposed in [29].

Size: [0.021λ_g x 0.042λ_g] realized on MgO.

Q factor= about 30000 at T=77K and f_0=1.75GHz.

Fabricated filters: A 6 pole filter in [24], with overall size [13x2.8]mm^2, f_0=1.75GHz, BW=15MHz and IL=0.35dB at T=77K. A 3 pole Chebychev filter in [29], with overall size [20x8]mm^2 on $LaAlO_3$, f_0=0.633GHz, BW=20MHz and IL=0.1dB at T=77K. A 4 pole quasi elliptic filter in [30] with overall size [15x20]mm^2 on $LaAlO_3$, f_0=1GHz, BW=35MHz and IL=0.2dB at T=77K.

Quasi lumped resonator with double spirals and inter-digital capacitors proposed in [31].

Size: [0.012λ_g x 0.026λ_g] on MgO.

Q factor= about 100000 at T=30K and f_0=610MHz.

Fabricated filters: A 8 pole quasi elliptic filter with overall size [22.85x6.1]mm^2, BW=5MHz and IL=0.3dB at 26K (see chapter 2) and a 7 pole Chebychev filter with overall size [20.35x5.05]mm^2, BW=5MHz and IL lower than 0.3dB at 26K.

Shunted open loop resonator proposed in [32].

Size: [0.0253λ_g x0.104λ_g] on MgO.

Q factor=28000 at T=77K and f_0=845MHz.

Fabricated filters=A 8 pole quasi elliptical filter with overall size [42x20]mm^2, BW=1.5MHz and minimum IL=1dB at T=77K.

Owing to its particular shape, this resonator is very insensitive to the changes of substrate physical parameters as the thickness.

In conclusion, fig.1.24 summarizes the dimensions (D_x and D_y in λ_g) of these resonators, including also for comparison those of the Koch-Minkowski and Hilbert resonators considered in our work.

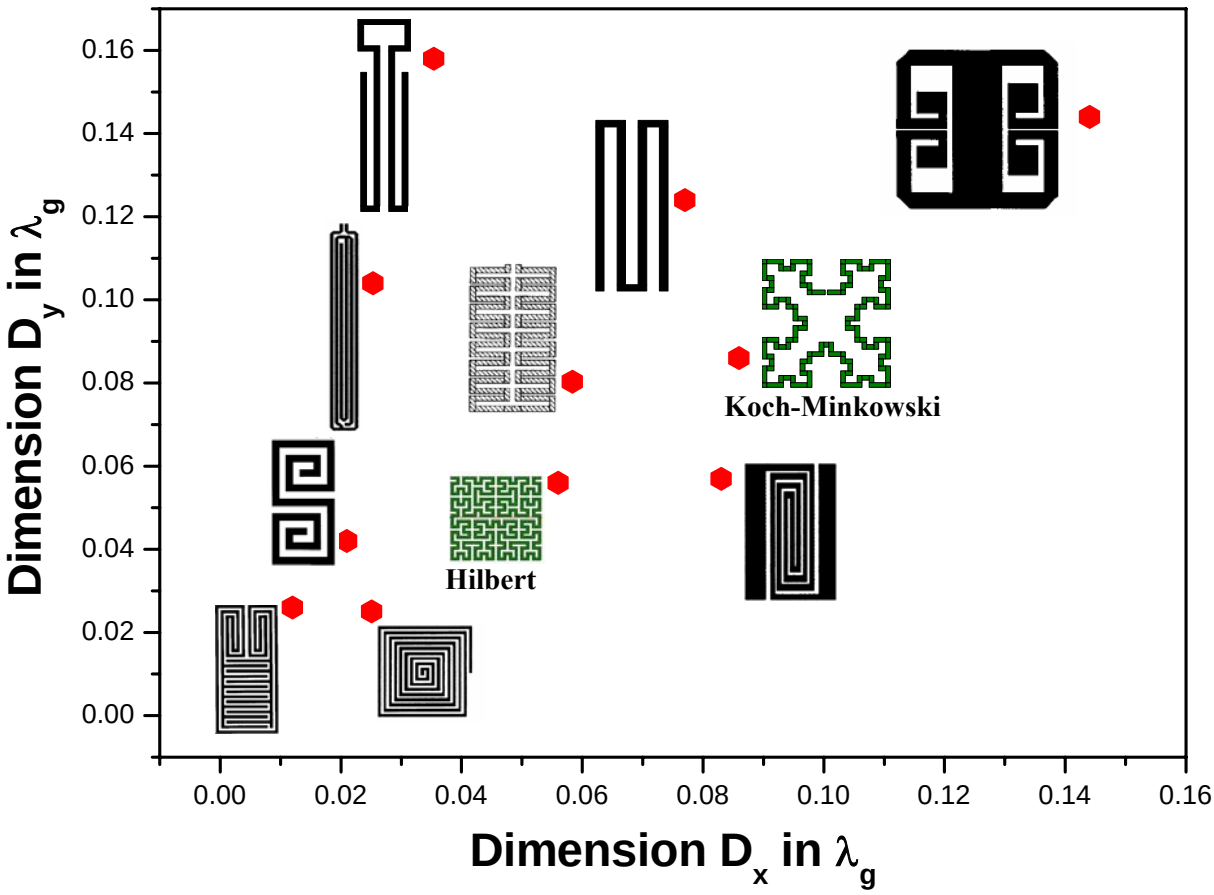

Fig.1.24 Dimensions of recently proposed HTS miniaturized resonators

1.6 Experimental set-up

In this last section, a short description of the fabrication process of the superconducting filters realized at University of Naples "Federico II", INFM Coherentia Labs, and of the corresponding experimental set-up used in the experimental tests is given.

Once optimized the simulation work, the filter layouts have been directly exported from EM simulators in DXF or GDSII format and printed in a 1:1 scale on chrome photo-masks, by a MM-250 system from Electromasks Company. The masks have been realized at University of Rome "Tor Vergata" and a resolution of the order of 0.7-0.8μm is guaranteed. Then, the tested filters have been fabricated on double sided superconducting films by a standard photolithography process and a wet etching process using a solution of HCl at 0.1%.

For the testing, the devices have been mounted into a copper housing with SMA connectors (fig.1.25). Silver paste or bounding with gold wires has been used to contact the feed lines to the SMA connectors. Usually, HTS film ground plane has been protected from chemical reactions by depositing an additional gold film (typical thickness 1μm) and then has been fixed to the housing ground by silver paste.

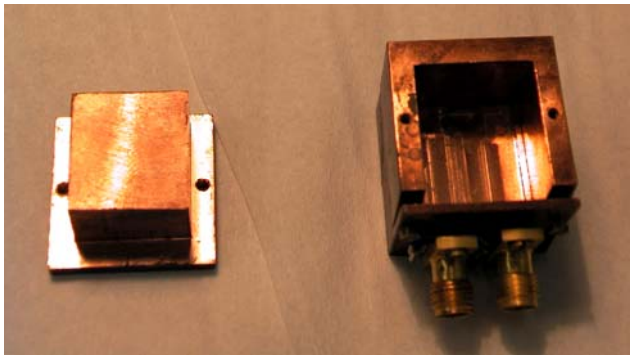

Fig.1.25 Typical copper box for the filter mounting

The experimental set-up used for the measurements of the filter scattering parameters is shown in fig.1.26. Device under test (DUT) performances have been measured by means of an **8720C Hewlett-Packard** network analyzer,

while a standard computer provided the experimental control and the data acquisition by Labview programs.

Since the maximum output power from network analyzer is 10dBm (10mW), in case of power handling test, a power amplifier with a gain of 33dB and a maximum output of 34dBm has been added to the basic measurement scheme. In this case, the input detector of the network analyzer, able to handle at maximum 20dBm, has been protected by an attenuator.

a)

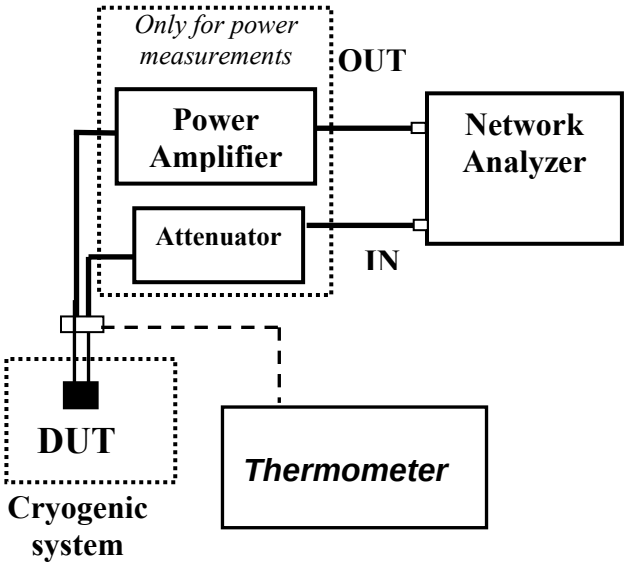

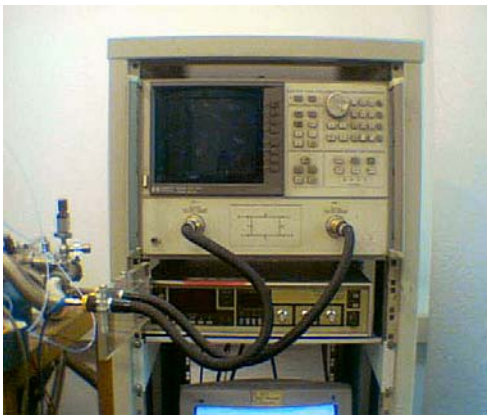

b)

Fig.1.26 a) Experimental set-up for the filter scattering parameter measurements b) 8720C Hewlett-Packard network analyzer

Usually, the HTS filter cooling has been carried out by Nitrogen liquid or by the cryo-cooler system depicted on fig.1.27. The refrigerator is a Gifford-McMahon (GM) type single stage cryo-cooler with a 3" cold finger. The cold head and the compressor specifications are reported below. In order to reduce the vibration, a bellows has been added to the cryo-cooler between the expander and the cold head. The unloaded cool down temperature is 26K, while refrigeration capacity is > 15 Watt at T= 50 K.

Obviously, in all scattering parameter measurements, in order to take into account the losses related to the cables between the analyzer and the DUT, a full two ports OSLT (open short load and thru) calibration in the frequency range of interest has been performed. To this regard, it should be considered

that, due to the available instrumental set up, the calibration has been carried out at room temperature. In this way, the cryogenic temperature effect on the cable losses has not been taken into account and this leads to an increase of the S-parameter magnitude in the order of 0.1dB.

a) 

b)

•Weight:	1.8 Kg
•Working temperature range:	25 - 350 K
•Cooling power	15 - 200 W @ 77K
•Lenght	360 mm
•Cold finger diameter 30 mm	30 mm

c)

Weight	**Dimension**	**Flexible lines**
43 Kg	400 x 430 x 560 mm	Variable length up to 15 m

Fig.1.27 a) Gifford McMahon cryo-cooler, b) GM cold head specifications and c) Air cooled compressor specifications

Finally, according to what discussed in section 1.4.2, fig.1.28 shows the standard two tone method experimental set-up, used to test the non linear behavior of the filters by intermodulation product (IMP) measurements. Two-tone signals f_1 and f_2 have been synthesized by two **Rhode&Schwartz** microwave generators: **SWM05 (50MHZ-18GHz)** and **SMT06 (50MHz-6GHz)**. The distortion related to the crosstalk between the two generators is avoided by two isolators. At the input port, f_1 and f_2 have been opportunely

combined and amplified (power combiner and power amplifier cascade), while the output frequency spectrum (f_1, f_2, $2f_1$-f_2 and $2f_2$-f_1) has been observed with a spectrum analyzer **Rhode&Schwartz FSEM30 (20Hz-26.5GHz)**. Also in this case, the experimental control and the data acquisition were governed by a computer with Labview programs.

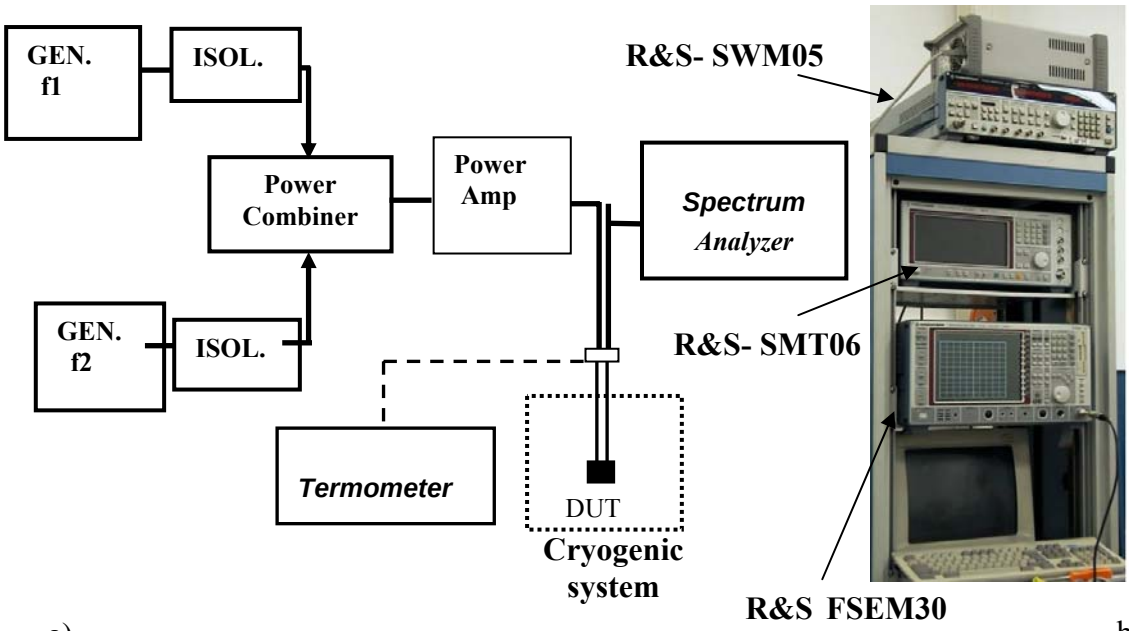

a) b)

Fig.1.28 a) IMP experimental set-up b) Two tone signal generators and spectrum analyzer

CHAPTER 2

HTS MICROWAVE SYSTEMS IN MODERN TELECOMMUNICATIONS

This chapter deals with the impact of HTS technology on improving the performances of some modern telecommunication systems. Our focus will be mainly concentrated on mobile communications of 2nd and 3rd generation and on satellite applications, which show very interesting perspectives of market growth. Recent new applications in the field of the radio astronomy will be also considered. For all applications, a review of recent efforts and advances will be provided.

2.4 Mobile communication systems

Today, mobile communications play a fundamental role in our society. The information age needs an increasing number of more and more sophisticated systems to support its development and wireless forms of personal communication have become undoubtedly essential for every person. To this regard, table 2.1 summarizes the foreseen number of subscribers for mobile telephony services in the first decade of 21th century.

Despite their differences, all mobile telecommunication systems are based on the concept of cell (fig.2.1). Substantially, in a cellular system, a desired coverage area is divided into sub-areas (cells) and for each of these, a base trans-receiver station (BTS) manages the communication traffic.

	Year 2000 in millions	*Year 2005 in millions*	*Year 2010 in millions*
Europe (EU 15)	*113*	*200*	*260*
Noth America	*127*	*190*	*220*
Asia	*149*	*400*	*850*
Rest of world	*37*	*150*	*400*
Total	*426*	*940*	*1730*

Table 2.1 Foreseen growth for mobile telephony subscribers [33]

It receives the signals from a mobile handset (up-link direction) and re-transmits (down-link direction) to a second user, completing the signal path. Usually, separated bands are dedicated to the up-link and down-link communications. It is also clear that, wherever the handsets are inside the covered area, the communication system has to be able also to define dynamically the control transfer of them, when they move from one cell to another (handover). This is done through a hierarchical structure of the cells network, where sophisticated functions of control are realized by specific BTSs.

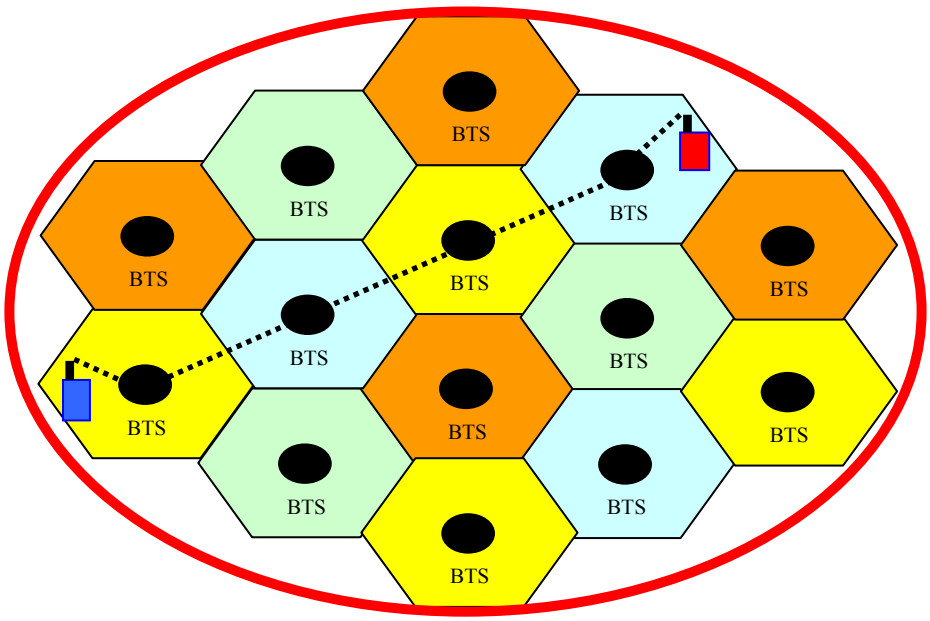

Fig.2.1 Division in cells of the coverage area

Historically, the first generation of mobile communication systems, known as TACS (Total Access Communication System), began its deployment at the mid of 80s and could support only analogue voice signals. In the early 90s, in order to define a standard system for all countries which made possible the international roaming, TACS was substituted by the GSM system (Global System for Mobile Communications). To satisfy the increasing traffic demand, a new digital technology with data service like fax and e-mail was adopted in the course of the GSM developing.

Finally, in the early 2000s, this trend towards the possibility to support more and more complex multimedia data has given rise to the birth of the UMTS (Universal Mobile Telecommunication System). In principle, this third generation will make available the full wireless access to Internet and images, videos and other highly structured data will be currently supported by the hand-held devices of next future. To this end, the new systems have to be capable to provide very high data rates, up to 2 Mbit/s versus 9.6Kbit/s for the basic GSM, and this means that the frequency spectrum available for every user has to be remarkably increased.

In all these communication systems, the overall bandwidth B has to be shared among different users and many techniques of "multiple access" can be defined to assure a correct utilization of the common spectrum resources. A first one is based on the frequency division multiple access (FDMA), where different bandwidths are assigned, simultaneously in time, to different communication links. On the contrary, in the time division technique (TDMA), more users utilize the same frequency channel but in different time intervals. Finally, in the case of the code division multiple access (CDMA), more signals share the same frequency channel at the same time and they are multiplied with different pseudo-random orthogonal binary sequences. In this way, every code identifies a single user making possible the correct demodulation of the signal. Presently, mobile communication systems utilize a combination of these techniques. In particular, in the GSM standard, TDMA is used with a FDMA structure. Usually, for every service provider, both for up-link and down-link bandwidths ([1710-1785] MHz and [1805-1880] MHz in Europe, respectively), a 25MHz

frequency band is divided, using a FDMA scheme, into 125 carrier frequencies, spaced one from each other by a 200KHz band. Furthermore, each carrier frequency is divided in time using a TDMA scheme, such that 8 different time slots can be accommodated in every channel. Every single slot, which lasts approximately 0.577ms, represents a different user.

As far as the UMTS system is concerned, fig.2.2 presents the corresponding frequency bands in Europe and, as shown, both terrestrial and satellite communication channels are considered.

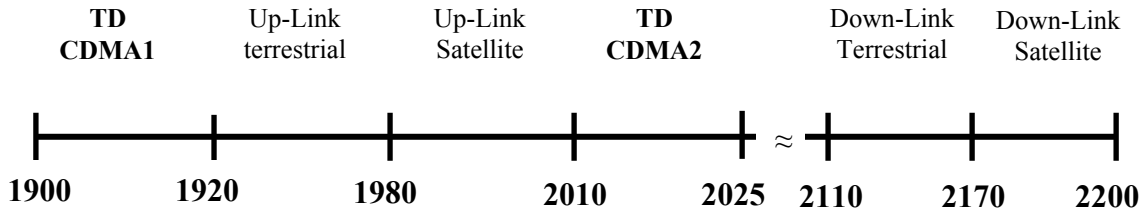

Fig.2.2 UMTS bands allocation

For the terrestrial channels, both for up and down-link communications, the band is divided into carrier frequencies with bandwidth of about 5MHz (generally two or three for every provider), where the so called W (Wide band)-CDMA, a technological evolution of the basic CDMA, is applied. The unpaired bands ([1900-1920] MHz) and ([2010-2025] MHz) are used for the communication of multimedia data and can support both up-link and down-link transmissions. In this case, a TDMA technique is combined with CDMA, where every frame is composed of 15 different time slots and lasts about 10ms.

The different multiple access techniques affect strongly the overall network organization. In the GSM system, every single cell does not use the overall frequency spectrum assigned to the corresponding provider, since the interference level due to the adjacent cells would be intolerable in this case. Consequently, the available frequency band is distributed over clusters of K cells and this distribution is repeated for the overall covered area. Practically, the frequencies used in a cell are not used in the adjacent ones, but they will be "reused" K cells away and the distance between the cells using the same frequencies must be sufficient to avoid interference. In the UMTS system,

owing to CDMA technique, the concept of reuse in frequency is not necessary and every cell manages all the spectrum of the corresponding operator. In this system, the interference scenario is quite different since, due to the sharing of the same frequencies in the same time intervals, every communication link sees all the others as interferences. This intrinsic feature of UMTS implies a dynamic relation between the communication quality and the maximum number of users. This last parameter is not fixed like for the GSM (number of carriers for number of time slots in a frame), but it is dynamically defined by a maximum tolerable interference level, which is also related to the other noise sources.

For a single service provider, the optimization of the overall system requires the maximization of the coverage area ($\underline{A}=\pi\underline{R}^2$) for each cell. Indeed, this allows reducing the number of BTSs necessary to cover a desired territory portion, with the consequent reduction of the costs. In a digital channel, $\underline{R}$ depends firstly on the so called BER (Bit Error Rate), which defines the maximum bit error rate that does not degrade irremediably the communication. BER is translated into a minimum level Λ, depending also on the modulation type, which has to be exceeded by the signal to noise plus interference ratio SINR to guarantee a correct communication [3]. Hence, the coverage area $\underline{A}$ is defined by the equation:

$$SINR = \frac{S_0}{PN_0 + I_0} \geq \Lambda(BER) \qquad (2.1),$$

where S_0 is the useful signal power and is strictly dependent on $\underline{R}$, PN_0 is the noise power, which is partially related to the noise environment and partially to the loss mechanisms present in the BTS receiver devices, while I_0 represents the interference noise. On turn, this term takes into account all interference sources, both external (other communication systems) or internal (other channels) to the considered BTS.

Another parameter related to the working quality of the single cell is the capacity $\underline{m}$, representing the traffic supported density normalized with respect to coverage area. For a BTS of the UMTS system, according to what discussed above, $\underline{m}$ is remarkably affected by the noise and interference scenarios.

2.1.1 HTS filter impact on BTS receiver front-ends

Within the last decade, many advanced research projects have confirmed that the use of HTS filters, with their low insertion losses and high selectivity, can strongly improve the sensitivity and the interference rejection capabilities of the modern BTSs. To better analyze this question, in fig.2.3, a double possible scheme, based on the HTS technology, of a BTS multi carrier digital receiver is depicted.

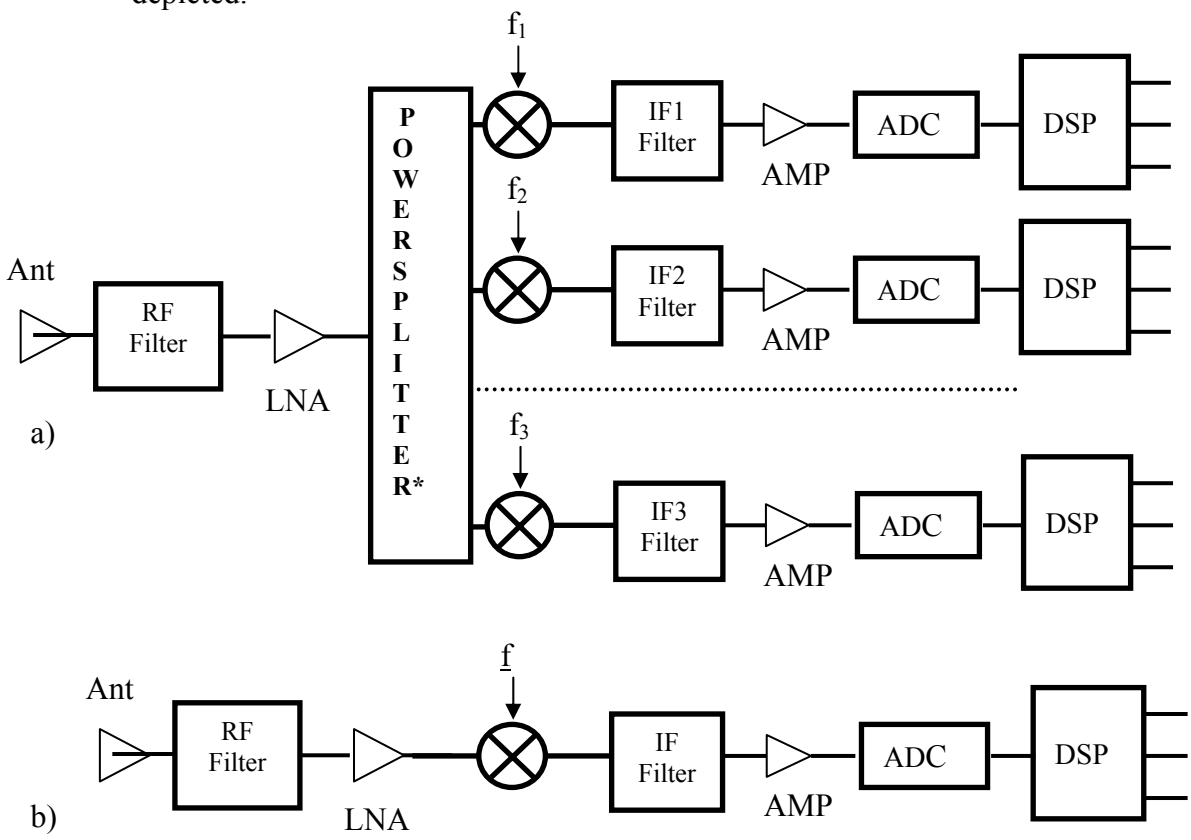

Fig.2.3 BTS receiver with (a) analog and (b) digital channel selection

After the reception by the antenna and before the digital conversion (ADC) and the subsequent processing (DSP), the signal is filtered, amplified and down-converted by the mixer. The down-conversion implies that the central frequency of the signal is down-shifted from the microwave range to an intermediate frequency range, where the signal is usually filtered again to avoid anti-alias problems. The (a) and (b) architectures, shown in fig 2.3, present two

different approaches for the channel selection, by which the single carriers are separated by the other frequencies. The scheme (a) represents a conventional architecture, based on a power splitter and a bank of receiving channels with different down-conversion frequencies f_i. Here, the channel selection is performed by means of narrow band IF filters. In the scheme (b), only one down-conversion cascade is employed and the channel selection is realized by the DSP (digital signal processing) block. This architecture is usually known as "software radio" and combines the reduction of the number of analog components and the processing flexibility typical of a software control. On the other hand, in this scheme, the role of the ADC (analog digital converter) is more delicate, since increased performances in terms of linearity and high dynamic range are required. In general, the modern innovation trend for digital systems is based on the attempt to move the ADC closer to the antenna. In future, the down-conversion stage should be eliminated and the digitalization will be realized directly on the RF signal. Clearly, this will be possible only by the development of a new generation of ADCs with very wide analog input bandwidths [3].

Beyond the different solutions, in all the above schemes, the RF pre-select pass -band filter is fundamental to assure good performances to the receiving chain. In particular, by using HTS filters, considerable advantages can be achieved by the cryogenic temperature, since the overall receiver sensitivity can be improved by cooling the Low Noise Amplifier together with the filter (cryogenic front-end). Indeed, at the input of the antenna, the RF signal power is very low and can be easily degraded by the introduction of further noise. This issue is fundamental and the performances in terms of noise of the first stages (antenna, filter and LNA) influence the overall receiver sensitivity. As depicted in fig.2.4, neglecting the interference contributions, at the output of the LNA the useful signal is superimposed by disturbing noise signal, composed by the external noise received by the antenna and by the internal noise (mainly thermal noise and shot noise in the amplifier) produced by the receiver blocks.

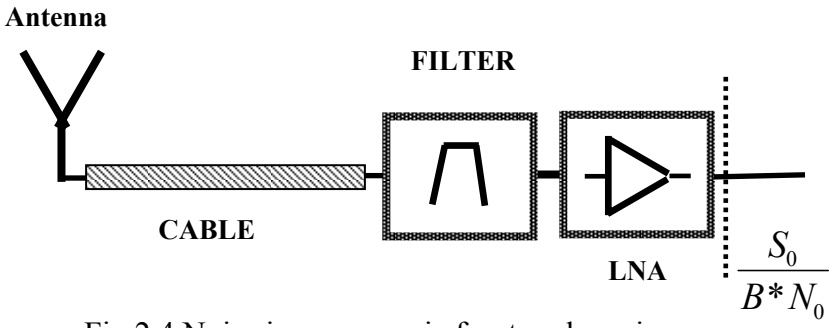

Fig.2.4 Noise in a cryogenic front-end receiver

The overall noise contribution is usually described by a uniform spectral power density N_0, which can be expressed by an equivalent effective temperature via:

$$N_0 = KT_{SYST} = K(T_{ANT} + T_{REC}) \qquad (2.2),$$

where K is the Boltzmann constant. The external noise received by the antenna is summarized by temperature T_A, while the internal noise is represented by T_{REC} and in turn is given by:

$$T_{REC} = (10^{0.1L_c} - 1)T_{CABLE}^{(PHYS)} + 10^{0.1L_c}(10^{0.1L_F} - 1)T_F^{(PHYS)} + 10^{0.1(L_c+L_F)}T_{ampl} \qquad (2.3),$$

where $T_{CABLE}^{(PHYS)}$ and $T_F^{(PHYS)}$ are the physical temperatures of the cable and the filter, respectively, L_C and L_F are the corresponding insertion losses in dB and T_{ampl} is the equivalent noise temperature of the LNA. Usually, in the modern systems, the contribution of $T_{CABLE}^{(PHYS)}$ and L_C is reduced, mounting the receiver very close to the antenna (TMA-tower mounted configuration).

Analyzing (2.3), it is evident that the use of a HTS filter in combination with a cooled LNA can reduce T_{REC} by the reduction of L_F, $T_F^{(PHYS)}$ and T_{ampl}, which decreases with the physical temperature. In the frequency range of mobile communications (0.9-2GHz), a cryogenic front-end receiver can reduce T_{REC} of a factor higher than 10 (1-2dB improvement in the noise figure NF, defined as $F_{REC} = 10 * \log(1 + \frac{T_{REC}}{290})$ [15].

In the rural areas, with limited external noise (T_A lower than 300K), the T_{REC} reduction can be immediately translated into an increased coverage area for the BTS. Rearranging (2.2) by (2.3) and neglecting the interference, it is possible to demonstrate that the maximum R is proportional to $T_{syst}^{-0.25}$ [3]. In these

conditions, if T_A is about 150K, a cryogenic front-end can produce an R increase close to 15-20%. However, it is clear that this direct improvement can be strongly limited by higher values of T_A, which in urban areas can be very close to 2000K. On the other hand, when a more realistic scenario with the interference contributions is considered, HTS filter selectivity becomes a very important feature for the optimization of the receiver performances. Indeed, if a filter with poor selectivity is utilized, possible strong interference signals in the adjacent bands are not opportunely attenuated (fig.2.5) [18].

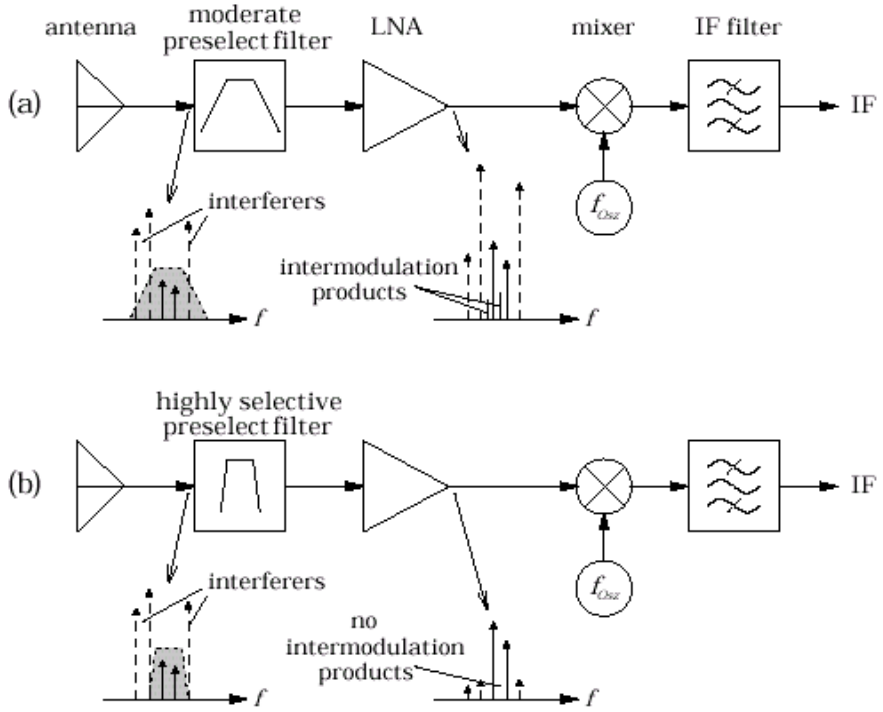

Fig.2.5 Intermodulation products generated by LNA in a receiver with (a) moderate and (b) highly selective filter

Since a LNA shows non linear behavior also at moderate power levels and considering moreover that the mixers are intrinsically non linear devices, the presence of interference signals can generate in-band intermodulation products. These can be superimposed to the useful signals, thus increasing the effective noise level and desensitizing the corresponding channels, with the possible reduction of the corresponding overall gain due to the saturation of the receiver components (blocking). To avoid this occurrence, large guard bands between

the different channels can be employed, but this reduces the spectral efficiency of the given application. On the contrary, nowadays the high number of provided services requires a strong optimization of the spectral occupation, such that the interest in the usage of very selective filters is extremely high.
The above considerations are quite general, but it is not difficult to understand that the interference effects can become even more dramatic in a CDMA system, where many subscribers are utilizing the same channel simultaneously. Hence, for these systems, the requirements in terms of high out-of-band rejection and low intermodulation products are more stringent, as summarized by the table 2.2 [34].

	TDMA IS-136	GSM	CDMA IS-95	W CDMA
Bandwidth (kHz)	30	200*	1250	5000
Receiver IIP3 (dB)	-4	-8	-18	-23
Minimum signal to produce in-band IMD (dBm)	-48	-45	-47	-50
Minimum signal to produce Blocking (dBm)	-15	-19	-29	-34

Table 2.2 Requirements on intermodulation product for different multiple access techniques

Moreover, it is necessary to take into account that (see fig.2.2) in the UMTS system, the TD-CDMA bands, where both up-link and strong down-link signals operate, are adjacent to the W-CDMA bands, with the weak up-link signals of the terrestrial and satellite channels.
Provided these considerations, the impact of HTS technology on the 3rd generation of mobile communications could be very significant. To this purpose, it is worthwhile to mention that a recent detailed analysis [35], based on a statistical approach, the only one possible to treat an inherently dynamic phenomenon as interference, has confirmed that the use of HTS filters can

increase the capacity of the BTSs in a CDMA system. In this analysis, the intermodulation products of the interference signals have been considered as a noise source, which can degrade remarkably SNIR, thus reducing the coverage area and increasing the amount of dropped and blocked calls.

2.1.2 Recent efforts in HTS front-end receiver design

The above discussed economical and scientific considerations explain fully the considerable interest that the research world has dedicated to the study and the realization of many HTS wireless systems for the mobile communications. Great efforts have been carried out to design new HTS filter configurations, able to combine compactness, high selectivity and easy integration with LNA. On the other hand, new cryogenic systems, with an increased maintenance free life, have been developed to satisfy the stringent requirements about the reduction of the power consumption and overall costs.

In USA, in 90s years, three companies have focused their activities on this subject: Superconductor Technologies Inc. (STI), Conductus (Inc) and Illinois Superconductor Corp (ILSC). The birth of these companies was also favored by the unique problems posed by the United States cellular telephony system. The up-link bands of the American Mobile Phone System (AMPS) are collocated in the frequency range from 824MHz to 849MHz and, in every region, the spectrum is shared by two different providers (A and B) in non contiguous sub-bands, according to what shown in fig.2.6.

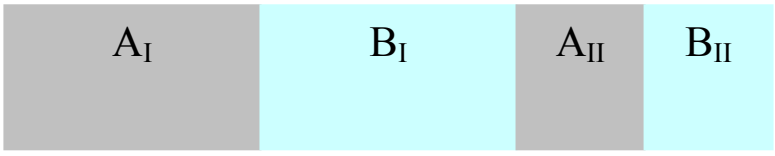

Fig.2.6 AMPS allocation bands

In this situation, since both providers can not control the power up-link signals of their competitor, the interference levels can result extremely high. Considered this scenario, the three USA companies have developed many different HTS subsystems, based on pass-band and stop-band filters, able to reduce the equivalent interference noise by their high selectivity. Since 2001, STI and Conductus have merged their efforts giving birth to a new company, called Superconductor Technologies [36]. At present, this company offers a large variety of HTS receiver subsystems for mobile applications (SuperFilter series), operating in different bands, both for USA and Europe applications. These systems contain different number of filters and the integration with LNA assures typical noise figure of about 0.5dB.

a) 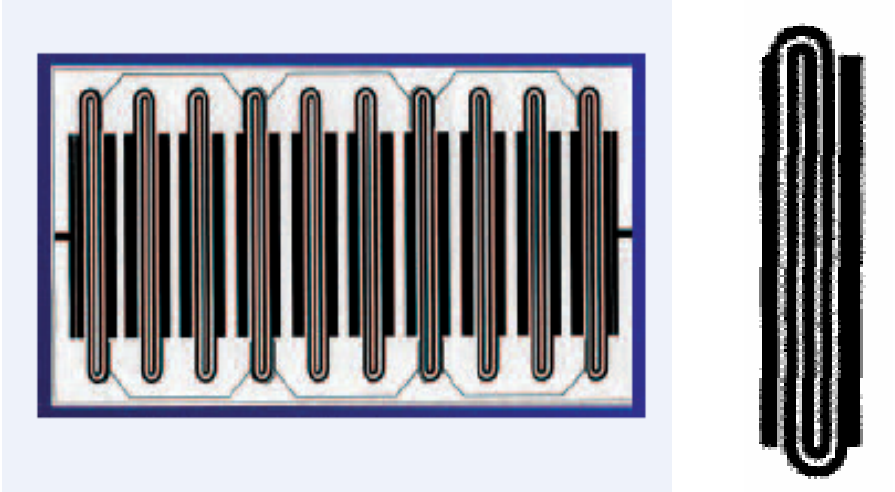 b)

Fig.2.7 a) Ten pole quasi elliptic filter by Superconductor Technologies and b) basic spiral-in spiral-out resonator

An example of a Superconductor Technologies filter is shown in fig.2.7. It is based on spiral-in spiral-out resonators [37,38] and a quasi elliptic response is obtained by opportune cross coupling transmission lines. In this layout, every cross coupling provides a different couple of transmission zeroes.

Superconductor Technologies has also promoted an extensive activity of field trials, in order to confirm experimentally the improved performances of real BTSs based on HTS technology. In this way, different advantages, shortly listed below, have been experimentally demonstrated:

- Extension of up-link Coverage for all systems

- Expansion of up-link Capacity for CDMA systems
- Improvement of the overall Service Quality (reduction of dropped calls and ineffective connection attempts)
- Improvement of in-Building Coverage
- Reduction of the Handset Transmit Power.

Fig.2.8 summarizes the results of one of these field trials, where cryogenic front- end receivers (CRFE) were installed in some BTSs (blue in figure) of a CDMA system covering a sub-urban area [39]. The data, concerning the transmitted power by a sample mobile over a prescribed route around the considered sites, were recorded before and after the installation of CRFE. For this analysis, a statistical approach was used and the data were collected for three weeks prior to and three weeks after the installation, moving at identical speed over the exact same route, at the same time of day.

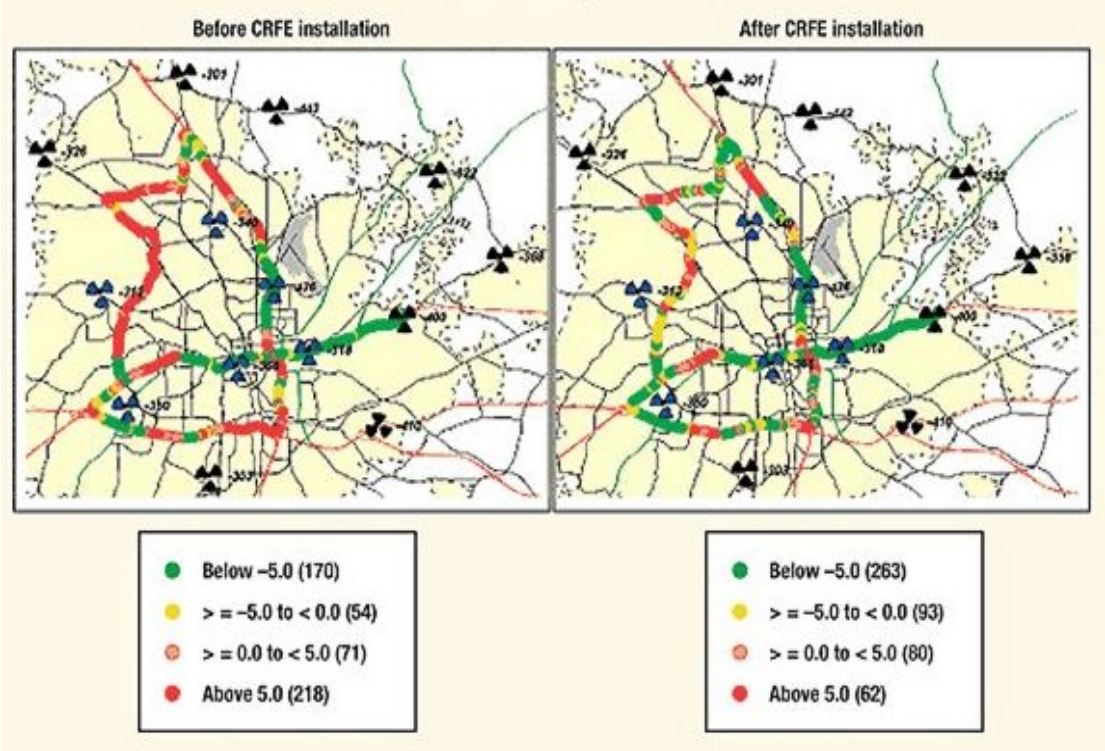

Fig.2.8 Superconductor Technologies field trials on transmitted power by a mobile sample before and after CRFE installation

As shown by the color code, owing to the best sensitivity of the CRFE, the points where the transmitted power is above 5dB, are significantly reduced and an average improvement of about 6.5dB is found over all the tested area. So, since a less number of mobiles are obliged to work close to the maximum power (23dBm), the density of dropped calls and connection failures is drastically reduced too. In [39], the average improvement in dropped call rate is estimated to be 40% for each site, while the ineffective attempts to connect to the network decrease by about 20%. The consequent improvement of the quality service is clear.

As far as Illinois Superconductor Corp (now ISCO International) is concerned, in the past it gained a great experience in the fabrication of HTS thick film coated filters. These are three dimensional filters based on metallic resonators, in particular split ring structures, coated with HTS thick films [40,41]. Usually, HTS thick films present much higher R_s than epitaxial thin films, but the large volume of the realizable resonators still guarantees high Q. In its history, ISCO demonstrated a large variety of superconducting systems, pioneering the market wireless system with 300 cryogenic BTSs sold in the last 90s.

In Japan, the efforts in HTS wireless system development have been mainly sustained by two multi-organization consortia: Western Alliance and Advance Mobile Telecommunications Technologies (AMTEL). In particular, AMTEL has fabricated many HTS planar filters with high number of poles (>10). LNA/Filter subsystems have also been fabricated, showing noise figure of about 0.5dB. In early 2000s, the first Japanese company called Crydevice inc. (now DENSO) was formed with the end to commercialize the HTS devices for third generation communication systems developed by AMTEL. Fig.2.9a shows the most significant example of these filters. It is a 32 pole filter, based on J-shaped hairpin resonators (fig.2.9b) and fabricated on the full area of 3-inches-diameter MgO wafer [42]. Fig.2.9c shows the measured response at T=70K. Similar efforts have been also carried out in Korea, in particular at LG Electronics Institute of Technology (Seoul) where, as summarized in [43], 12 and 16 pole Chebychev filters assembled with LNA have been designed for GSM applications.

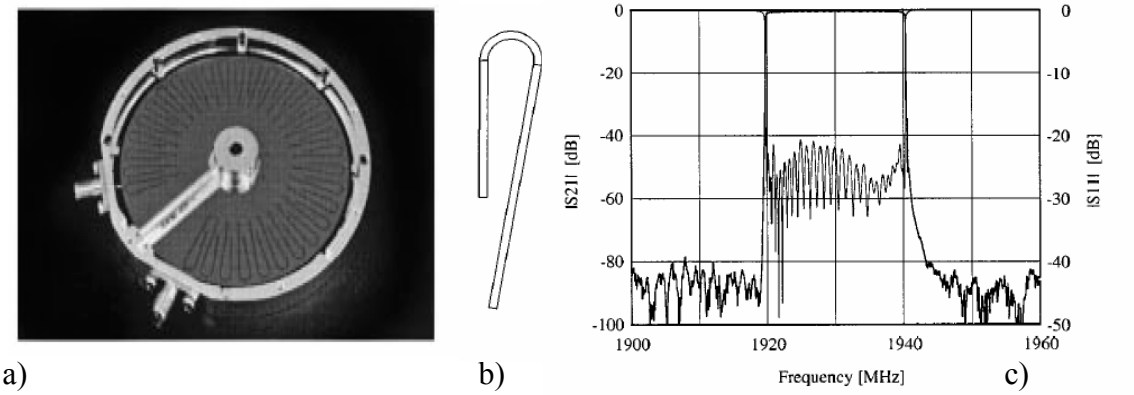

a) b) c)

Fig.2.9 a) 32 pole filter developed by AMTEL b) J shaped hairpin resonator and c) measured response at T=70K

In Europe, a first relevant contribution to the fabrication of HTS wireless systems was initially provided by Superconducting Systems for Communications (SUCOMS) project, sponsored by European Commission. This project involved many companies (GEC-Marconi, Great Baddow, Chelmsford Essex, U.K., Thomson CSF, Gennevilliers, France, and Lybold, Koln, Germany) and two universities (Birmingham University, Edgbaston, Birmingham, U.K. and Wuppertal University, Wuppertal, Germany). The main project goal was the fabrication of an HTS based trans-receiver for the second generation digital system GSM (DCS 1800). In particular, HTS planar pre-select filters able to cover a 15MHz sub-band in the range 1710-1785MHz were designed on both $LaAlO_3$ and MgO substrates. The layout of an 8 pole SUCOMS filter is presented in fig.2.10a [23,44]. In this case, the basic resonator is a meandered open loop and the desired quasi elliptic response with two transmission zeroes (fig.2.10b) was obtained by the classic quadruplet configuration, with the combination of magnetic and electric couplings. The overall dimensions on an MgO substrate are $(39x22.5)mm^2$. In this project, a particular attention was also dedicated to the realization of an adequate encapsulation of the Filter/LNA systems, in order to obtain a good thermal isolation from the external ambient.

Fig.2.10c shows three HTS filters assembled with LNAs in a RF connector ring. The measured noise figure of LNA and filter was about 0.3dB.

a)

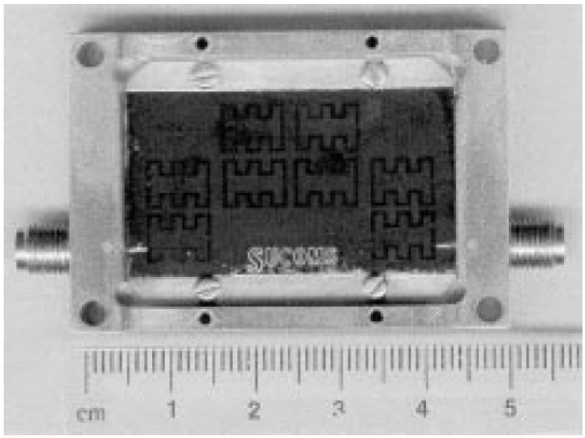

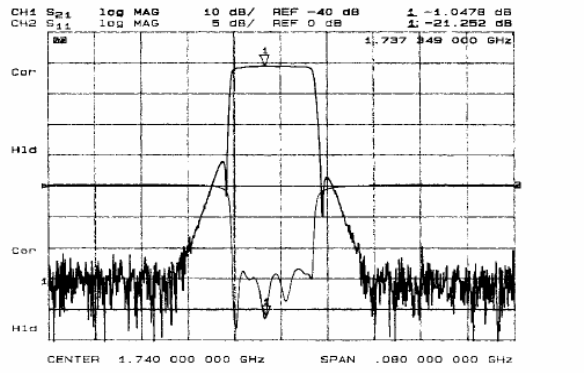

b)

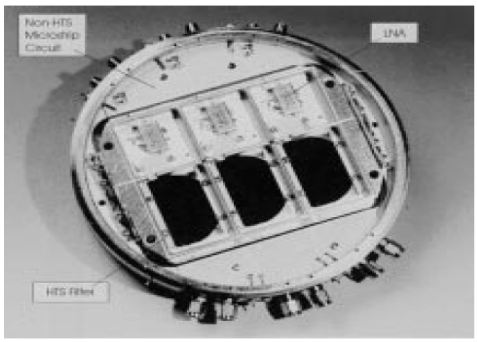

c)

Fig.2.10 a) Sucoms 8 pole quasi elliptic filter b) Measured response at T=77K and c) Three filters with LNAs in an RF connector ring

In Europe, other considerable results were achieved in the framework of the German program "Superconductors and Ceramics for future Communication Technology", funded by German Ministry of Education and Research and mainly based on the innovative filter design techniques developed at Wuppertal University. Also in this case, a demonstrator prototype for an HTS pre-selection filter integrated with a LNA amplifier was fabricated [15]. One of the new filter configurations proposed is shown in fig 2.11a. This 9 pole filter, with overall size [39x14.5]mm^2 on $LaAlO_3$, presents a quasi elliptic response and is based on the innovative principle that the coupling between adjacent resonators is achieved by disturbing the basic resonator symmetry. In this way, narrow band filters can be realized with closely spaced resonators [18]. In fig.2.11b, the measured responses at T=55K for two filters with 10MHz and 15MHz are reported.

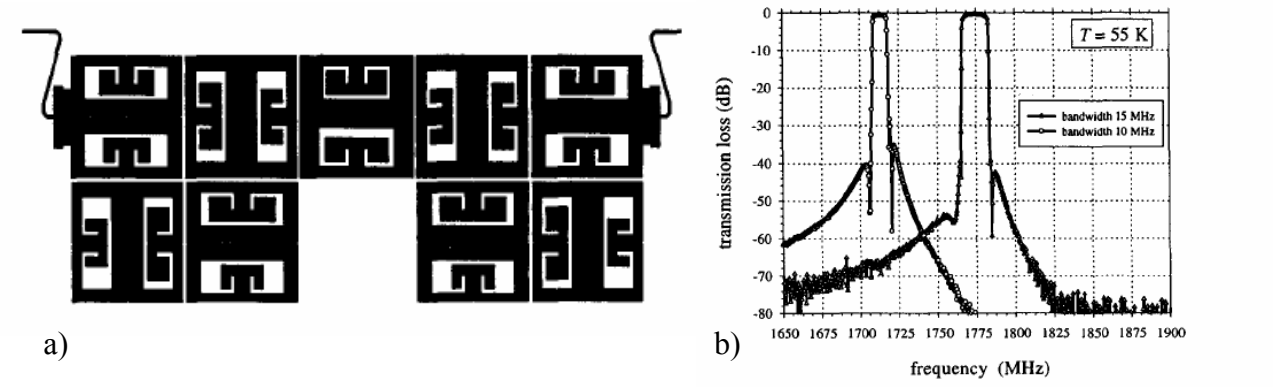

Fig.2.11) Layout of a 9 pole quasi elliptic filter developed at University of Wuppertal and b) measured responses at T=55K

The experience matured at Wuppertal University has favored also the birth of a new company (CRYOLECTRA GmBH). Presently, Cryoelectra commercialize HTS filters based on a novel coupling scheme, defined "triple mode", which, according to what shown in fig.2.12, allows to obtain two poles and three transmission zeroes with only two resonators. The basic structures are two $\lambda_g/2$ resonators rearranged in a cross configuration [45]. By this principle, many filters with high number of poles (9.13,17) have been fabricated and integrated with LNAs in adequate RF connector rings.

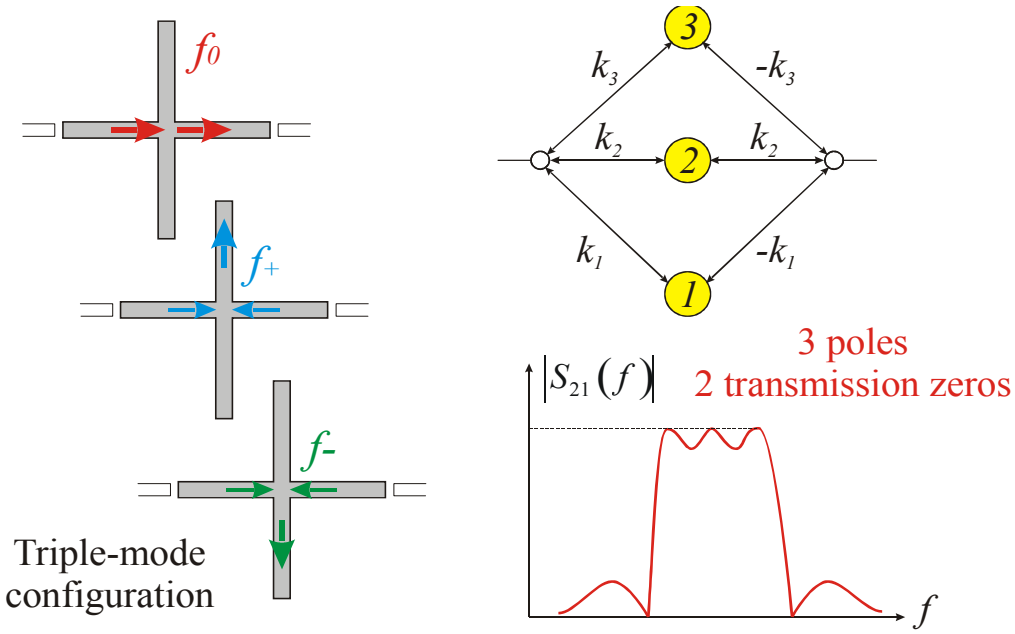

Fig.2.12. Triple mode configuration

2.1.3 HTS wireless system research in Italy

In Italy, the first research and development activity on HTS wireless systems was realized in the framework of the "Progetto-Sud Filtri Superconduttivi", starting in 1997. This project was funded by INFM (National Institute of Physics of Matter) and involved the Universities of Naples, Salerno and Catania, the telephony provider OMNITEL (now Vodafone) and the company Ansaldo CRIS for the fabrication of a new cryo-cooler system. One of the main goals of this project was the fabrication and the test of a prototype HTS receiver for GSM applications. To this regard, two 7 pole filters with 75 and 25 MHz bandwidths, based on the forward coupling scheme, were fabricated using 2" double sided YBCO films.

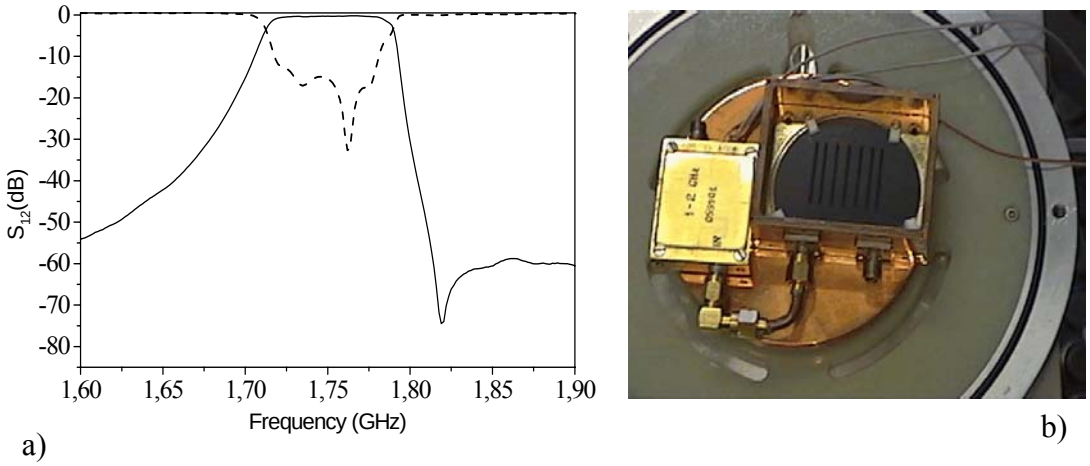

Fig.2.13 a) Measured response at T=77K of a 7 pole inter-digital filter b) Filter/LNA assembling

The filters were tested both in nitrogen liquid and in a closed cycle cryo-cooler, showing insertion losses ranging form 0.2 to 0.5dB (fig.2.13a), up to power input of about 2W. Furthermore, the 75MHz filter was assembled with a commercial LNA (fig.2.13b) and a sensitivity trial was performed in an OMNITEL BTS. At 77K, the HTS receiver showed a reduction of about 1dB of the minimum input power signal necessary to not exceed the maximum tolerable BER [46].

More recently, since 2002, PIRELLI Labs and Telecom Italia Lab, the R&D divisions of PIRELLI and the telephony provider Telecom Italia, have renewed the interest for HTS cryogenic front-end receivers, exploring their potentialities with respect to the new UMTS system. Substantially, their activities can be summarized in three main actions:

- Preliminary field trials on up-link coverage area of a CDMA BTS with a prototype HTS receiver
- Design and fabrication of a front-end system for a UMTS BTS, containing a new HTS receiver system
- Realistic simulations on the impact that the HTS receiver can have on the coverage and capacity of the UMTS wireless network.

The field trials have been performed following a similar procedure to that considered by Superconductor Technologies, as above discussed. An example of the collected data is reported in fig.2.14a. The different colors are still associated to the different levels of the transmitted power by a sample mobile, when this moves along a route (specified by the longitude and latitude) in the covered area. The data recorded in presence of a conventional TMA receiver and of a HTS front-end receiver are compared.

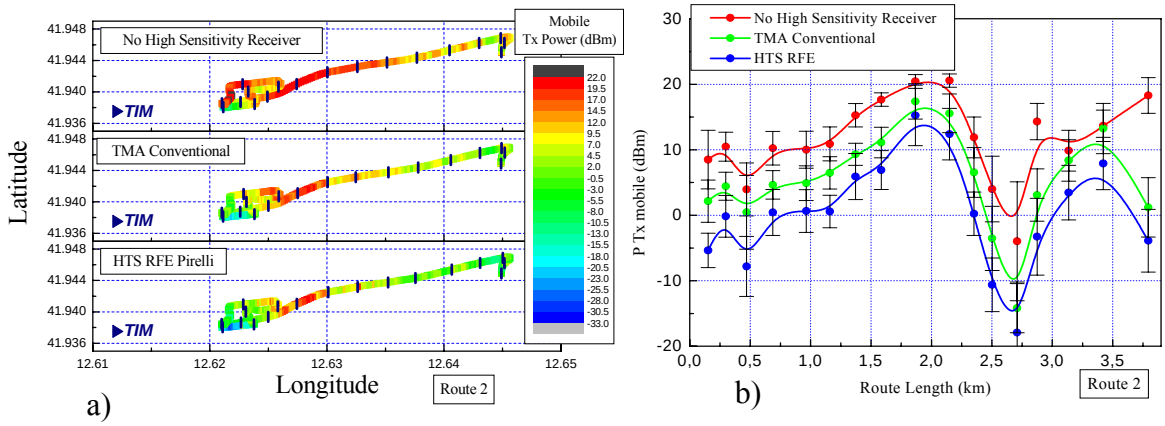

Fig.2.14. Field trials for the sensitivity of a BTS with conventional and HTS receiver

Fig.2.14b reports the same data as a function of the distance in km from the starting point of the route. For the reported example, the data show that the HTS receiver assures a handset transmitted power reduction ranging from 2 to

7dB. This test has been considered only preliminary and, according to the authors' opinion, the data interpretation needs a more accurate analysis. Nevertheless, it should be specified that, even in this case, trials performed in laboratory showed an improvement of about 1dB of the BTS sensitivity. In 2003, Pirelli Labs and Telecom Italia Lab, with the scientific support of the INFM National Center *Coherentia*, based at University of Naples, have started the development of a new front-end system (fig.2.15) with a HTS receiver channel for UMTS applications.

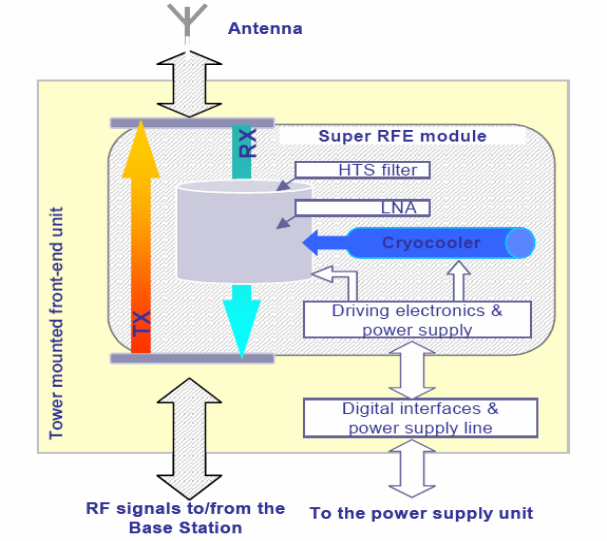

Fig.2.15 Block scheme of a new HTS front-end receiver

The duplexer scheme allows using the same antenna for transmission and receiving side and its generic function is twofold:

1) To route the received signal from the antenna to the receiver channel filter

2) To route the high-power Tx signal from the Tx filter to the antenna.

In this project, the duplexing function has been realized by using T-junctions and opportunely determining the lengths of the transmission line branches connecting the different devices. A new prototype HTS four pole filter, shown in fig.2.16a, has been designed to operate in the UMTS full up-link band (1.92-1.98)GHz with overall dimensions of about (13.5x27)mm^2 on $LaAlO_3$. It is based on two dual mode square patch resonators, where the coupling between the degenerate modes is realized by an elliptic slot situated in the resonator centre region. In this way, the coupling strength can be governed by the

ellipticity and the angular orientation of the slots [47]. Furthermore, by exploiting the peculiar characteristics of the dual mode resonators, a quasi elliptic response with two transmission zeroes has been obtained with the measured in-band insertion losses in the range of 0.2-0.3dB (fig.2.16b) at T=77K.

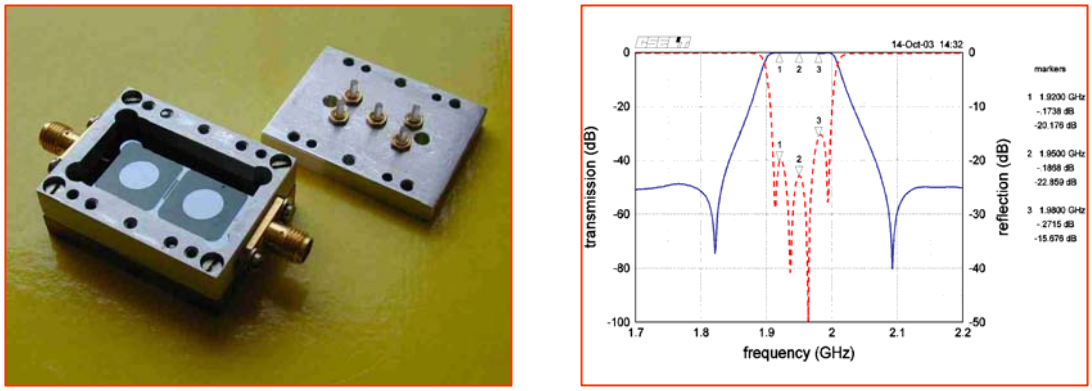

a) b)

Fig.2.16 a) Pirelli Labs-Telecom Italia Lab HTS four pole filter and b) corresponding response at T=77K

Then, the filter has been assembled with a commercial LNA and a noise figure of about 0.8dB (gain higher than 20dB) has been measured in a not optimized encapsulation system.

Finally, the third part of the activity has been dedicated to perform realistic network simulations to assess the impact of a HTS receiver in a UMTS wireless network [48]. This investigation has been performed by advanced codes for cell planning, developed by Telecom Italia Lab. Substantially, it was demonstrated that a HTS receiver can increase network coverage and capacity, when the total power available at the base station (downlink) is not the limiting factor. Provided this condition, in particular it was found that:

- Fewer sites are required to ensure proper coverage in a given area. In realistic rural and dense urban scenarios, the possible reduction of the sites is about 10% if a sensitivity improvement of 1 dB is realized. Furthermore, a better coverage can also be exploited in terms of better indoor service penetration.

- If the number of sites is kept fixed, the HTS technology performances can be exploited to improve the up-ink capacity, in terms of higher robustness against traffic peaks. The capability to carry significant excess of traffic (up to 5% of the network total traffic), without change in the quality of service level, has been estimated.

2.2 HTS systems in satellite communications

Satellite applications represent another field of commercial interest for HTS microwave technology since, even in this case, the present technological trend towards new systems with advanced signal processing capabilities can be sustained only by more and more complex architectures, requiring an increasing number of basic devices. The possible impact on satellite systems of the HTS technology, where the use of miniaturized and high performing devices allows the mass reduction of the necessary electronic equipment, is evident. To this regard, suffice it to mention that a satellite launch costs approximately 50.000 USA dollars per Kg. A basic scheme of a satellite structure, which well represents historically the early systems, is depicted in fig.2.17. This architecture was introduced for the first time in INTELSAT IV satellite (1971) and is based on a channel structure, where the received signal, with a 500 MHz bandwidth, is split by means of circulators in many sub-channels (transponders) with bandwidths typically from 36MHz to 72MHz (Input Multiplexer-IMUX). This is necessary to avoid the problems associated with high power amplifiers (HPAs), which are really linear only in very narrow bands. Hence, to avoid the non linearity effects of a common amplifier, the signals in the sub-channels are amplified separately and then recombined by another set of pass-band filters, to be finally re-transmitted by a common antenna. The output manifold block is usually composed of a set of transmission line branches of adequate lengths, which are necessary to

minimize the mutual interaction of the output filters (Output Multiplexer – OMUX).

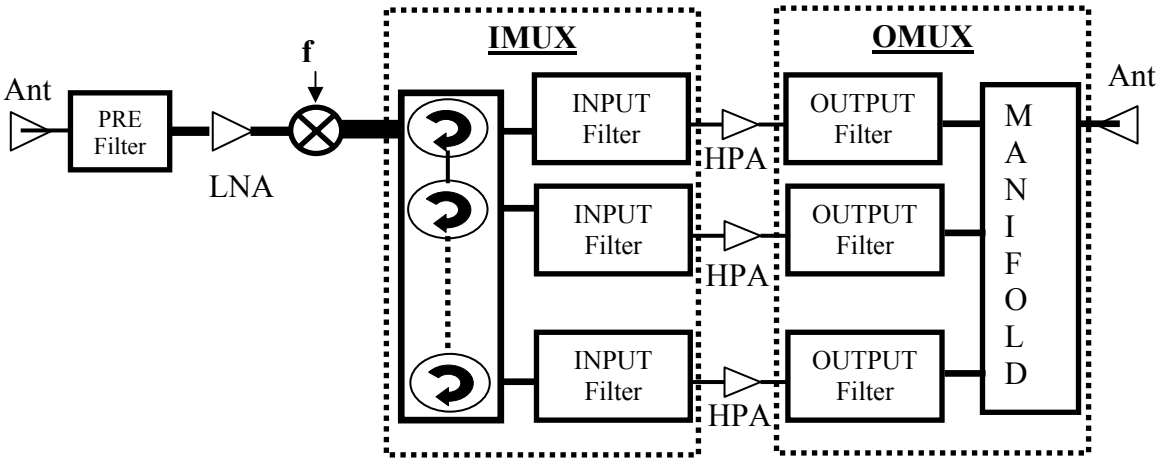

Fig.2.17 Basic structure of the first generation satellites

Future satellite systems (regenerative satellites) will be based on an extension of this basic architecture, with the possibility to use more input and more output antennas and to combine arbitrarily the links between the receiving and transmitting channels. This concept will extend tremendously the processing capabilities of the system, with the obvious drawback to necessitate a high number of filters, antennas and multiplexers.

Still focusing our attention on the basic configuration of fig.2.17, it is clear that HTS technology can be used potentially not only for the pre-select filter, thus improving the system noise figure, but also for the IMUX and OMUX filters, with drastically different required characteristics. As far as the IMUX filters are concerned, the selectivity performances are very important. Indeed, high selectivity allows strongly reducing the guard bands between the transponders, thus improving the spectral efficiency. Moreover, in order to avoid an irremediable distortion in phase and amplitude of the final recombined signal, it is necessary that the IMUX filters present special properties of flatness both for the group delay and the amplitude of the in-band response. Historically, the first input multiplexers (operating in C band) were based on single mode waveguide filters with additional phase equalizers. Since 1983, these filters are based on dual mode dielectric resonators. For example, in INTELSAT VIII

(1996), the IMUX filters are 10 pole self-equalized dielectric resonator filters (with 60 transponders versus 2 transponders for INTELSAT I). Obviously, HTS technology allows satisfying the IMUX requirements by planar filters, with a consistent miniaturization if compared with other conventional technologies. To this regard, fig.2.18 shows the dimensions of different filters operating in C band.

In last years, some important research and development projects have been funded for the qualification of HTS systems in space applications. The first of these projects was HTSEE, funded by Naval Research Laboratory in 1988 and involving different companies. Its first goal (HTSEE1) was the test, in a space environment reproduced in laboratory, of some HTS devices, such as planar resonators, filters with wide and narrow bandwidths, delay lines, patch antennas and 3dB couplers [49].

Fig.2.18 Comparison between different filter technologies in C band

The first phase was followed by HTSEE II, with the design of new advanced HTS devices and subsystems (see table 2.3), which were launched in orbit with ARGOS satellite in 1999 [50]. In particular, following different approaches, two 4 channel input multiplexers in C band were developed by Westinghouse (now Northrop Grumman) and Com Dev. The Westinghouse device, with some fabrication details, is shown in fig.2.19.

Category	Major Features	Provider
Channelizers and Filters	4 Channel mux @ 4 GHz 4 Channel filter @ 4 GHz 5 Channel mux @ 8 GHz	COM DEV Westinghouse Loral
Receivers	60 GHz Comm. Receiver Wideband Cueing Receiver > 2GHz Chirp BW Hybrid 9 GHz Channelized Receiver with MMIC mixer Low Noise HTS/GaAs Downconverter; 7 → 1 GHz	TRW Lincoln Labs NRL NASA/JPL and NASA Lewis
A/D Converter	Josephson junction logic module	Conductus
Digital IFM	5 bit, 16 MHz resolution f_c = 4 GHz, BW = 500 MHz	Conductus
Digital Multiplexer	HTS SQUID logic module	TRW
Delay line	40 nS, spiral in/out design	Westinghouse
Antenna array	Adaptive nulling design 4 elements, f_c = 5 GHz	Univ. of Wuppertal and Siemens
HTS environmental effects	Measure space radiation effects on J_c and R_s	NRL

Table 2.3 HTSSE II systems and corresponding providers

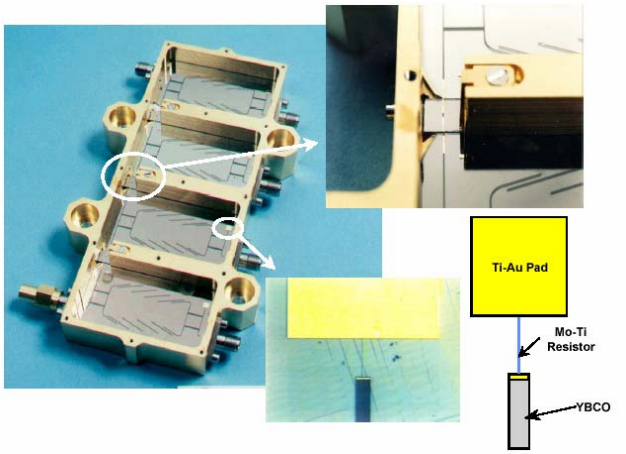

Fig.2.19 Four channel multiplexer based on planar hybrid couplers

In this case, the channelization is not realized by circulators, but by means of planar hybrid couplers. Every channel is composed by two twin HTS filters in backward coupling configuration. The combined actions of the couplers and filters, with different constructive or destructive interference paths for the signal, provide the desired multiplexing function. Certainly, the main purpose of this approach is the elimination of the losses associated to the circulators (0.2-0.3dB), favoring the fabrication of an all planar device.

On the other hand, the multiplexer developed by COM DEV, with overall dimensions (7.8x8.1x11.4)cm^3, was composed by four channels comprising circulators and 8 pole quasi elliptic filters based on hybrid dielectric/HTS (DR-HTS) resonators [51]. The basic concepts of this new resonator typology are shown in fig.2.20.

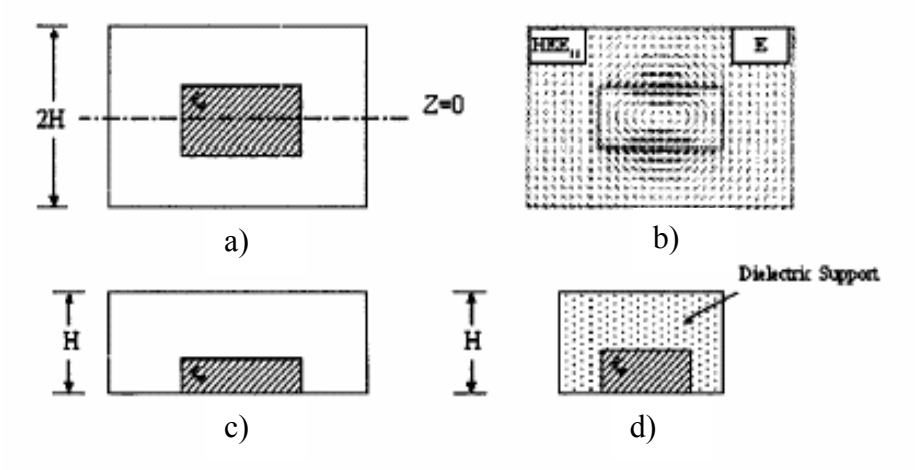

Fig.2.20 DR/HTS resonator basic principle

Considering a conventional DR resonator in HE_{11} mode, as shown in fig.2.20a and 2.20b, it is possible to note that the tangential component of the electric field is zero at z=0, such that a conducting wall (image plate, fig.2.20c) can be introduced without changing the boundary conditions and the consequent mode configuration. Moreover, if a HTS image plate is used, the Q_0 factor performances are preserved. Hence, by this technique, the resonator size is halved without affecting the resonant frequency and Q_0 factor. A further reduction can be achieved by a dielectric support which fills the whole cavity (fig.2.20d). The resulting superconducting multiplexer volume is less the one fifth of that of a conventional dielectric one.

While in Europe, efforts for the development of HTS systems for communication satellites have been carried out only in the German program "Superconductors and Ceramics for future Communication Technology", another important project in North America has been realized by a consortium consisting of COM DEV Ltd., Cambridge, Ont., Canada, Lockheed-Martin Advanced Technology Center (LM-ATC), Palo Alto, CA, Lockheed-Martin Communication and Power Center (LM-CPC), Newton, PA, and DuPont,

Wilmington, DE. This project was funded by Defense Advanced Research Project Agency (DARPA), with the aim to develop two complete HTS subsystems:

- A 60-channel HTS multiplexer (operating in C band) that duplicates the requirements of the INTELSAT 8 program
- Ka band Beam-link subsystem that duplicates the typical requirements of multimedia satellites.

In particular, for the 60 channel input multiplexer, the filters were based on a new planar resonator defined “quasi dual mode” by the authors (fig.2.21a) [52].

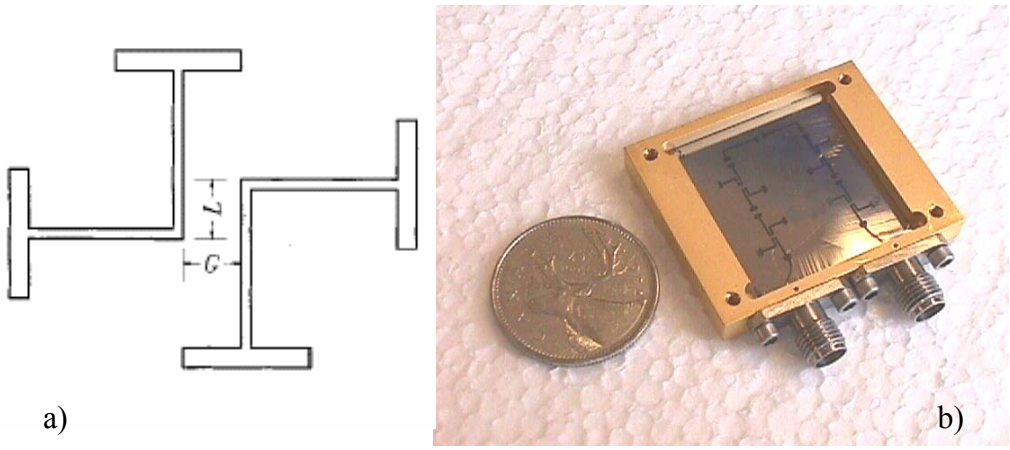

a) b)

Fig.2.21 a) Quasi Dual mode resonator and b) a 10 pole quasi elliptic self-equalized filter

Practically, this structure is composed of two stepped resonators (see chapter 4), which are coupled by opportunely fixing the gap G and the offset L. This particular resonator has been chosen in order to fabricate filters with both quasi elliptic and flat phase (self-equalized) response. To this end, it is necessary to consider resonators which allow easily the realization of cross couplings with different signs and, in this configuration, this can be achieved by an opportune choice of G and L. Fig.2.21b shows one of the realized 10 pole filters.

In this project, a particular care has been also dedicated to the design and optimization of the cryogenic packaging (shown in fig.2.22), where 4 real filters and 56 dummy filters were mounted in six stacks each to an aluminum support structure. This was machined from a single block of 6063 aluminum in

order to increase its stiffness and contemporarily decrease the thermal resistance through the filter stacks.

Fig.2.22 Cryogenic packaging for 60 filters

Indeed, in this type of project, where many HTS devices are required, it is important to minimize the thermal gradient, guaranteeing a stable working temperature for all filters. To this end, it is necessary to remember that HTS planar filters, due to the kinetic inductance, can exhibit a frequency shift of about 300KHz for every temperature change of 1K. For a satellite application, a 1MHz shift from the desired centre frequency can be in many cases not tolerable. Another critical aspect of this project was the cryo-cooler design, which had to satisfy special requirements on the stability and efficiency. Firstly, all possible heat leaks had to be avoided and, to this purpose, special cables with very low thermal conductivity for the connection of the cryogenic package to the room temperature ambient have been used. Usually, this can be obtained by fabricating long and wide cables at the expense of increasing losses. In this case, a trade-off between the different needs is essential.

Table 2.4 summarizes the mass and volume of the realized IMUX, comparing them with those of the original INTELSAT system. As reported, the percentage savings are higher than 50%. In future systems, where the number of channels could grow up to some hundreds, this feature should be fundamental.

Parameter	**Mass**	**Size**
Conventional DR technology (including mounting hardware)	25 Kg	0.005 m^3
HTS technology including 2 cryo-coolers and 2 electronic controllers (for redundancy)	12.2 Kg	0.0024 m^3
Percentage savings	**> 50%**	**> 50%**

Table 2.4 Mass and volume comparison between conventional and HTS technology for INTELSAT VIII IMUX

As far as the OMUX filters are concerned, usually not high selectivity is required and four or five poles are considered sufficient. It is clear that HTS OMUX filters can reduce remarkably the insertion losses and this can decrease the required output power amplifier. A reduction of the insertion loss of only 0.1 dB for every filter can result in an about 3W transmitted power reduction for channel. Obviously, to be convenient, this power reduction has to compensate the power required to the cryo-cooler. In first place, this implies a minimum value for the Q_0 factor of the considered resonators, but requires also that the cooling process has to be highly optimized, minimizing all heat dissipation mechanisms which tend to increase the cooling burden. For superconducting high power multiplexers, the heat dissipation sources are mainly three:

1. Insertion loss filters
2. Heat load of input/output cables
3. Heat leaks through support structure and radiation.

Presently, the most difficult to minimize are the losses related to the cables, since it is very complicated to fabricate cables with low insertion loss, low heat conduction and able to handle high power (up to 100W). In this case, due to high power signals, the situation is much more complex than that for the IMUX cables. The development of these transitions is essential to exploit fully the HTS potentialities, with the possibility to relax considerably the mass and power requirements of the cryo-cooler. However, some prototype superconducting OMUXs have been realized. A 4 channel superconducting output multiplexer, operating in C band and with a manifold realized using coaxial lines, is shown in fig.2.23, where is compared with a waveguide realization. The superconducting multiplexer occupies less than 5% of volume of the conventional device.

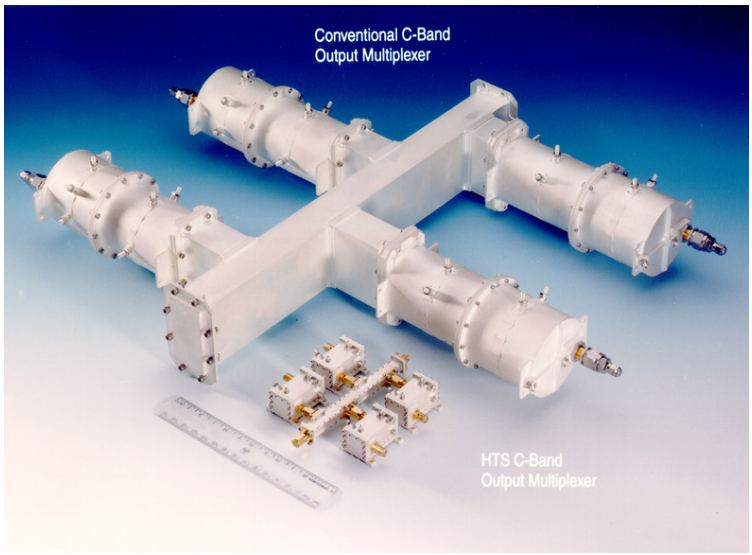

Fig.2.23 Comparison between 4 channel superconducting and conventional output multiplexers in C band

In this case, to support the high power signals, DR/HTS resonators are employed. For them, differently form the microstrip structures, the current density is quite uniform without edge peaks. Moreover, no etching process is needed, avoiding a further film degradation. In this way, the power handling is increased up to 50W [14].

As reported in the chapter 1, the only planar resonators able to handle so high power levels are those operating in modes with edge free currents, as the TM_{010} disk patches. A quasi elliptic four pole filter based on this concept and developed for a satellite output multiplexer is reported in [17]. However, this structure is based on a multilayered approach, where two disks are patterned on different layers and are coupled by a hole with opportune size, positioned in the common ground plane. Finally, fig.2.24 shows a last example of resonator, based on HTS films, for OMUX filters [53,54]. Basically, it is a dual mode hemi-spherical dielectric resonator, mounted on a ground plane of a cylindrically shaped metallic shielding cavity. The $HE_{11\delta}$ degenerate modes are coupled by means of opportunely positioned dielectric screws and the dielectric hemisphere is separated from the ground plane by another dielectric spacer.

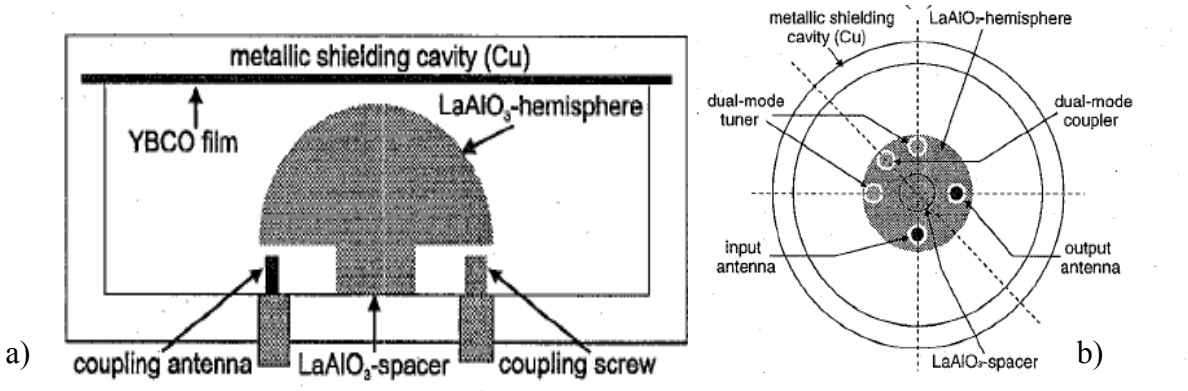

Fig.2.24 a) Side view and b) top view of the dual mode dielectric hemisphere resonator

Due to the field distribution inside the shielding cavity, beyond the tanδ of the dielectric, the main loss contributions are related to the ohmic losses in the top plate, which are much higher than those coming from the side walls or the bottom plate. Consequently, the Q_0 resonator has been improved by using a HTS film as top plate, with a final value of about 85000 measured at T=77K. By this resonator, two and four pole filters with quasi elliptic response have been fabricated and tested up to 35W of the input power, without showing appreciable degradations of the in-band insertion losses (about 0.1dB).

2.3 Radio astronomy receivers

Radio astronomy applications represent the most recent field where the front-end receivers based on HTS filters have demonstrated their capabilities. In order to reduce the system noise and improve the overall sensitivity, modern radio astronomy receivers are already cryogenic (working temperatures at 20-30K). In this way, the cooling system for HTS filters is already available and their integration in these receivers can improve remarkably the performances in terms of rejection of high interference signals. Indeed, the "observation" of weak signals coming from the space is very sensitive to interference disturbs and this is a more and more critical condition, due to the present proliferation of the communication channels. Most of the work in the development of HTS filters for radio astronomy has been carried out by the group supervised by prof. M.J. Lancaster at University of Birmingham, which in the last years have designed many HTS filters for Jodrell Bank Radio Observatory (University of Manchester). Table 2.5 summarizes some of the observation bands and the corresponding interference signals, deriving especially from commercial communication services [55].

L-Band	1550 – 1730 MHz	Observing noise and spectral lines from distant galaxy but interference from mobile communications
L-Band	1330 – 1430 MHz	Observing noise and spectral lines from distant galaxy but interference from air traffic control
L-Band	1330 – 1730 MHz	Observing noise and spectral lines from distant galaxy but interference from mobile communications and air traffic control
UHF	606 – 614 MHz	Pulsar observation cutting out interference from television signals
UHF	406-410 MHz	Removing interference from television signals
UHF	400.5-402.5 MHz	Receiving communications signals from deep space probes (Beagle II).

Table 2.5 Observation bands for radio astronomy signals

The first filter developed for Jodrell Bank Radio Observatory is shown in fig.2.25. This filter was designed to have a very wide bandwidth from 1330MHz to 1730MHz (26.4%). In this case, very high couplings are required

and it is difficult to obtain them by conventional filter configurations. To this end, a different structure based on half wavelength stubs was adopted [56].

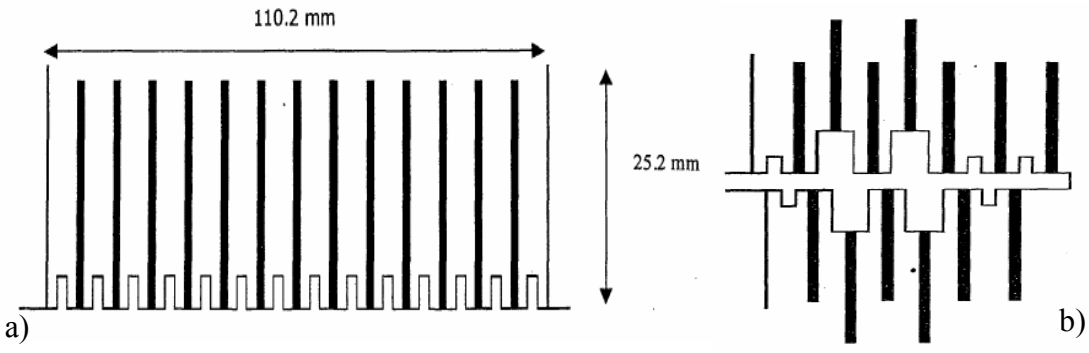

Fig.2.25 15 pole filter based on half wavelength stubs

Basically (fig.2.25a), the filter is composed of fifteen $\lambda_g/2$ stub resonators, which are connected by meandered $\lambda_g/4$ lines. The filter specifications can be satisfied by opportunely determining the admittance of the stubs and that of the connection lines, according to what reported in [2]. In order to fit the available superconducting area (3 inches diameter wafer), a more compact layout was realized (fig.2.25b).

More recently, another HTS filter configuration was proposed for the same bandwidth (fig.2.26) [57].

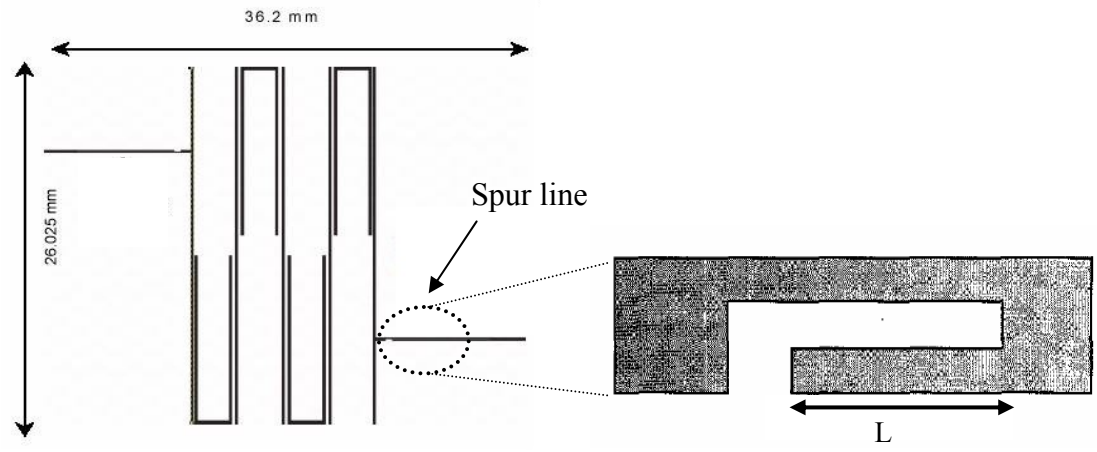

Fig.2.26 9 pole filter with basic $\lambda_g/2$ and hairpin resonators. Spur line filters are embedded in the feed lines

The 9 pole filter, fabricated on a $LaAlO_3$ substrate, is based on a combination of basic $\lambda_g/2$ and hairpin resonators. This structure, with the alternate

orientation of the hairpins, allows maximizing the couplings between the adjacent resonators. In this way, the filter was designed according to the Chebychev model, thus neglecting the cross couplings between non adjacent resonators. Furthermore, in order to suppress the second harmonic, a spur line filter is embedded in each of the two 50Ohm feed lines. The spur line filter is fundamentally a notch filter, which consists of a pair of coupled lines with L length, connected together at one end. At other end, one line is open-ended. This structure guarantees a notch-band, centered at the frequency at which $L=\lambda_g/4$. In this filter, the notch-band is centered at about 2.85GHz, corresponding approximately to the filter second harmonic.

As indicated in table 2.5, the observation of pulsars in UHF band is made difficult by the presence of strong interference signals. To this regard, narrow band filters, centered at 610MHz, have been designed on MgO substrates, with the main goal to strongly reject the television interferences at 605.25MHz and 615.25MHz. These filters are based on the quasi lumped resonator shown in fig.2.27.

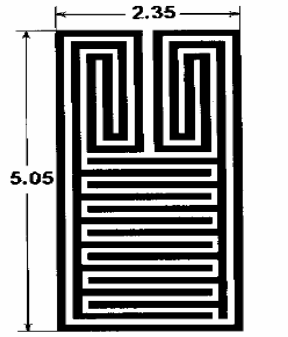

Fig.2.27 Quasi lumped HTS resonator with double spiral inductors and inter-digital capacitors

This resonator consists of symmetrical double spiral (spiral-in spiral-out) lines, loaded with inter-digital capacitors [31]. Despite the strong miniaturization, with a strip width of only 50μm, a Q_0 factor of more than 10^5 has been measured at T=30K, with P_{in}=-10dBm.

Due to its structure, the resonator magnetic energy is mainly stored in the double spiral (inductive) section, while most of the electric energy is stored in the inter-digital finger area. At resonance, this condition is translated into a strong confinement of the overall energy near the surface of the substrate.

Substantially, this confinement allows also weakening the coupling between adjacent resonators and low couplings at short distances can be obtained, reducing further the dimensions of the final filter. Fig.2.28 shows the layout and the corresponding dimensions on MgO of an 8 pole quasi elliptic filter based on this resonator [58].

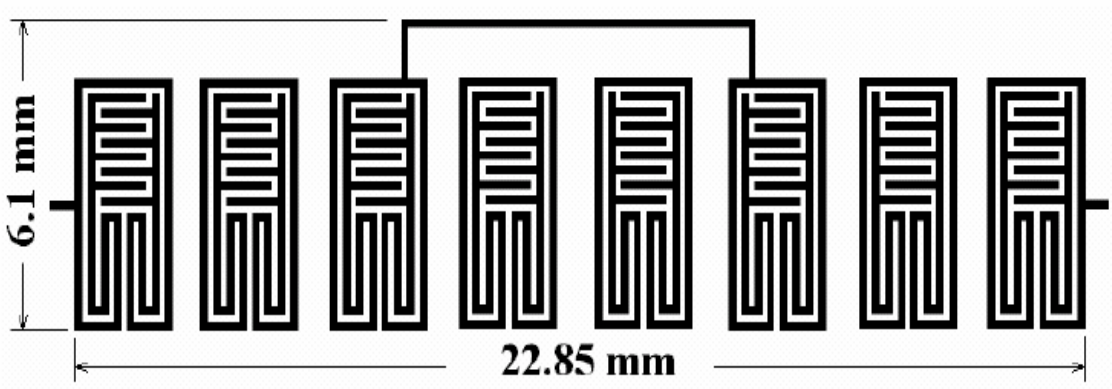

Fig.2.28 Layout of an 8 pole quasi elliptic filter with f_0=610MHz

The filter was designed to have the bandwidth lower than 1%. Two transmission zeroes have been realized by cross coupling the third and the sixth resonator by a tapped transmission line. Here, the tapping point position defines the coupling strength. Fig.2.29a reports the final response of the radio receiver based on this filter, compared with the corresponding performances achieved by the conventional filter. It is evident that the HTS filter guarantees a strong selectivity improvement, which provides an adequate rejection of the TV interference signals collocated at 605.25MHz and 615.25MHz (fig.2.29b).

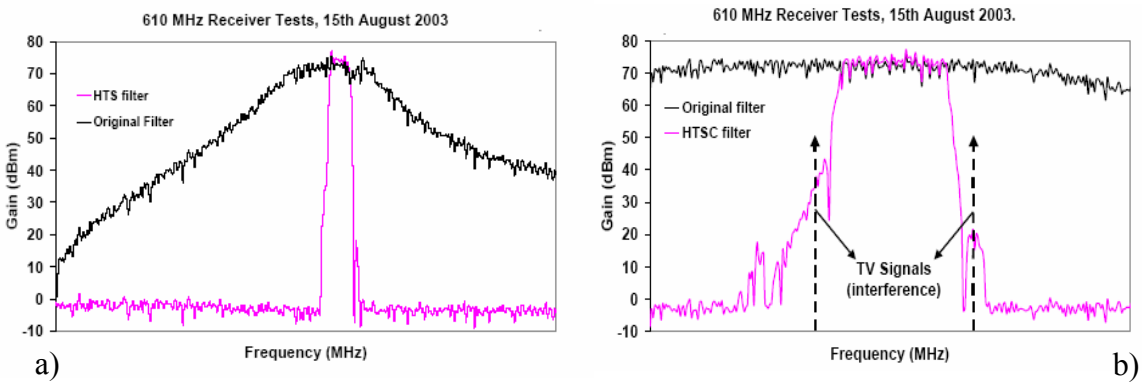

a) b)

Fig.2.29 Comparison between the performances of receivers based on the HTS filter (magenta line) and the conventional filter (black line)

As far as the radio astronomy applications in the frequency range around 400MHz are concerned, the Birmingham group has proposed the 8 pole filter shown in fig.2.30. This filter (f_0=408MHz and BW=3.7%) is based on the single spiral resonator and the overall dimensions on MgO are only [18x32]mm^2, confirming the high miniaturization levels achievable by this kind of resonator. The feed lines are provided with $\lambda_g/4$ coils, which are coupled to the external resonators by a capacitive gap. This particular arrangement allows largely extending the achievable Q_{ext} range.

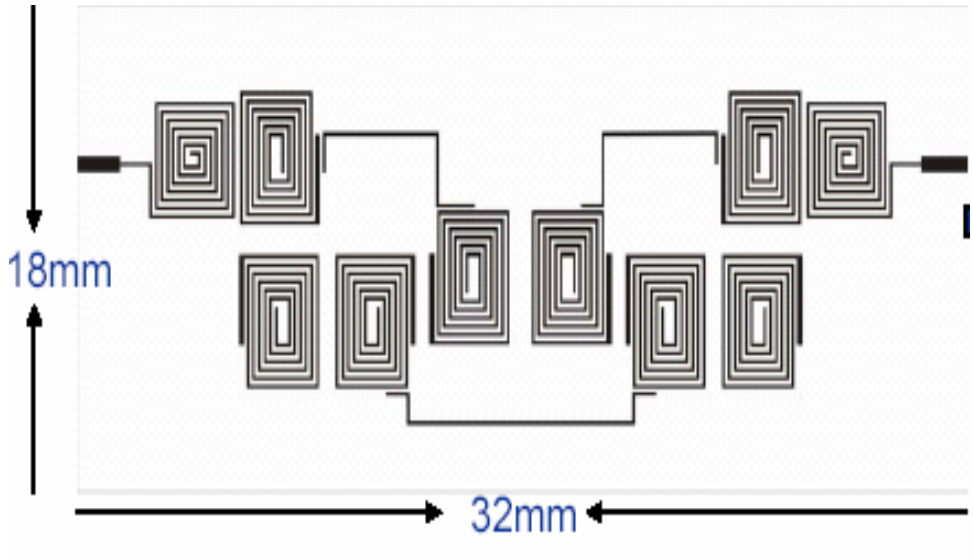

Fig.2.30 Layout of a quasi elliptic 8 pole filter based on the single spiral resonator

The single spiral resonator was introduced for HTS applications in [24], where its main features were discussed. In particular, since the current in adjacent arms flows in the same direction, the energy results mainly stored in the substrate region below the resonator and not close the surface. This guarantees a low sensitivity to the fabrication tolerances. Differently from those reported in [24], the filter in fig.2.30 is based on the quasi elliptic model, where four transmission zeroes are realized by adding three cross couplings to the original Chebychev filter. Finally, fig.2.31, where the signal has been down converted by a local oscillator signal of 435MHz in order to obtain a 30MHz intermediate frequency (IF), confirms that the use of HTS filters allows cutting the interference signals close to the band.

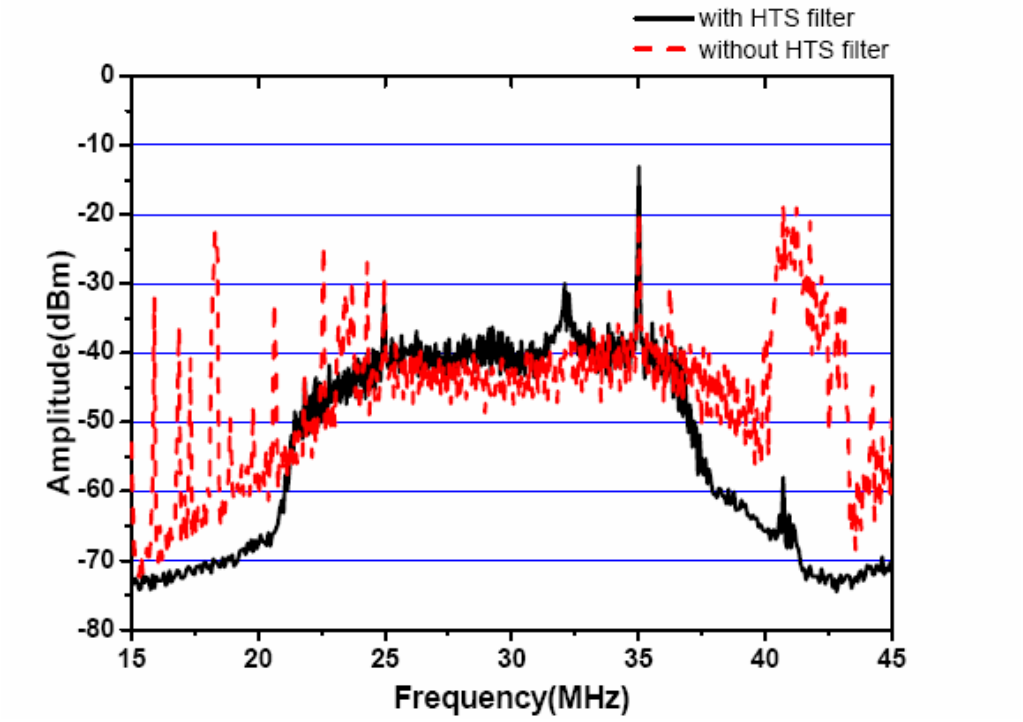

Fig.2.31 Intermediate frequency signal, down converted from UHF band radio astronomy signal with (continuous line) and without (dashed line) HTS filter

CHAPTER 3

MINIATURIZED HTS FILTERS BASED ON FRACTAL LAYOUTS

This chapter is devoted to the design and fabrication of highly miniaturized superconducting filters, realized by using novel resonators based on fractal layouts. In particular, our attention has been focused on Koch-Minkowski and Hilbert space filling curves. We have explored the miniaturization levels achievable by these resonators, emphasizing the parameters which allow obtaining a good trade-off between compact size and losses. Several prototype four pole filters, with Chebychev and quasi elliptic responses, have been designed and fabricated. The main experimental measurements are reported here as well.

3.1 Fractal space filling curves

According to the meandering technique discussed in section (1.5), in our work we have analyzed the miniaturization performances of Koch-Minkowski and Hilbert fractal curves in the fabrication of HTS filters (fig.3.1).
In general, fractal geometries are realized from classical ones by the iterative application of a generator method. This procedure leads to *self-similar* structures, where some parts of the figure repeat the entire scaled figure at any magnification [59,60]. Fractal electrodynamics is the application of fractal

concepts to the electromagnetic theory. For example, the fractal description of some geometries present in nature and too complex to be described with Euclidean geometry, allowed the characterization of interaction between these structures and electromagnetic waves, leading to the solution of problems such as land or ocean surfaces diffraction or random media propagation [61].

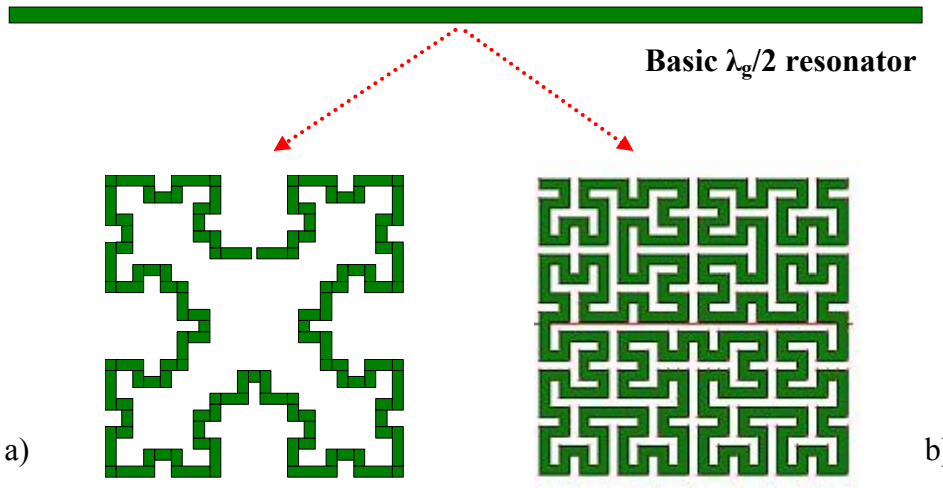

Fig.3.1 a) Koch-Minkowski and b) Hilbert resonator examples

The use of fractal curves in the design of miniaturized superconducting microstrip devices was suggested for the first time in [62], by a group of researchers working at the Universitat Politecnica de Catalunya (UPC), where a part of our investigation has been developed.

In particular, Koch-Minkowski and Hilbert fractals (fig 3.2) are realized by one-dimensional generators, thus showing peculiar space-filling features. Usually, they can be characterized by a non integer geometrical dimension which can be determined by [63]:

$$D = \frac{\log N}{\log s} \qquad (3.1),$$

where N is the number of copies of the generator and s is the scale factor of consecutive iterations. For example, at k^{th} iteration of a Hilbert curve, each generator occurrence is substituted by four copies, each one scaled by a factor 4, so that $D = \frac{\log N}{\log s} = \frac{\log\left[\left(4^k - 1\right)/\left(4^{k-1} - 1\right)\right]}{\log\left[\left(2^k - 1\right)/\left(2^{k-1} - 1\right)\right]}$. Consequently if k>>1, it results

that $D \approx \frac{\log\left[4^k / 4^{k-1}\right]}{\log\left[2^k / 2^{k-1}\right]} = 2$ and this means that the Hilbert curve ideally fills all the available two-dimensional area.

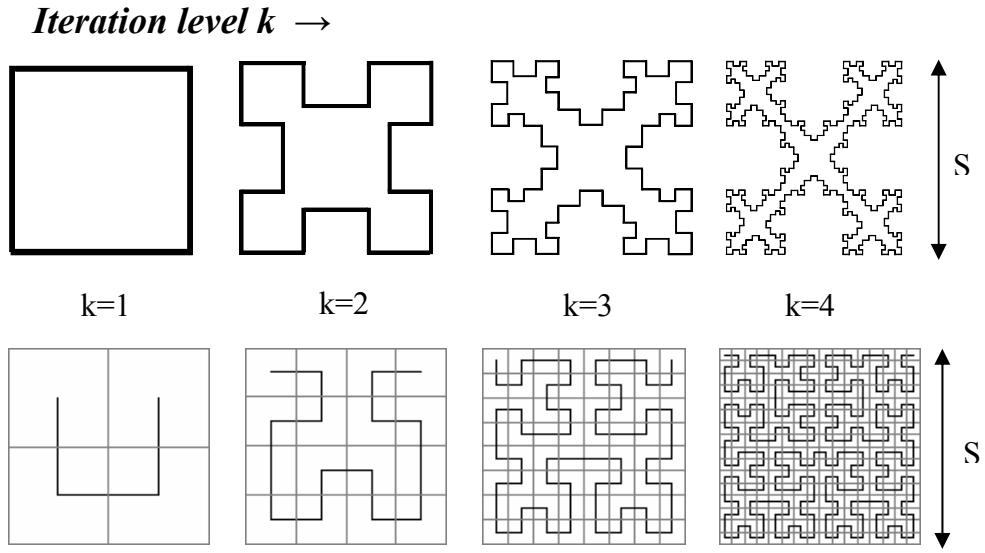

Fig.3.2 First four iterations of Koch-Minkowski (upper side) and Hilbert (lower side) curves

With the reference to a resonator, when the number k of the applications of the generator method is increased, the space filling capability allows increasing its length without changing the external side S and this is the basis for the miniaturization. As a drawback, in a real planar resonator, higher levels of fractal iteration imply lower values of the microstrip width, thus increasing the dissipative losses with a corresponding degradation of the quality factor. Hence, for these structures, the compromise between miniaturization and quality factor is simply defined by an adequate fractal iteration level.

Before analyzing in details our results, it is worth to remember that recently these same fractal shapes have been utilized to fabricate miniaturized planar antennas [64,65,66,67,68,69,70]. These studies have clearly shown that, increasing the iteration level k and keeping fixed S, the resonant frequencies of a fractal antenna lowers, but contemporarily its radiation characteristics worsen, with a rapid decreasing of the radiation resistance and the efficiency. On the other hand, these results confirm also for these HTS fractal resonators

the occurrence that high miniaturization levels (high k) reduce contemporarily the housing losses related to the radiated field.

3.2 Koch-Minkowski resonators

The generator method for the square Koch-Minkowski fractal curves is represented in fig.3.3. At the first stage, one third of the square side is substituted with an indentation step of length S; at the second stage, this method is applied to every single segment of the figure and so on. For such a loop, at k iteration step the perimeter P_k is related to P_{k-1} by the formula:

$$p_k = \left(1 + \frac{2}{3}w\right).^k p_{k-1} \qquad (3.2),$$

revealing that the overall length of the curve exponentially increases with k. In this case, the fractal dimension, defined according to (3.1), is D=1.262 (if k>>1).

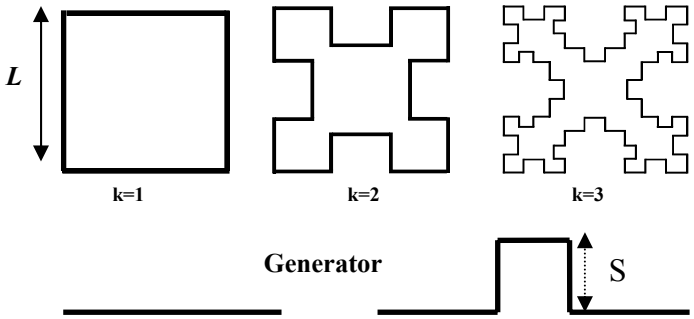

Fig.3.3 Generator method and first three iterations of square Koch-Minkowski curves

As better shown in the following, these curves present a lower space-filling feature if compared with the Hilbert ones and consequently a lower miniaturization power. However, they are easier and faster to simulate and their particular shape allows reduced coupling coefficients between adjacent resonators, even if the distances are very short [67]. Therefore, this geometry can be useful for the design of narrow band filters, where low couplings are required. In our work, Koch-Minkowski resonators have been rearranged as

half wavelength resonators by cutting one side of the origin fractal closed curves (fig.3.4a). This configuration makes also these resonators suitable to the realization of quasi elliptic responses by the quadruplet configuration, which is based on the combination of electric and magnetic couplings [1]. In particular, considering the fundamental mode, the electric field has a maximum in the cut region, while the magnetic field has a maximum at the midpoint of the resonator. Fig.3.4b shows the resonance frequencies on MgO substrate of the first three Koch-Minkowski resonators (k=1,2,3), as a function of the external side L. This plot confirms that higher k assure lower resonant frequencies, once fixed the external side.

In order to give some reference values of the obtainable miniaturization levels, we can compare the values of L for different k at a fixed resonance frequency. For example, at f_0=1.95GHz (UMTS application), L results 8.1mm for k=1 and it is reduced up to 5.4mm for k=3. This result corresponds to a reduction of about 30% and this value is almost constant in all the analyzed range. However, it is intuitive that for low values of L the fractal details introduced in the resonators are smaller and smaller, thus giving a lower contribution to the miniaturization process. Practically for L≤3mm (f_0≥ 4GHz), the resonators with k=2 and k=3 present very similar f_0.

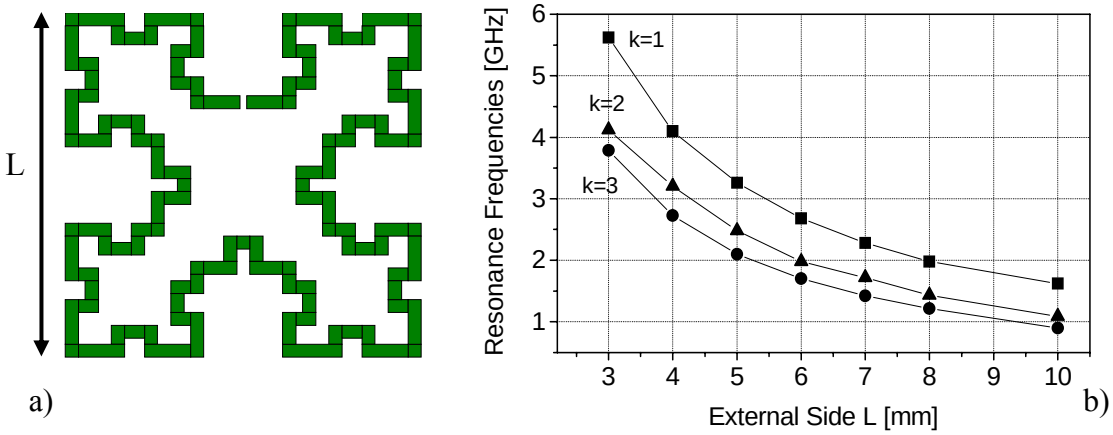

Fig.3.4 a) Open loop Koch-Minkowski resonator b) Resonance frequencies of resonators with k=1,2,3 as a function of L on MgO

In this study, we have focused our attention on Koch-Minkowski resonators with k=3, since the case with k=4 provided negligible changes in the device

miniaturization for all the practical values of L [68]. Furthermore, the microstrip widths for resonators with k=3 range from 0.1mm to 0.3mm, guaranteeing high quality factors (>$3*10^4$).

As aforementioned, besides the miniaturization of the resonator itself, the fractal layout allows also the reduction of the coupling coefficient between resonators, once fixed the distance. To this regard, the plot in fig.3.5 shows a comparison between the couplings, as a function of the distance, for Koch-Minkowski resonators with k=1 and k=3, both resonating at 1.95GHz. In this case, the orientations of the adjacent resonators have been considered opposite and as shown, at the same distance, from k=1 to k=3, there is a reduction of about one third of the evaluated coupling.

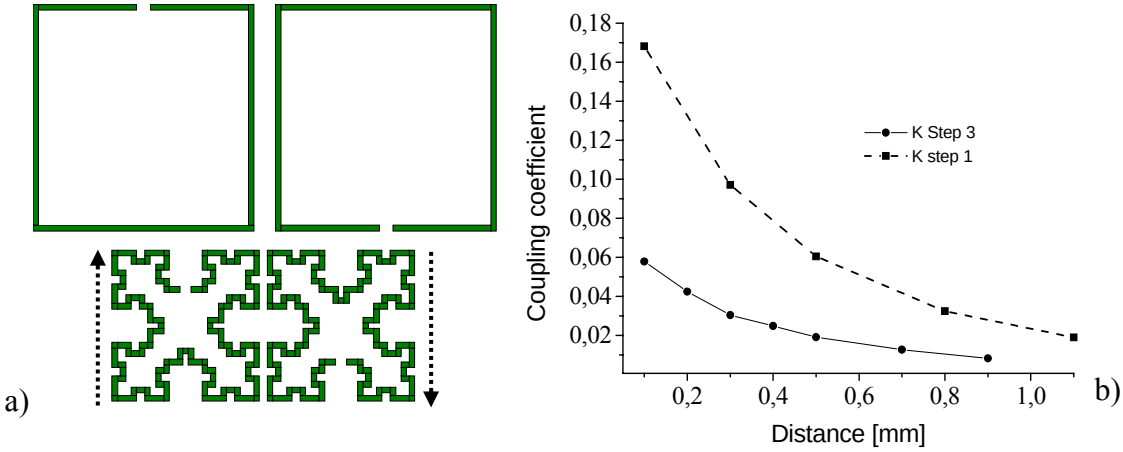

Fig.3.5 a) Layout of coupled resonators with opposite orientations and b) corresponding curve as a function of the distance for Koch-Minkowski resonators with k=1 (dashed curve) and k=3 (continuous curve)

A further reduction of the coupling between resonators with k=3 is achievable choosing the same orientation for both the resonators (fig.3.6a). Indeed, the comparison (fig.3.6b) with the previous configuration based on the opposite orientation shows again a reduction of about one third. This last feature can be explained considering that, in both the analyzed configurations, the coupling nature is mixed, since both the electric and magnetic fields give a contribution to the overall coupling. Actually, in the configuration based on the opposite

orientation the magnetic coupling results to be in-phase with respect to the electric coupling.

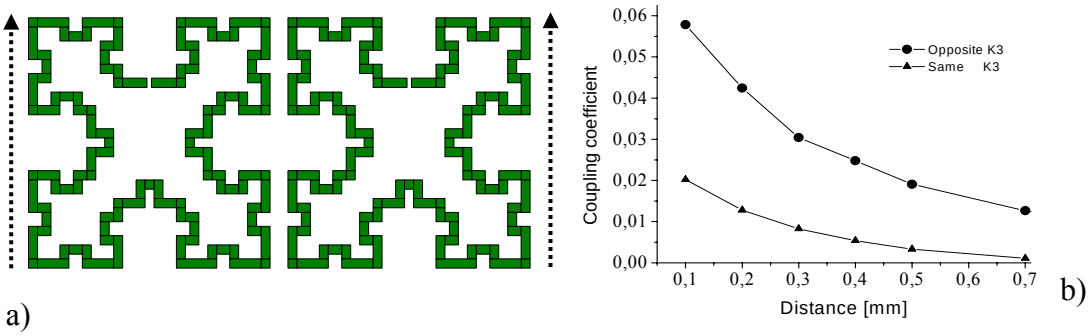

a) b)

Fig.3.6 a) Coupling layout for Koch-Minkowski resonators with k=3 and the same orientation and b) Comparison between the couplings as function of the distance for resonators with opposite (circle) and same (up-triangle) orientation

In this way, their contributions tend to add, thus increasing the overall coupling. Instead, in the other case, the magnetic and the electric coupling contributions are out of phase and tend to cancel each other lowering the overall coupling effect [71]. In conclusion, by using the same orientation, typical coupling values for Koch-Minkowski resonators with k=3 are lower than $1*10^{-3}$ in the distance range around 1mm, leading to very interesting performances if compared with those of other microstrip resonators [32].

3.2.1 Filters based on Koch-Minkowski layout

By using Koch-Minkowski resonators with k=3, several prototype four pole filters, with both Chebychev and quasi elliptic responses, have been designed. In a first part of this work, we focused our attention on the frequency range around 1.95GHz. At this frequency, as mentioned above, the external side of a Koch-Minkowski resonator with k=3 is 5.4mm on MgO ($0.086\lambda_g$, where λ_g is the wavelength at 1.95GHz for a 50Ohm transmission line). The width of the microstrip is 200μm. As a comparison, it should be remembered that, at the

same frequency and on the same substrate, a basic $\lambda_g/2$ resonator is long about 30mm, while a square dual mode resonator has an external side of 25mm.

A first possible layout for a Chebychev four pole filter is reported in fig.3.7a. It was designed to satisfy the following specifications: f_0=1.95GHz, r=0.01dB, *BW(%)*=0.65% (12MHz). As shown, all the resonators have the same orientation, thus favoring the realization of the required low couplings. Indeed in this case, for k_{12}=0.00709 and k_{23}=0.00502**,** the necessary distances are 0.35mm and 0.42mm, respectively. Q_{ext} is higher than 100 and is realized by a capacitive gap between the external resonators and the feed lines. The overall dimensions of the filter are only [24.2x5.42]mm^2 and are less than the half of a equivalent realization based on $\lambda_g/2$ resonators (forward coupled configuration).

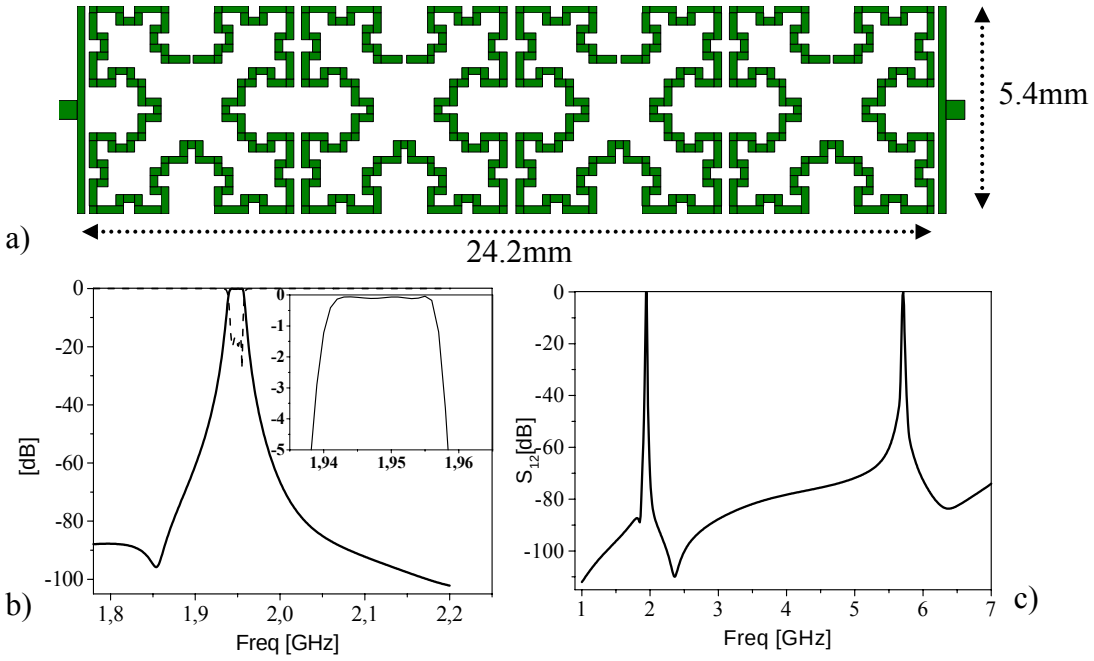

Fig.3.7 a) Chebychev four pole filter: a) Layout, b) in-band and c) wideband frequency response

The simulated response, realized by IE3D from Zeland Software, predicts minimum insertion losses in the range of 0.1dB (fig.3.7b). Furthermore, it should be noted that the filter presents the first spurious response only at about $3f_0$ with an out-of-band rejection higher than 80dB. The absence of the second mode at $2f_0$ is typical of capacitively loaded resonators. Indeed, at this

frequency, since the length of the resonators is one wavelength, charges of the same sign are present at their ends and this reduces considerably the equivalent capacitance [31]. As mentioned above, these resonators are also suitable to realize quasi elliptic responses. In fig.3.8a, a very compact filter layout (overall dimensions [12x11]mm^2), rearranged in the classic quadruplet configuration is shown. The simulated filter response with f_0=1.95GHz, r=0.04dB and *BW(%)*=4% (corresponding about to the whole UMTS up-link bandwidth, [1.92-1.98]GHz) is reported in fig.3.8b. A tapped line configuration has been adopted for Q_{ext} (about 20) and, also in this case, the expected minimum insertion losses are in the range of 0.1dB.

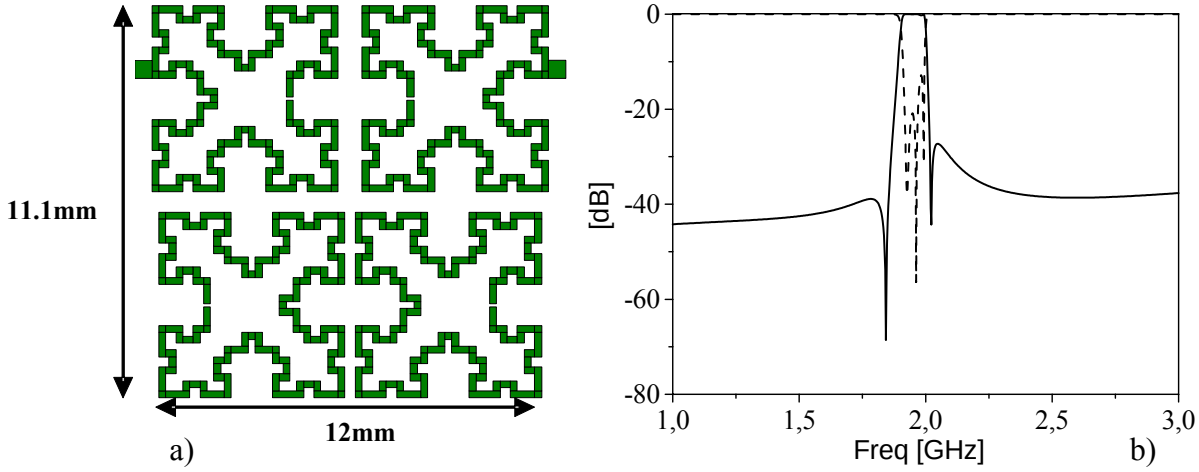

Fig.3.8 a) Quasi-elliptic filter layout and b) simulated response

Finally, a prototype four pole quasi elliptic filter, operating in the UHF band (f_0=0.67GHz and *BW(%)*=1%), of interest for radio astronomy applications, has been fabricated on a $LaAlO_3$ substrate, with the overall dimensions fitting exactly in a 20x20mm^2 area [72]. Also this filter is based on the quadruplet layout, but the feed line configuration was realized by a capacitive coupling with the external resonators (fig.3.9a). In order to extend the obtainable Q_{ext} range, even the feed lines stub has a fractal shape.

Moreover, this particular rearrangement of the four pole filter provides a further direct coupling k_{SL} between the two feed lines, what produces the presence of other two extra zeroes in the response [73]. The k_{SL} strength (-0001768 in our filter) is related to the feed lines length H, which can be

changed in order to control the extra zeroes position. This situation can be modeled in the corresponding quasi elliptic equivalent circuit, in which a further k_{SL} coupling between the ports is added.

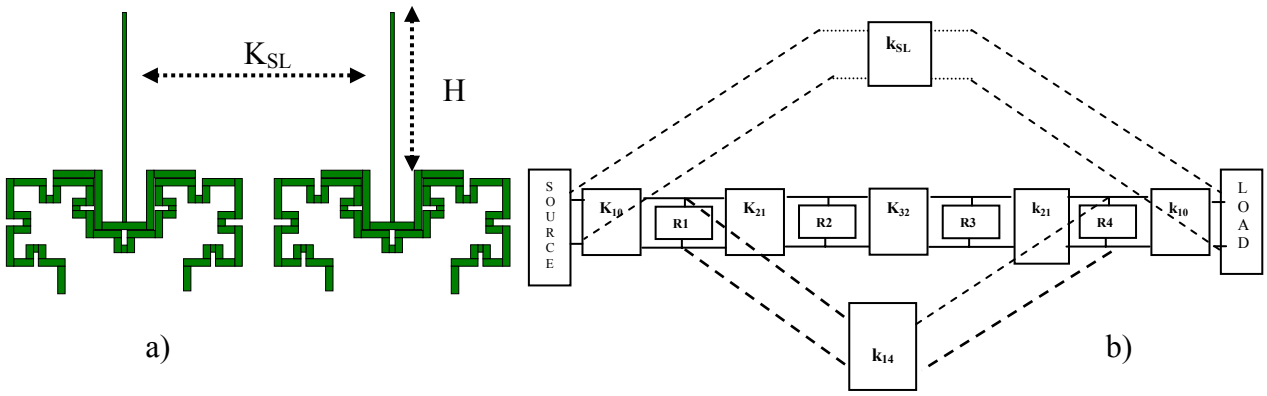

Fig.3.9 a) Direct coupling between the feed lines for the UHF band quasi elliptic filter b) Equivalent lumped circuit

The filter was fabricated by using a Niobium 1000nm thin film (fig.3.10a) and tested in liquid Helium at T=4.2K. The simulated response realized by Ensemble, is presented in fig. 3.10b (dashed curve) and is compared to the experimental measurement (continuous curve), obtained without the use of tuning dielectric screws.

The measured center frequency coincides with the simulated one if ε_r=23.7 is considered in the simulations. The minimum insertion losses (about 0.2dB) and the bandwidth are in good agreement with the expected values, but the measured response presents an undesired in-band ripple of about 2.5dB. This last condition is probably due to the lost of accuracy of Ensemble, unable to refine the mesh at the edges of the microstrip. In fact, in this design, the resonant frequencies of the first and last resonators have been slightly modified, to compensate the feed lines effect. Probably this modification has not been accurately realized by Ensemble.

Other simulations (dotted curve in fig.3.10b) by IE3D, with a more dense edge mesh, have proved the detuning condition of the designed filter, giving however an in-band response worst than the experimental one. Finally, the measured response confirms the presence of the extra zeros, even if they are

not evident as in the Ensemble simulations. To this regard, due the low value of k_{SL}, the box effect should be carefully analyzed.

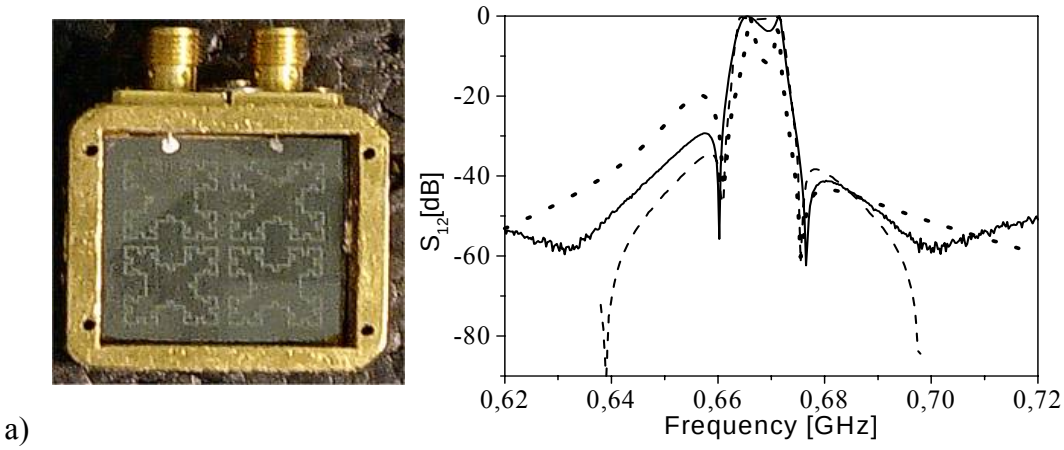

a) b)

Fig.3.10 a) Photo of the UHF band filter mounted in its box b) Comparison between measured response (continuous curve), Ensemble simulation (dashed curve) and IE3D simulation (dotted curve)

3.3 Hilbert resonators

In 1892, while studying the existence of special curves with space filling capabilities and the property of being everywhere continuous, the German mathematician David Hilbert presented the set of curves shown in fig.3.2(lower side, for the first four iterations). As evidenced by the background grid, the Hilbert curve with k=1 connects the centers of the four parts in which the original square is divided. For k=2, the same criterion can be applied dividing the square in 16 parts and connecting the centers in the same way. For the general k^{th} iteration, 2^{2k} divisions are realized and consequently the curve will be composed of $(2^{2k}-1)$ segments, all with the same length. Another and probably more intuitive vision suggests that, at every stage, the geometry can be obtained by putting four copies of the previous iteration, opportunely oriented and connected by additional short segments. For every curve, the total length *L(k)* exponentially increases with k and can be written as

$$L(k) = (2^k + 1)S \qquad (3.3),$$

being S the length of the external dimension side [64]. As mentioned above, the fractal dimension D of the Hilbert curves approaches the value 2 for very large values of k. In this way, among other fractal curves, the Hilbert ones present the best space-filling capability and consequently the best miniaturization perspectives for superconducting resonators [74]. However, while in an ideal Hilbert curve the line width is zero, in a real Hilbert resonator the microstrip width w and the interspacing g between the turns are the parameters which actually define the trade-off between miniaturization and quality factor Q_0.

To illustrate this, fig.3.11 shows the resonance frequency f_0 and quality factor as a function of the external side S, obtained by using Momentum-Advanced Design System on several Hilbert resonators on MgO, with iteration level 3, 4 and 5. In this first case, the ratio w/g was kept constant to 1. For all simulated resonators, the parameters of the superconducting films are taken from the data at 77 K of a commercial supplier, namely, surface resistance $5f^2\mu\Omega$, with f in GHz, and London penetration depth λ_L=200nm. Fig.3.11a shows the simulated f_0 as a function of S values ranging from 3mm to 10mm. For comparison, the corresponding f_0 (dashed curve) for Koch-Minkowski resonators with k=3 are reported too.

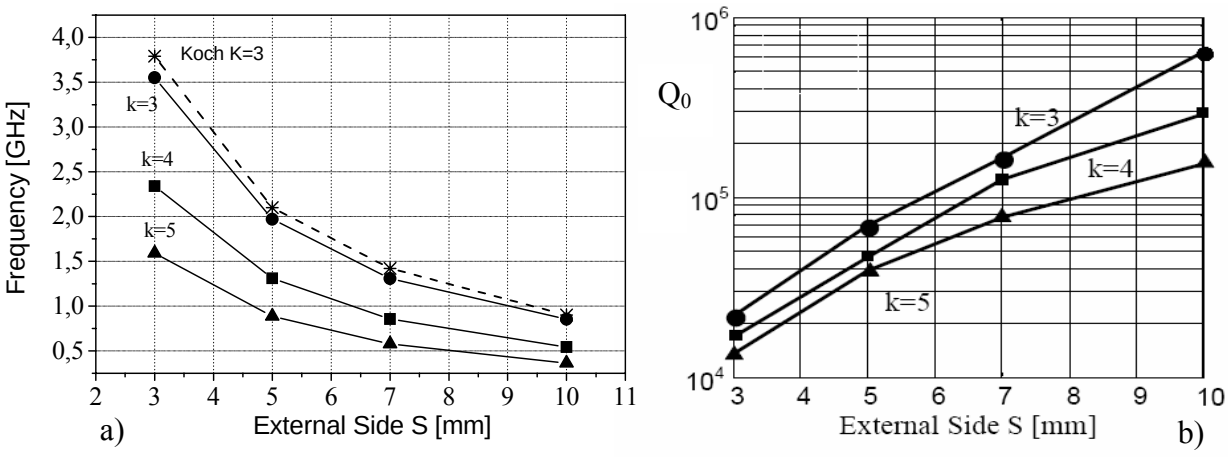

Fig.3.11 a) Resonance frequencies on MgO and b) unloaded quality factor of Hilbert resonators with k=3,4,5 as a function of external side S

As a reference point for the achievable resonance frequencies in this range of dimensions, it should be mentioned that for S=3 mm and k=3, f_0 is around 3.6 GHz, whereas for S=10 mm and k=5, it is around 0.35GHz.

Firstly, for a given S, we can observe that, although according to (3.3) the length of the resonator almost doubles at each iteration from k to k+1, the fundamental resonance frequency does not halve. This phenomenon is due to the coupling between the different turns of the Hilbert resonator, which practically define an equivalent shorter path for the signal. Obviously, this effect gets stronger with the increase of k, since a reduction of the interspacing among the turns takes place. In this way, for large values of k, the ratio $f_0(k+1)/f_0(k)$, between the resonance frequencies of two iterations, tends to grow towards 1. This means, from a practical point of view, that only iterations with $k \leq 6$ guarantee an effective miniaturization improvement. Secondly, it is clear that, for every value of S, the resonators with k=5 show lower resonant frequencies, but as evidenced in fig.3.11b, these same resonators present also lower quality factors. Indeed, taking into account w and g, the external side S of a Hilbert resonator can be written as a function of k by:

$$S(k) = 2^{(k-2)} * (4w + 3g) + (2^{(k-2)} - 1) * g \qquad (3.4).$$

Analyzing this formula, valid for every $k \geq 2$, it is possible to conclude that keeping fixed S(k), the value of w almost behalves for two next iterations, leading to the rapid degradation of Q_0 because of the current density increase. Practically, for a given application, by these two plots it is possible to identify completely the maximum miniaturization level that one could achieve if a minimum Q_0 is required.

In a second phase, also for these resonators, the attention has been focused on the applications at frequencies close to 2GHz. In this case, we have evaluated how the w/g ratio affects Q_0 and S. Table 3.1 summarizes the width of the strip, the external side and the quality factor for the resonators with k=3,4,5 and w/g=(0.5, 1, 1.5). As shown, for every w/g series, S almost halves comparing k=3 with k=5, but w is reduced from 8 to 10 times which significantly lowers Q_0, of a factor between 6 and 8. On the other hand, increasing w/s and keeping

fixed k, S(k) slightly increases, making the resonator less miniaturized but contemporarily improving Q_0 since the microstrip width increases.

	w(mm)	**S(mm)**	**Q_0**
w/g=0.5, k=3	0.2	4.6	56.100
w/g=0.5, k=4	0.069	3.33	18.500
w/g=0.5, k=5	0.024	2.35	6.800
w/g=1, k=3	0.33	4.95	64.200
w/g=1, k=4	0.115	3.58	24.800
w/g=1, k=5	0.041	2.58	8.700
w/g=1.5, k=3	0.4	5.09	67.700
w/g=1.5, k=4	0.142	3.71	27.900
w/g=1.5, k=5	0.051	2.71	10.400

Table 3.1 External sides, microstrip widths and quality factors of Hilbert resonators on MgO with k=3,4 and 5 at frequency close to 2GHz

From this preliminary analysis, the Hilbert resonator with k=4 and w/s=1 (fig.3.12a,b) appeared to be the best candidate to assure a good trade-off between miniaturization level and Q_0 factor. In this case, the strip width w is 115 microns and the external dimension S is only 3.58mm ($0.056\lambda_g$).

The k=4 resonator was realized on a $10x10mm^2$ double sided 700nm YBCO thin film on MgO. The resonator was tested at T=77K in a liquid nitrogen bath and the loaded resonant frequency was 1.84GHz, 80MHz lower than the expected value from simulations (fig.3.12c). This discrepancy between measured and simulated centre frequency was mainly due to an over-etching of the resonator during the photolithographic process. Consequently, the microstrip width resulted to be about 80 microns and this explains clearly the reduction of the resonance frequency, since the coupling among the different

turns of the resonators decreases and its equivalent length increases. Despite this occurrence, a Q_0 of about 27000 was measured. This value is in a very good agreement with the value predicted by Momentum software and is very similar to those reported in very recent papers for other compact resonators.

Finally, in order to complete our study about the characteristics of the k=4 Hilbert resonator, its properties have been compared with those of its meander line counterpart (fig.3.13a), since the meander line achieves the same length for the same strip width, gap and external side.

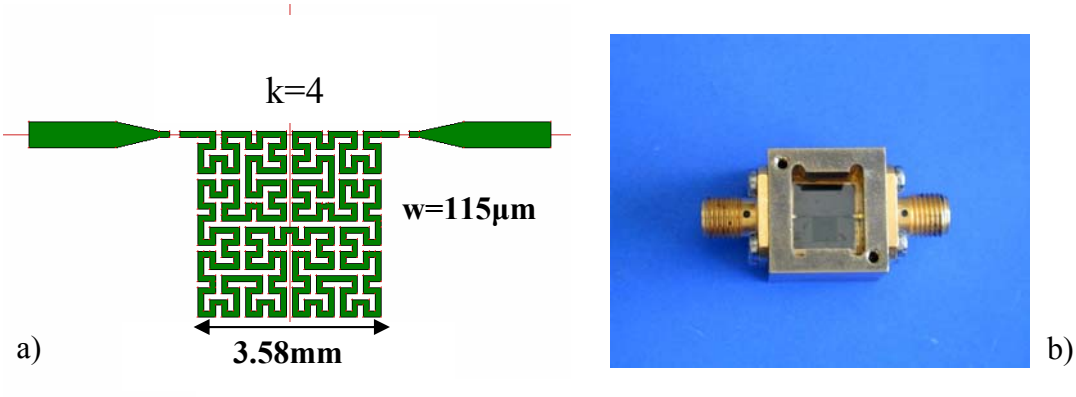

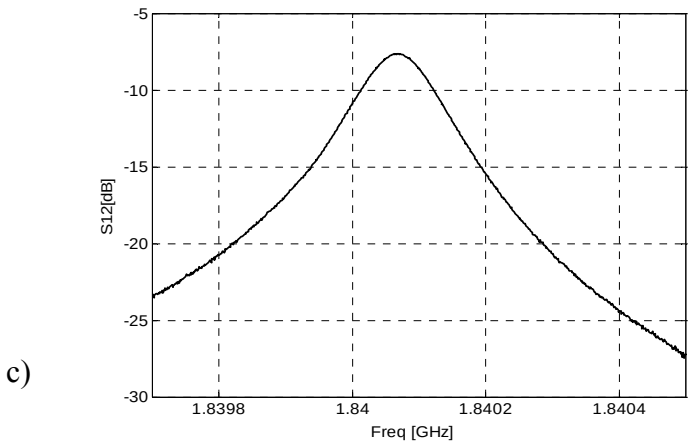

c)

Fig.3.12 a) Layout and b) photo of the fabricated Hilbert resonator with k=4, c) measured loaded f_0 at T=77K

The simulations reveal that the meander line has the same quality factor and resonates at almost 30MHz higher than Hilbert, which confirms the results contained in [63] and obtained by comparing Hilbert and meander antennas. This result can be explained considering that in a meander resonator the coupling among the turns is higher due its longer confronted length.

Consequently, the equivalent reduction of the path current is slightly stronger than that produced in the Hilbert device.

The higher coupling between the turns of a meander resonator makes also its electromagnetic behavior more dependent on the variations of physical parameters, like the substrate thickness h. Fig.3.13b shows the shift on the resonant frequency for these resonators as a function of the h changes. For a change of h around ±5%, the frequency shift of the Hilbert resonator is ±1% while for the meander is ±1.5%. For comparison, in this plot the same frequency shift is also reported for the basic $\lambda_g/2$ resonator and Koch-Minkowski resonator with k=3 (f_0 close to 2GHz). In this case, the shift results to be respectively ±0.18% and ±0.8%. This plot suggests how, in general, the miniaturization process can also make more critical the resonator behavior.

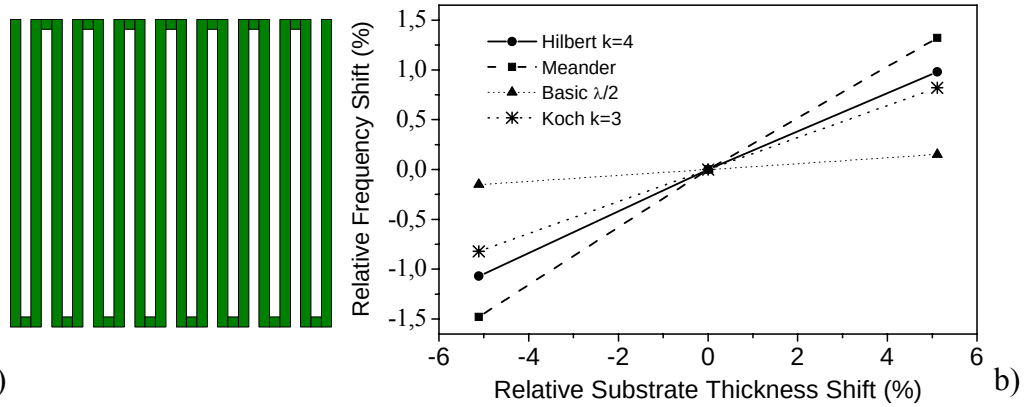

a) b)

Fig.3.13 a) Meander resonator and b) Comparison between the relative resonance frequency shift as a function of h changes for Hilbert resonator with k=4 (continuous curve with circle symbols), the counterpart meander (dashed curve with square symbols), the Koch-Minkowski resonator with k=3 (dotted curve with star symbols) and the basic $\lambda_g/2$ resonator

3.3.1 Quasi elliptic filters based on Hilbert layout

As stated above, quasi elliptic filters need out of phase couplings between not adjacent resonators which can be achieved by the combination of electric and

magnetic couplings. To this regard, as shown in fig.3.14a, the basic Hilbert resonator has been provided with a capacitive load, where the electric field has a maximum, by lengthening and coupling the ends of the resonator. At f_0=1.95GHz, the dimensions of this resonator are [3.38x3.74]mm^2 on MgO, while the microstrip width is 110μm.

Based on this first rearrangement and following the classic procedure described in [1], several four pole quasi elliptic filters have been designed with the conventional cascaded-quadruplet topology.

a) 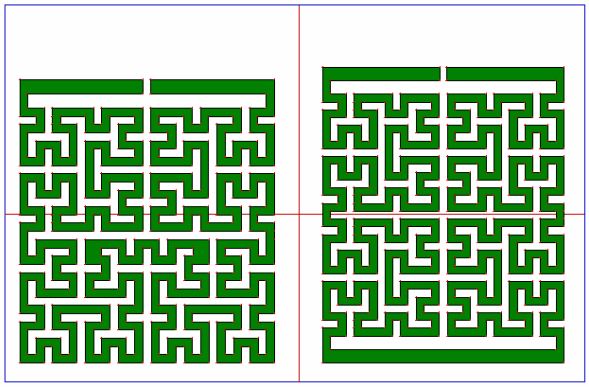 b)

Fig.3.14 a) Hilbert resonator with capacitive load b) Hilbert resonator arrangement with accessible centre point

Also in this case, the feed lines can be coupled to the first and last resonators by a capacitive gap or by a direct connection (tapped line configuration). According to our analysis, the capacitive gap allows Q_{ext} larger than 200, suitable for fractional bandwidth filters lower than 0.5%. Instead, tapped feed lines allow Q_{ext} lower than 20 (BW larger than 3%). Therefore, by the structure of fig.3.14a, it is not possible to reach the intermediate values of Q_{ext} and this is substantially due to the not accessibility of the centre point. This last limitation has been simply overcome by rearranging the Hilbert resonator as depicted in fig.3.14b. Here, the orientation of two of the four component elements with k=3 has been changed, in order to provide a double axial symmetry which makes accessible the resonator midpoint. In this way, simply by shifting the tap point, Q_{ext} in the range between 40 and 200 can be obtained.

At f_0=1.95GHz, this new Hilbert resonator is 3.15mm wide and 3.9mm high, with a microstrip width of 105μm. Fig.3.15 shows the layout with the in-band and out-of-band responses, simulated by IE3D, of a four pole quasi elliptic filter with bandwidth of about 15MHz (0.77%). In this case Q_{ext} is 110. The overall dimensions are [10.2x7.5]mm^2 and are quite lower (a reduction of about 40% is achieved) than those of an equivalent filter based on Koch-Minkowski resonators.

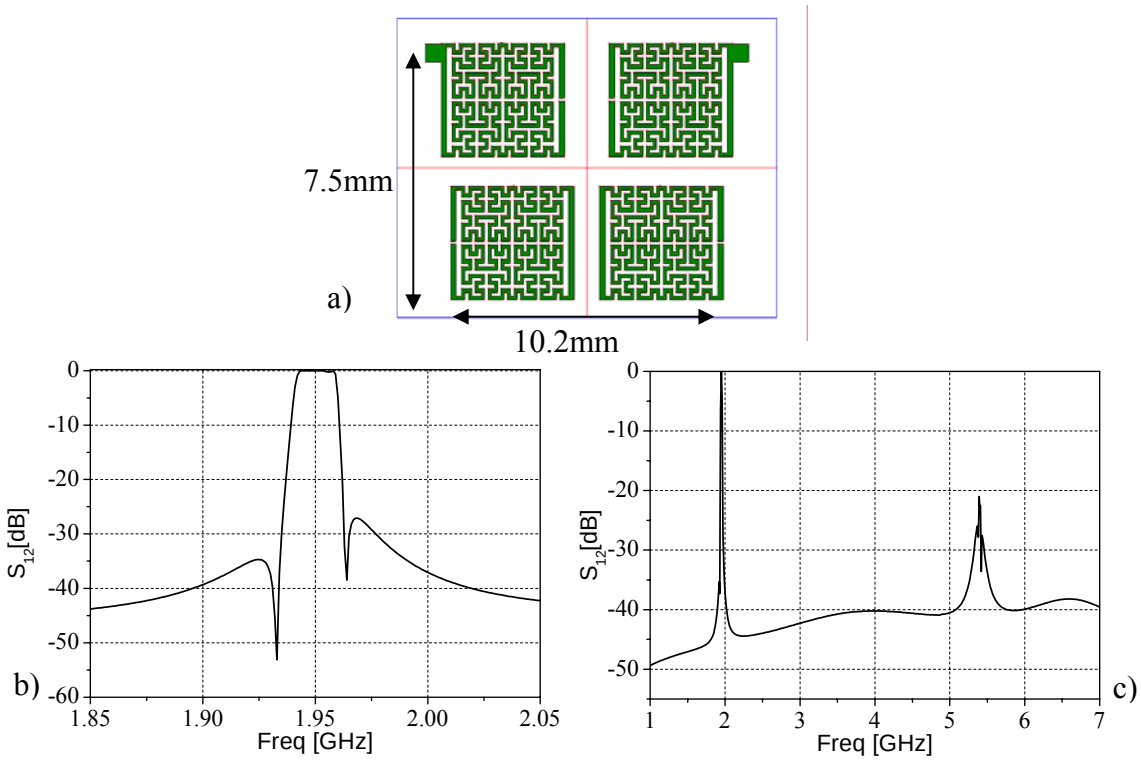

Fig.3.15 a) Quasi elliptic four pole filter based on Hilbert resonators b) In-band and c) out-of-band responses at f_0=1.95GHz

Considering the wideband response, it is significant to outline also in this case the absence of the second harmonic peak at $2f_0$. Similarly to what reported for the filter in fig.3.7, this is mainly due to the effect of the capacitive load (charges of the same sign at the ends of resonator at $2f_0$). Moreover, in this layout there is a further effect related to the magnetic field distribution. Indeed, while at f_0 the magnetic field has a maximum at resonator midpoint, at $2f_0$ it is minimum in the same region, thus resulting in a very poor coupling between the same resonators.

By using the same layout and moving simply one of the tap points symmetrically respect to the centre (fig.3.16a), a new filter response with the same bandwidth (same Q_{ext}) but with four zeroes near the pass-band, improving the selectivity performance, can be obtained (fig.3.16b). Indeed, in this new position, the relative shift between the feed line tap points produce a further double possible path for the signal, introducing a destructive interference and the consequent presence of other extra two zeroes [75].

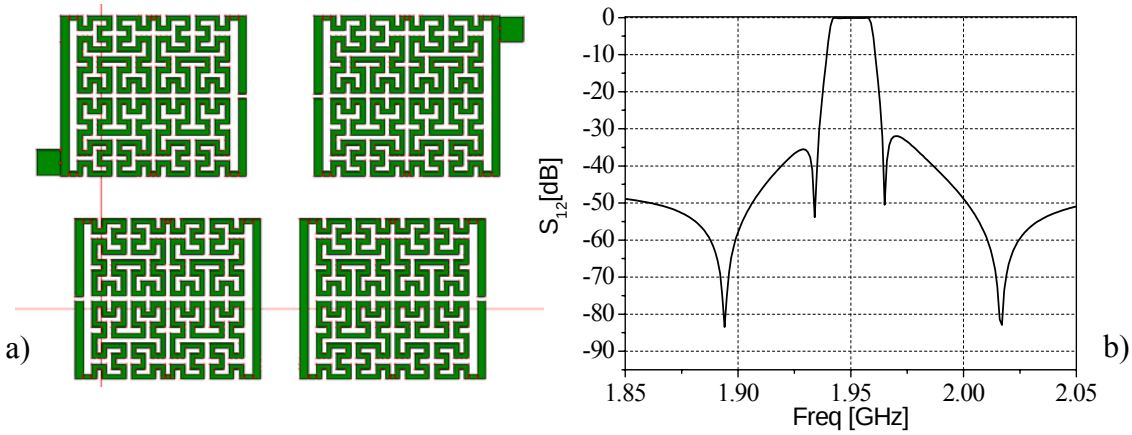

Fig.3.16 a) Layout and b) response of the four transmission zeroes Hilbert filter

Finally, by using the basic quadruplet configuration, a quasi elliptic filter with f_0=2.45GHz and BW=20MHz (0.8%) has been fabricated by using a commercial [10x10]mm^2 double sided YBCO 700nm thin film, grown on 0.508mm thick MgO substrate [74]. The basic resonator dimensions are [2.68x2.28]mm^2 with a microstrip width of 90μm. The overall dimensions of the filter are [7.9x6.2]mm^2. The filter has been tested in a liquid nitrogen bath at P_{in}=0dBm. In fig.3.17, the measured performances, obtained without the use of dielectric screws and compared with IE3D simulations, are reported.

A little discrepancy (not reported in fig.3.17, where the simulated response has been shifted) has been found between the simulated f_0=2.45GHz and the measured one (about 2.438GHz). A slightly difference between the real and simulations permittivity can partially justify this occurrence. In particular, in the permittivity range (9.6-9.7), the simulated centre frequency is shifted down of about 12MHz. Minimum insertion losses are about 0.2dB, but the in-band

response suffers a ripple distortion (maximum ripple 0.6 dB, minimum return loss in reflection 8dB) due to a little detuning condition.

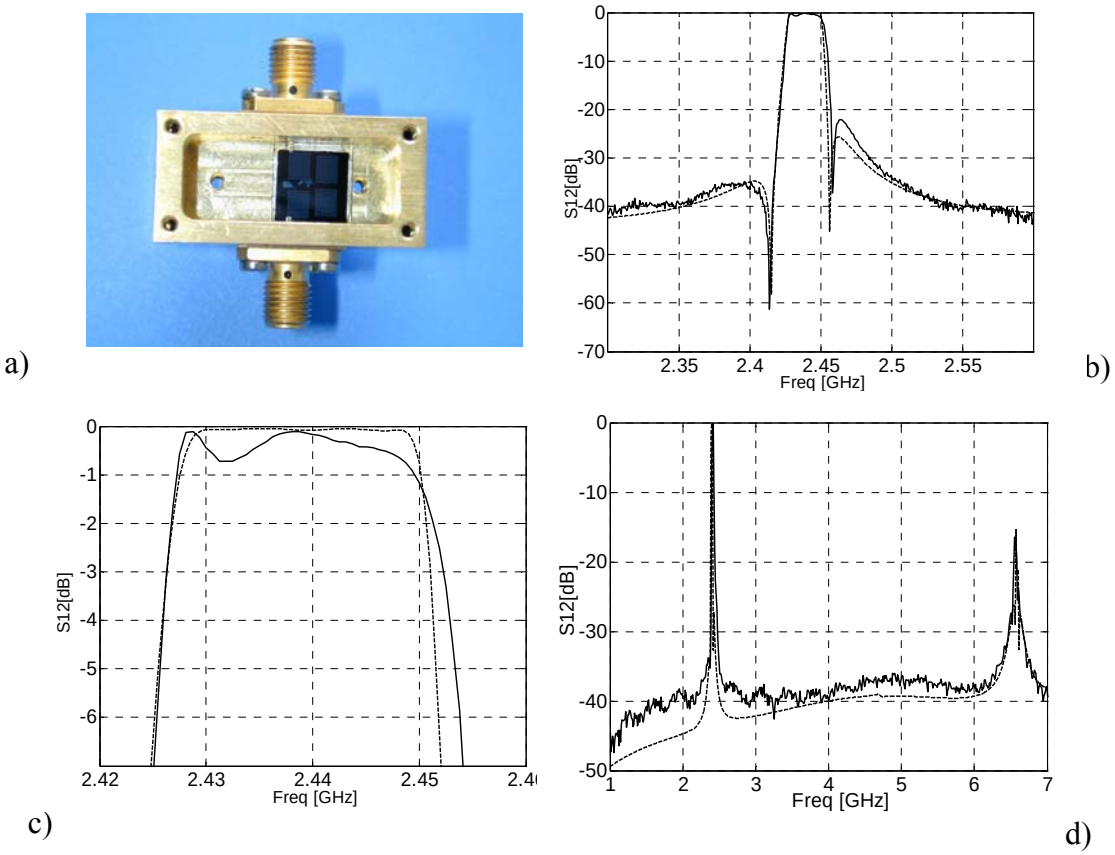

Fig.3.17 a) Quasi elliptic filter mounted in its metallic box b) Comparison between measured (continuous line) and simulated (dashed line) responses of the four pole quasi elliptical filter. (c) In-band and (d) out-of-band responses

By the use of an equivalent lumped circuit, a difference of about 3MHz between the central frequencies of the internal and external resonators has been estimated. The measured and simulated 3dB bandwidths (fig.3.17b) differ of about 1MHz and also this can be attributed to the detuning distortion which reduces the steepness at upper bound of the pass-band and degrades the symmetry of the response. This detuning distortion may come from many parasitic effects, such as unwanted coupling, deviation in the thickness substrate, tolerance in the fabrication process and so on. At last point, it worthwhile to observe the perfect agreement for the wideband responses which confirm the absence of the second harmonic peak.

3.3.2 Chebychev filters based on Hilbert layout

Similarly to the analysis realized for the quasi elliptic configurations, many four pole Chebychev filters in the frequency range of 2GHz have been investigated. The same considerations made in previous section, about the possibilities to utilize different feed line configurations for the desired bandwidths, can be repeated. As example, in fig.3.18, the layout and the simulated response of a four pole filter, with f_0=1.95GHz and BW=70MHz, is reported. The filter results 14mm wide and 3.6mm high. Also in this case, as for the Koch-Minkowski resonators, the fractal shape of the resonators and the choice to put them in the same orientation allow obtaining very low couplings even at short distances. In particular, in this filter the distances are only 0.05mm and 0.114mm. More in general, the couplings for a fixed distance are comparable with those realized by Koch-Minkowski resonators (see fig.3.6b).

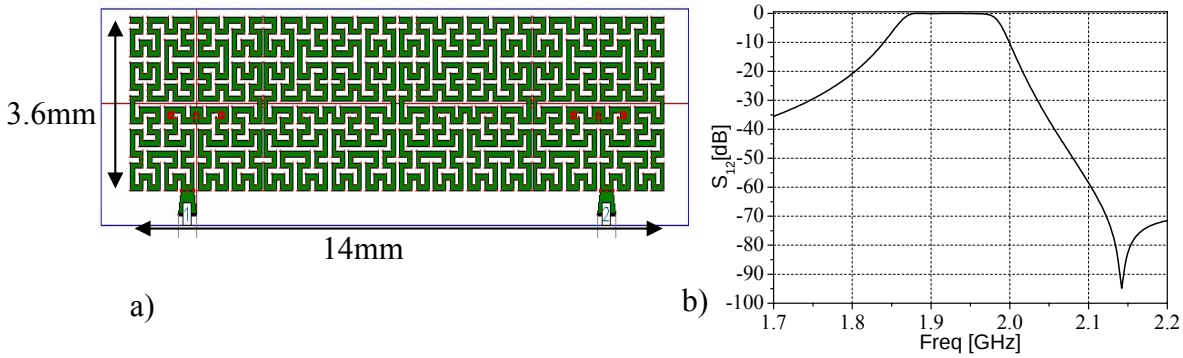

Fig.3.18 a) Layout and b) simulated response of a four pole Chebychev filter based on the original resonator

From this first example, it is evident that four pole Chebychev filters with 2 GHz central frequency would not fit in a [10x10]mm^2 thin film on a MgO substrate, by using any of the resonators presented so far. To this purpose, a new rearrangement of the basic Hilbert resonator has been proposed. In this case, we have changed the orientation and disposition of the component k=3 structures, rearranging them in a vertical sequence. At f_0=1.95GHz, the obtained resonator is 1.83mm wide and 7.91mm high, with a microstrip width

of 120μm. With this topology, a four pole filter with a bandwidth of 50MHz has been designed (fig.3.19), occupying an area of [8.2 x7.93]mm^2.

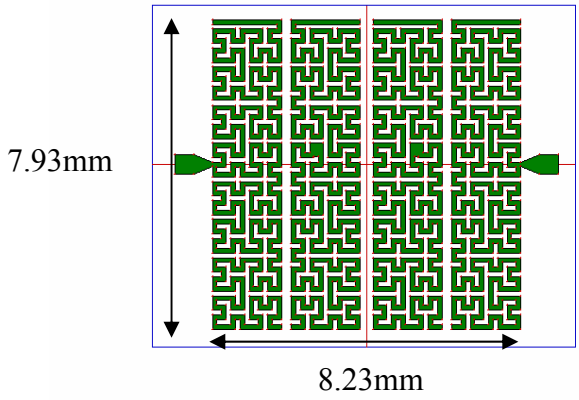

Fig.3.19 Chebychev four pole filter layout

As shown, every resonator is provided with a final straight termination. Its length allows extending the range of Q_{ext} obtainable by a tapped line, making the tap point to be closer or further to the resonating centre line. Note that also in this case, the distances are lower than 0.3mm. This filter was fabricated by a doubled sided YBCO 300nm thin film on MgO and tested at T=65K, in a closed cycle cryogenic system. The measured response and a comparison with the simulations are presented in fig.3.20.

The measured centre frequency f_0 results to be about 1.9GHz so that a discrepancy of about 50MHz is found between measurement and simulation (the frequency scale of the simulated data has been shifted to match the measurement). The measured 3dB bandwidth was also 10MHz lower than expected. Probably, factors as a not uniform value of the permittivity or the film thickness may have influenced strongly in the filter performance, since it occupied almost all the thin film area. Moreover, also in this case, the effect of the metallic box, whose dimensions are only [12x12]mm^2, have not been considered. Certainly, its reduced dimensions have also limited the out-of-band rejection value (about 40dB around f_0), with a behavior similar to that described in [24].

However, the in-band performances in terms of insertion losses (0.1dB as minimum value) and ripple (0.2 dB as maximum value) were very good, demonstrating again the good trade-off between quality factor and

miniaturization that this kind of resonator can offer. It is also noteworthy that, despite the reduced dimensions, the filter performances have been tested up to P_{in}=10dBm and no response distortion was observed.

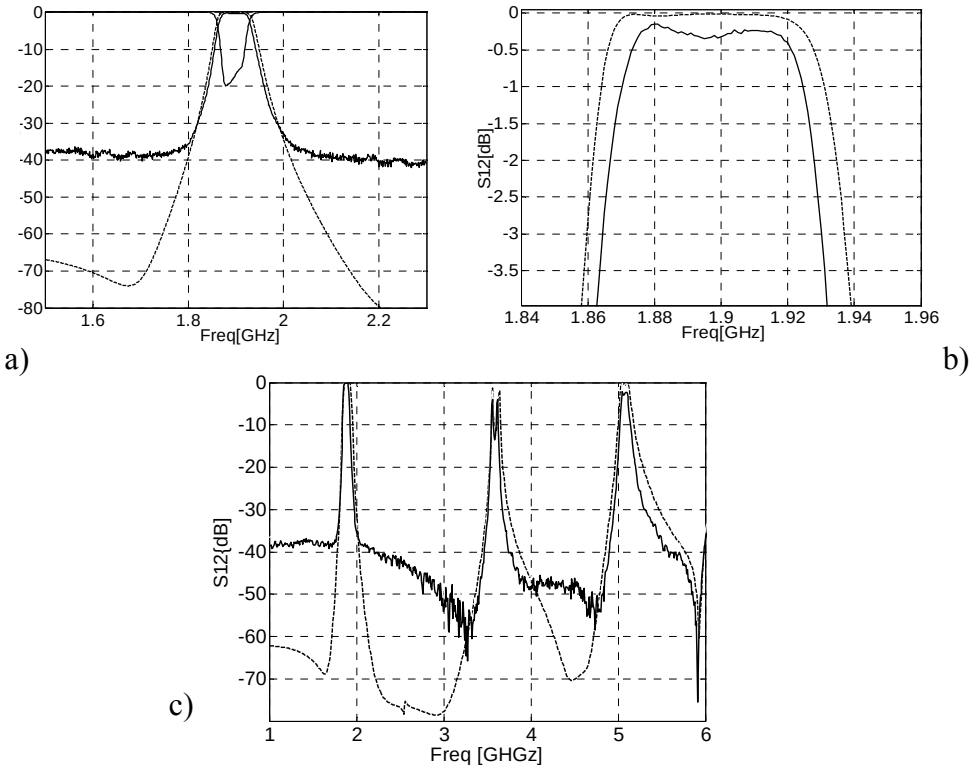

Fig.3.20 a) Measured (continuous line) and simulated response (dashed line) of a four pole Chebychev filter response at 65K. b) In-band and c) out of band responses

Finally, as evidenced in Fig. 3.20c, the wideband response from 1GHz to 7GHz presents a strong spurious response at each harmonic of the fundamental frequency. As done in the quasi-elliptic configuration, this can be explained from the electric and magnetic field distribution of the resonant modes. The magnetic and electric field maxima for the fundamental and second resonances are confronted between sequential resonators, so that the strength of the couplings does not change significantly from the first and second mode. This evidence suggests the possibility to design filters with multiple pass-bands, taking advantage of the geometrical properties of the fractal Hilbert curves.

CHAPTER 4

MINIATURIZED DUAL MODE FILTERS AND INTEGRATION WITH LNA AMPLIFIER

In the design of superconducting filters, dual mode resonators, owing to their geometrical symmetry, allow combining size compactness and relatively high power handling capability, since two modes, having a widely spread current distribution, are used in a single element [4,14]. The aim of this chapter is to describe the features of a novel dual mode resonator (cross slotted patch), miniaturized by the presence of surface cuts. Two and four pole HTS filters have been designed and tested in L and C band. Moreover, a new highly compact filter configuration based on the combination of stepped impedance resonators and cross slotted patches is presented. An L band 4 pole filter, based on this configuration, has been integrated with a LNA amplifier for satellite UMTS and here we report on the measured scattering parameters and noise figure.

4.1 Dual mode principle

Dual mode principle for 2D and 3D resonators is well known and has been the subject of extensive studies since the early 70s [76]. This principle is typical of all the resonators provided of geometrical symmetry that, for this reason, are able to give rise to degenerate modes with the same resonant frequency. When the symmetry is kept intact, the two modes are orthogonal and they can not exchange microwave power. On the contrary, when the geometrical symmetry

is opportunely broken, the resonator boundary conditions change allowing the coupling between the modes. Consequently, two modes can be contemporarily present at slightly split frequencies.

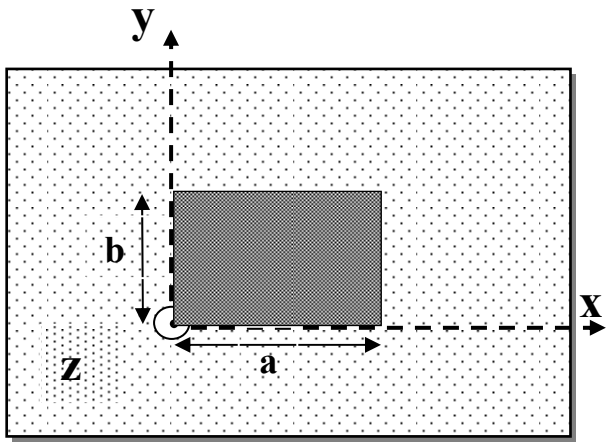

Fig.4.1 Top view of a generic rectangular patch

Considering for example the rectangular patch resonator (top view in fig.4.1), the application of the simple cavity model reveals that in this case the modes are transverse magnetic TM, with the magnetic field orthogonal to z axis. In particular, for the generic TM_{mn} mode, the magnetic field can be expressed by [8]:

$$\mathbf{H_{nm}} = \frac{1}{j\omega\mu}\left[\frac{m\pi}{b}\cos(\frac{n\pi}{a}x)\sin(\frac{m\pi}{b}y)\mathbf{i}_x - \frac{n\pi}{a}\cos(\frac{m\pi}{b}y)\sin(\frac{n\pi}{a}x)\mathbf{i}_y\right] \quad (4.1).$$

Analyzing the modes TM_{10} and TM_{01}, it is immediate to prove that in the former the magnetic field is directed only along the y axis, while in the latter it is directed along the x axis. Consequently, the surface current $J_S = \mathbf{i}_z \times \mathbf{H}_t$ is directed only along x in TM_{10}, while it is directed along y in TM_{01}. Furthermore, the resonant frequency of every mode is given by:

$$f_{nm} = \frac{c}{2\pi\sqrt{\varepsilon_r}}\left[(\frac{n\pi}{a})^2 + (\frac{m\pi}{b})^2\right]^{1/2} \quad (4.2),$$

where ε_r is the dielectric permittivity and c is the light speed in the empty. By (4.2), it results that:

$$f_{10} = \frac{c}{\sqrt{\varepsilon_r}} \frac{1}{2a} \text{ and } f_{01} = \frac{c}{\sqrt{\varepsilon_r}} \frac{1}{2b} \qquad (4.3).$$

Then, it is evident that for a square patch (a=b), TM_{10} and TM_{01} are degenerate modes, since they have the same resonant frequency and can separately and orthogonally (without power exchange) excited, as shown in fig.4.2. However, as stated above, the modes can be coupled by introducing an adequate geometry distortion, such that the changed boundary conditions can be satisfied by the contemporary presence of the two modes. The final surface current distribution is then a superimposition of the original orthogonal currents and this justifies, also intuitively, the classical placement at right angle of the feed lines.

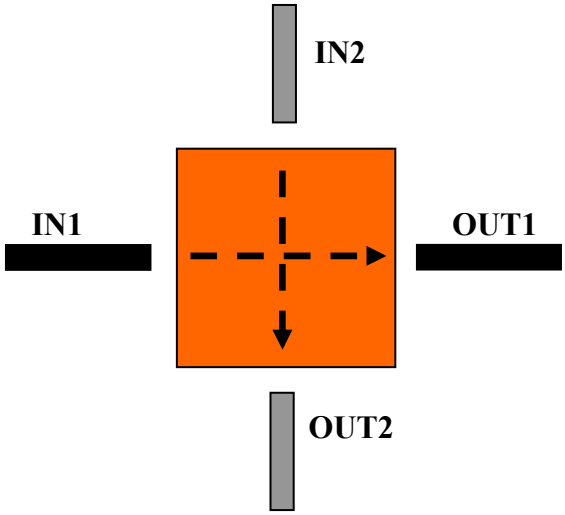

Fig.4.2 Current distribution of the orthogonal modes in the basic square patch

Fig.4.3 shows some dual mode resonators recently proposed for the fabrication of superconducting filters. Among these, probably the most common is the square patch resonator (fig.4.3a), where the orthogonal modes are coupled by cutting one of the corners ([14,77]. Another patch example is the elliptic disk proposed in fig.4.3b and considered as a distortion of the circular disk. The coupling strength between the modes is related to the introduced ellipticity [78]. On the contrary, dual mode resonators depicted in fig.4.3(c-e) are derived from the basic ring resonator and are miniaturized by a meandering technique [79,80,81]. Despite their reduced dimensions if compared with patch resonators, usually they are able to assure high Q_0 factor (about 30000 at 77K)

minimizing the housing losses that for a superconducting patch resonator can be quite relevant. Clearly, lower power handling can be managed.

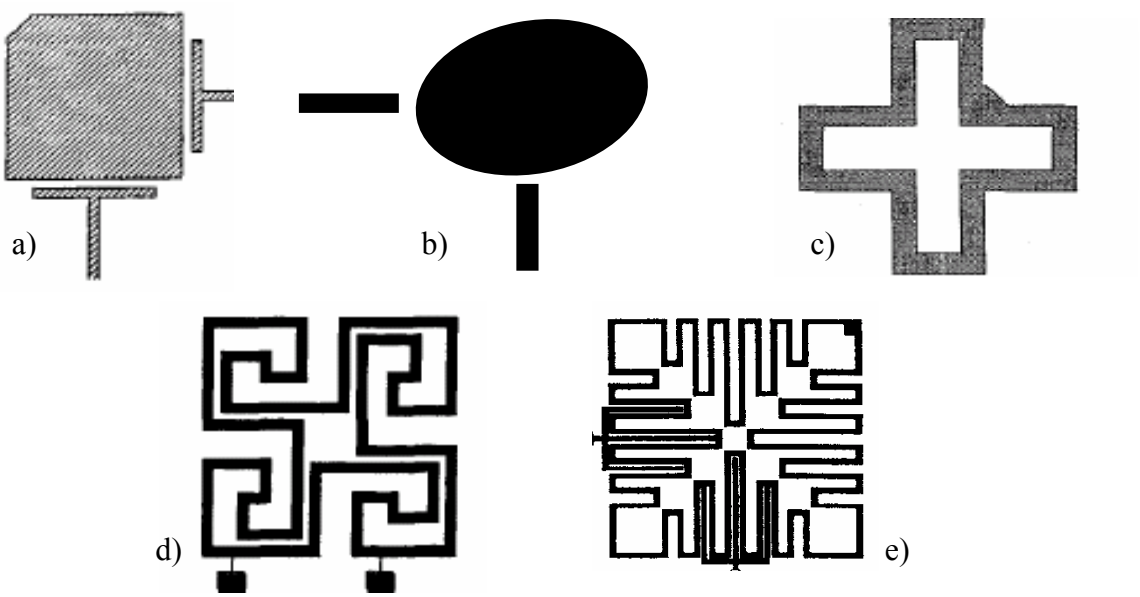

Fig.4.3 Superconducting Dual mode resonators recently proposed [77,78,79,80,81]

4.2 Cross slotted patch for miniaturized Dual Mode filters

In our work, a new superconducting dual mode resonator, able to offer a good trade-off between miniaturization, Q_0 factor and power handling, has been proposed. The basic structure, named cross type (fig.4.4a), was introduced and described in detail by Zhu et al. [82].

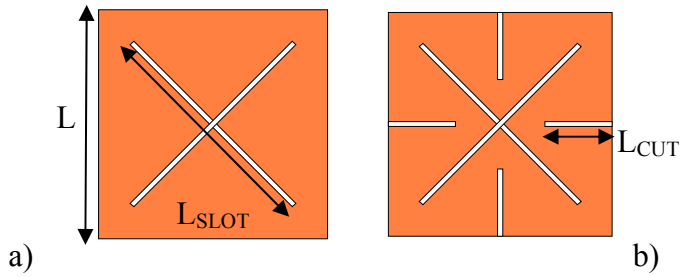

Fig.4.4 Cross and star type dual mode resonator

In this resonator, the presence of the diagonal cuts on the patch surface obliges the current to lengthen its path and this corresponds to a down-shift of the resonance frequency. Hence, this technique produces an equivalent increase of the resonator effective dimensions without changing the external side. Practically, the miniaturization is achieved by meandering the current and not all the resonator, in the attempt to preserve the power handling features of the patch resonator.

In terms of the equivalent lumped circuit, the deviation of the current lines produces an additional contribution to the shunt inductance, while the overall capacitance remains substantially unchanged. Indeed, the electrical field underneath the patch is almost unperturbed, while the magnetic field distribution is strongly changed. As a drawback, this last condition leads to a higher sensitivity of the resonant frequency to the thickness substrate tolerances if compared with a traditional square patch, whereas similar performances are found as far as the sensitivity to ε_r changes is concerned.

Fig.4.5a shows how the resonance frequency, obtained by the 2.5D simulator Ensemble from Ansoft Software, of a patch with external side L of 15mm on MgO can be reduced from 3.2GHz up to 2.05GHz (about 35% reduction), when L_{slot} goes from 0 to 15mm (100% of L). In our study, we have developed this structure introducing other transverse surface cuts (star type resonator in fig.4.4b). As shown in fig.4.5b, with $L=L_{slot}=15$mm, f_0 is reduced up to 1.54GHz when L_{cut} is 40% of L_{slot}.

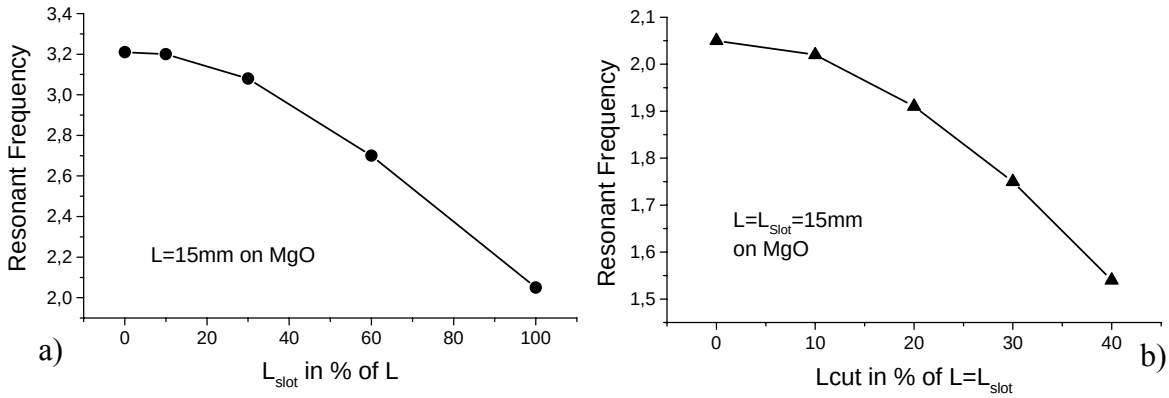

Fig.4.5 Resonance frequencies for cross and star type resonators

In conclusion, the original resonant frequency of the traditional square patch resonator with L=15mm is practically halved, corresponding to a miniaturization of the 50% of the external side, if the resonance frequency is fixed. For better appreciating the miniaturization capabilities of this technique, it can be useful to analyze the curves in fig.4.6. In this case, we have studied the resonance frequencies as a function of the external side L, for traditional square resonators and for cross resonators with $L=L_{slot}$. Both MgO and $LaAlO_3$ substrates have been considered. In particular, it is interesting to observe the superimposition of the performances of a traditional resonator on $LaAlO_3$ (up-triangle symbols) and those of a cross resonator on MgO (circle symbols). Practically, in a material perspective, the miniaturization achieved by the realization of the surface cuts can be considered equivalent to an increase of the substrate dielectric permittivity from 9.6 to about 24.

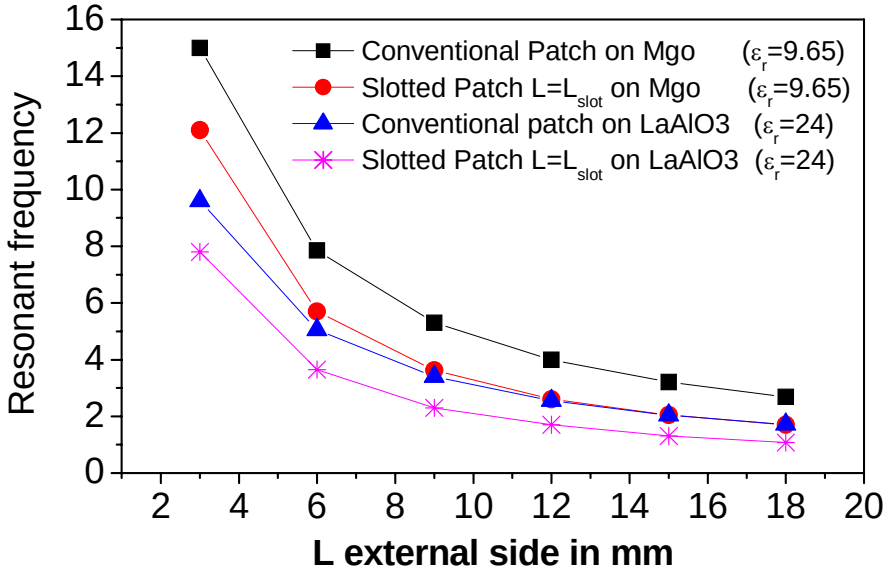

Fig.4.6 Resonance frequencies as a function of the external side L, for traditional square resonators (square symbols on MgO and up-triangle symbols on $LaAlO_3$) and for cross resonators with $L=L_{slot}$ (circle symbols on MgO and diamond symbols on $LaAlO_3$)

For all L values able to cover the frequency range from 1 to 10GHz, the possible miniaturization levels of the cross type resonators with respect to the

traditional patch are always in the range of 25-35%, increasing up to 35-50% when the transversal cuts are added (star type resonators). As further reference point, if a resonant frequency close 2GHz is desired, for a traditional patch L is about 25mm on MgO and 16mm on $LaAlO_3$, while for a star patch with $L=L_{slot}=3L_{cut}$, L is 13.5mm on MgO and 9mm on $LaAlO_3$. It is not difficult to show that these resonators present better compactness if compared with the quasi dual mode resonators introduced in [52], for satellite applications and depicted in fig.2.21a.

Similarly to what above discussed for the meandered ring resonators, in the original work by Zhu, it was also stressed the capability of this novel resonator to strongly reduce the radiation losses and the related housing losses, thus improving the overall unloaded quality factor. From the antenna theory, it is well known that the radiation efficiency η of a structure is directly related to the ratio $\frac{A}{\lambda^2}$, between its area and the square of the wavelength at resonance frequency. It is clear that the f_0 dropping without changing the area surface A, produces for these resonators a lowering of $\frac{A}{\lambda^2}$ with a direct consequence on η. More intuitively, fig.4.7 represents schematically the main current profile on the cross resonator. As shown, the current flow is split in an upward and a downward orientation which substantially give a very low contribution to the radiated field.

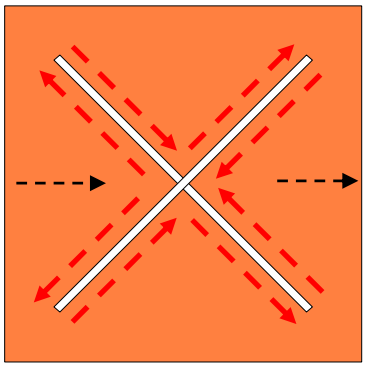

Fig.4.7 Schematic current profile over the single mode cross type resonator

To confirm this feature, in fig.4.8 we report the transmission response of a cross resonator with L=6mm on $LaAlO_3$ as a function of the length of L_{slot}. In this case, the feed lines are provided of a large stub and the coupling with the resonator is achieved by a capacitive gap D. Increasing L_{slot} and keeping fixed D, it is possible to observe, besides the down shift of the resonant frequency, also an increasing of more than 3dB of transmission peak maximum amplitude. A similar trend can be obtained if we consider the star type resonator with increasing L_{cut} for patches with fixed L and L_{slot} [83].

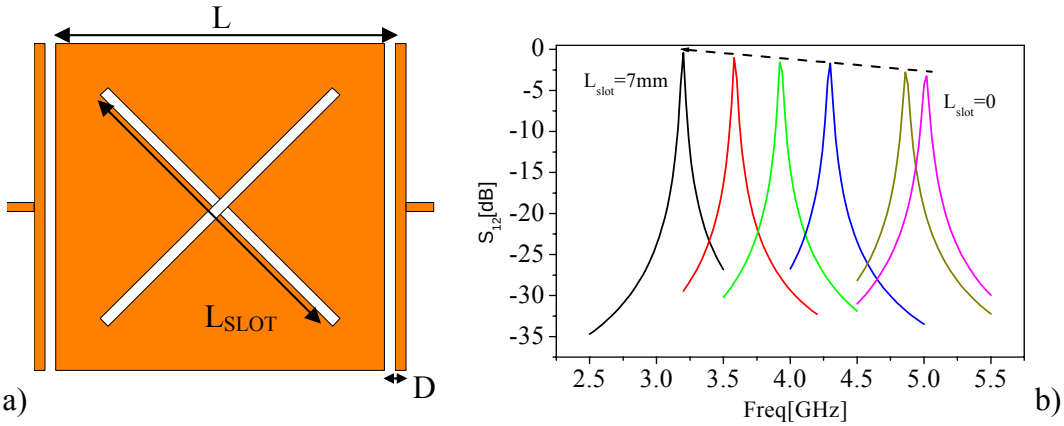

Fig.4.8 a) Cross patch coupled to the feed lines by a capacitive gap D b) Transmission peak amplitude of a cross patch with L=6mm, D=100μm as a function of L_{slot}

4.2.1 Single Stage Dual Mode filters design

In new miniaturized dual mode resonators (cross and star type), the coupling between the degenerate modes is obtained by using an adequate difference ($\Delta L=L_2-L_1$) between the two diagonals (fig.4.9a). To this regard, in fig.4.9b, for a cross patch with $([L_2+L_1]/2)=L=6mm$ on $LaAlO_3$, $|S_{12}|$ is reported for different values of ΔL. As shown, increasing ΔL from 0 to 0.1 mm, $|S_{12}|$ first moves rapidly upward toward the ideal 0dB and then it splits in two visible peaks. It is worthwhile to observe that ideally there would be no coupling between the two modes with ΔL=0, but the simulation shows that in this case

$|S_{12}|$ is however about -30dB. This phenomenon testifies the presence of some intrinsic mechanism of coupling between the modes and can be ascribed to the 90° arrangement of the feed lines. As it will be discussed in detail later, this same feature can explain the occurrence of two transmission zeroes which are not predicted by the Chebychev model.

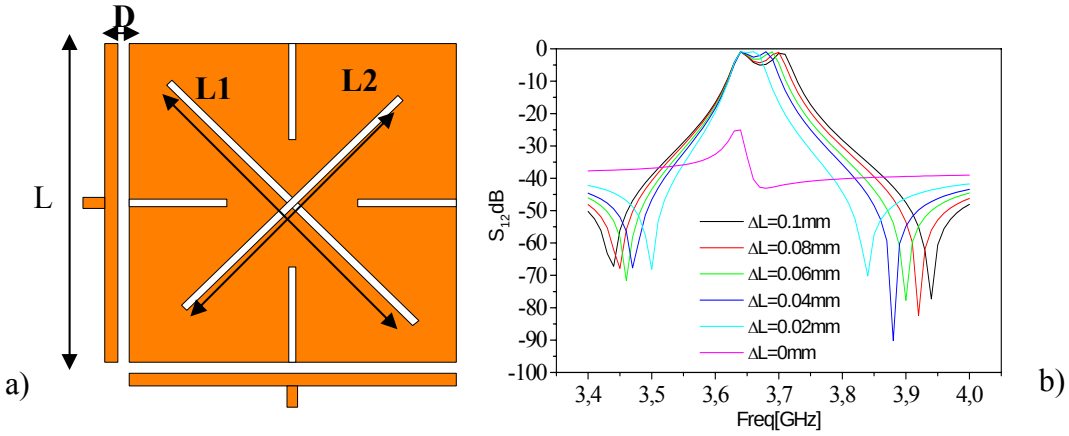

Fig.4.9 a) Dual mode filter based on the star type resonator b) Simulated $|S_{21}|$ of a cross type filter on $LaAlO_3$ as a function of ΔL

A typical plot of the degenerate modes coupling as a function of ΔL is reported in fig.4.10a, for a star type resonator with $L=L_{slot}=6mm$ and $L_{cut}=1.7mm$. In all the analyzed cases, the k_{12} dependence on ΔL results to be approximately linear, for all the range of interest for practical filters (bandwidths between 1% and 10%) [84].

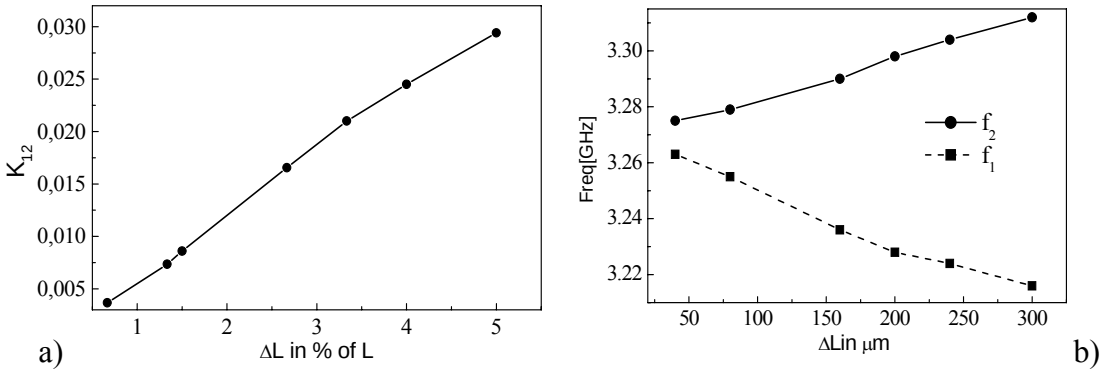

Fig.4.10 a) Coupling coefficient k_{12} as function of ΔL for a star type resonator ($L=L_{slot}=6mm$ and $L_{cut}=1.7mm$) b) Split frequencies f_1 and f_2 of the orthogonal modes

It should be pointed out that, in order to refer all the couplings to the same centre frequency f_0, it is necessary that both slots are symmetrically changed. In this way, the variation of the orthogonal modes frequencies f_1 and f_2 are symmetrical with respect to the center frequency f_0 (fig.4.10b). As far as Q_{ext} is concerned, both tapped and capacitive configurations can be considered. In particular, in the latter, rectangular stubs are added to the 50Ohm feed lines and the coupling is achieved by fixing the gap D between the stubs and the resonators. A typical Q_{ext} plot is shown in fig.4.11 with D ranging from 0.1 to 0.5mm. In this way, bandwidths lower than 2% can be achieved, while for larger values it is necessary to consider tapped line configurations opportunely rearranged.

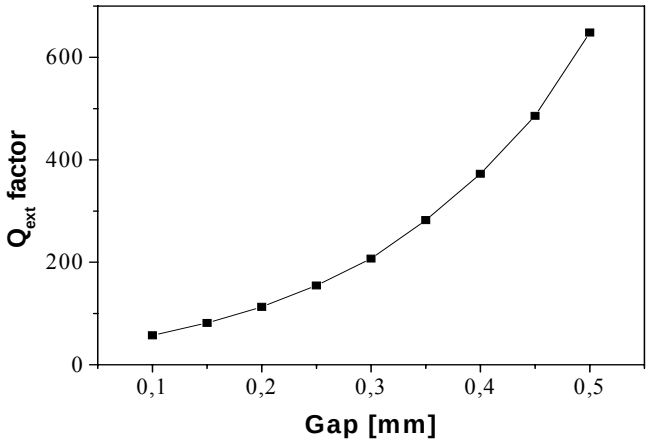

Fig.4.11 Q_{ext} as a function of the capacitive gap for the star type resonator

To assess the above introduced design principles, three two pole filters with $L=L_{slot}=6$mm have been fabricated using double sided $YBa_2Cu_3O_{7-\delta}$ (YBCO) 360nm thick films, deposited on (10x10x0.5)mm^3 $LaAlO_3$ substrates (fig.4.12). For these films, typical values of inductively measured critical temperature and current density are T_C=91K and $J_C \geq 1 \times 10^6$ A/cm^2 respectively. The features of these filters are summarized below:

1- a cross type filter with tapped feed lines (f_0=3.85GHz and BW≈10%)
2- a cross type filter with capacitively coupled feed lines, D=0.1mm (f_0=3.78GHz and BW≈1%)

3- a star type filter with capacitively coupled feed lines, D=0.1mm and L_{cut}=1.7mm (f_0=3.34GHz and BW≈1%)

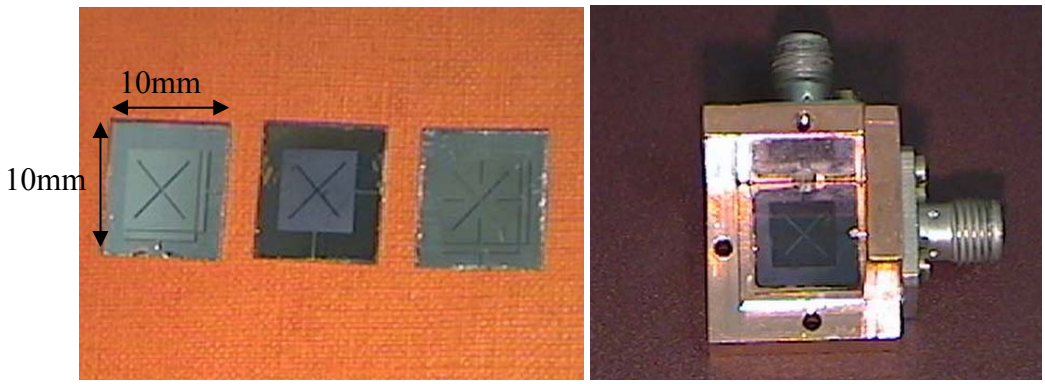

Fig.4.12 Fabricated HTS two pole filters based on cross and star type resonators

To investigate experimentally the performances of the new resonators, independently from the HTS film quality, some two pole filters have been also fabricated using Niobium 1000nm thick films and tested in liquid helium (T=4.2K). The experimental responses of the Niobium filters with capacitively coupled feed lines are reported in fig.4.13.

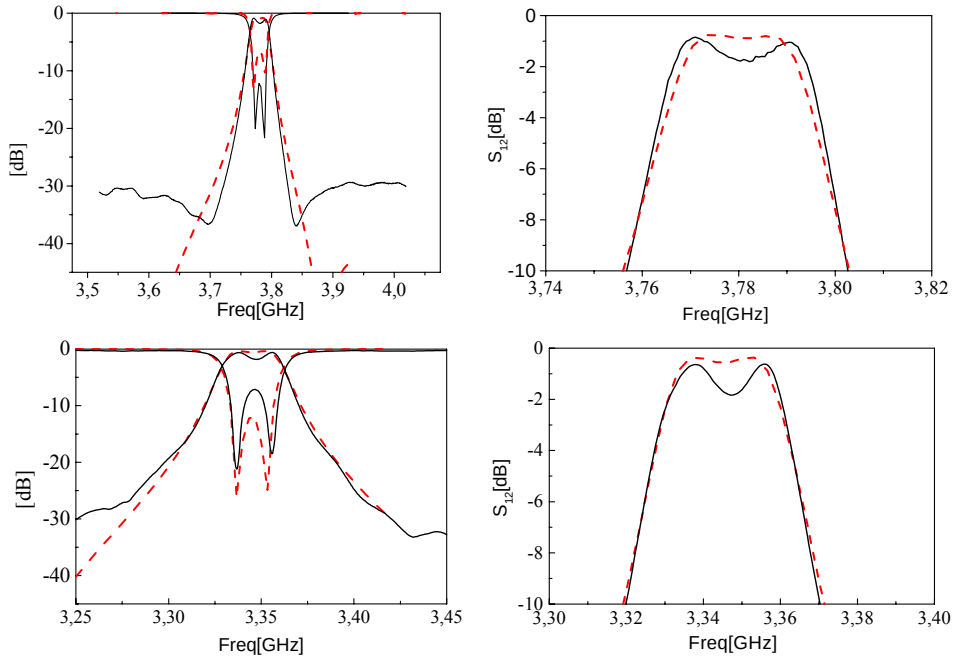

Fig.4.13 Experimental scattering parameters at T=4.2K (continuous curve) and simulated response (dashed curve) for the cross type filter-2 (Upper side) and for star type filter-3 (Lower side)

Here, the centre frequencies of the simulated responses have been up shifted in order to match the experimental measurements. This condition is firstly due to the real value of the $LaAlO_3$ permittivity which resulted lower than the value (24) used in the simulations. As shown, the measured responses present an enhanced pass-band ripple, (0.7–1)dB, whereas the bandwidths and the insertion losses (0.7 and 0.5dB for the cross and the star type, respectively) are in good agreement with the simulations. The measured insertion losses confirm also that the introduction of the transverse cuts in the star type resonators tend to improve the unloaded quality factor. The corresponding YBCO filters measured at 77K show higher insertion losses with minimum values of 1.1dB and 0.7dB. It is worth to mention that similar values of insertion losses have been measured with Niobium filters at the same reduced temperature (T=7.5K), proving that the YBCO filter response is limited neither by the film thickness, which is only twice the penetration depth, nor by the value of the surface resistance, which is larger than Niobium at the same reduced temperature.

Power handling capabilities of the fabricated two pole filters have also been tested. To this regard, fig 4.14 shows the responses as a function of the input power (P_{in}) for the Niobium and YBCO cross type filters.

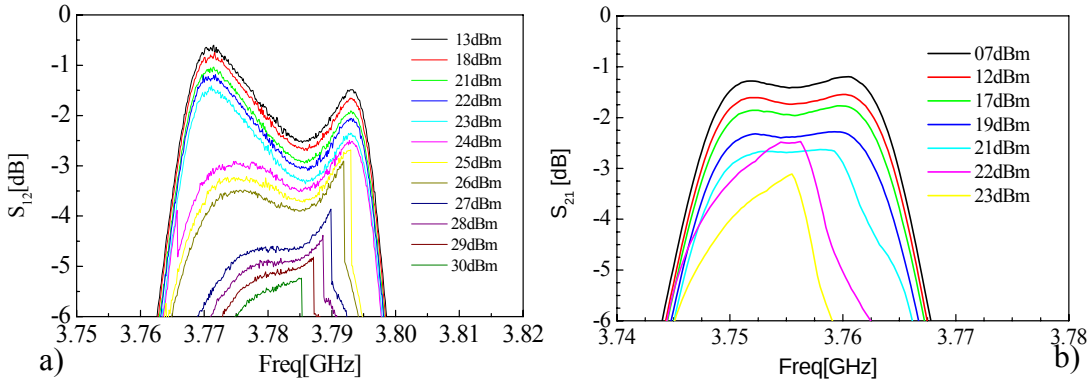

Fig.4.14 Measured $|S_{12}|$ responses of (a) Niobium and (b) YBCO cross type filters as a function of the input power

The final results are summarized in fig.4.15, where the minimum insertion losses are plotted as a function of P_{in}. For both Niobium filters (square and circle symbols for cross and star type filters, respectively), a fair field dependence up to 20dBm is observed, followed by a rapid increase of the in-

band insertion losses due to the strong distortion of the filter response, likely related to thermo-magnetic breakdown. In the same figure, IL vs P_{in} is shown for the HTS star type filter, at T=4.2K and T=77K (triangle and diamond symbols, respectively). In this case, the response degradation starts at lower input power (P_{in} ≥12dBm), but with smoother power dependence. Above 20dBm, a strong S_{12} distortion is clearly evidenced. The difference observed in the IL power behavior can be explained invoking the quite different microwave dependence of R_S values of Niobium and YBCO films.

Nonlinearity in the device response has also been investigated performing at T=77K intermodulation products (IMP) measurements on the star type YBCO filter. The standard two tone method is employed to examine intermodulation distortion characteristics [85], having the two tones set equal to amplitudes and with frequencies f_1=3357.5MHz and f_1=3362.5MHz.

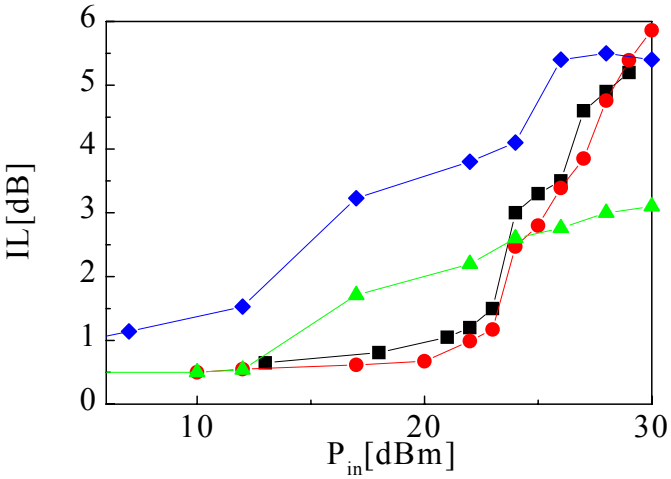

Fig.4.15 Insertion loss (IL) measured as a function of input power P_{in} for cross type Niobium filter at T=4.2K (Squares), star type Niobium filter at T=4.2K (Circles), star type YBCO filter at T=4.2K (Triangles), star type YBCO filter at T=77K (Diamonds)

The fundamental tones and IMP amplitudes as a function of the input power are reported in fig 4.16. IMP start to appear above the noise floor (-120dBm) at about P_{in}=-20dBm, and then show a quadratic dependence on the input power. For comparison, the IMP curve measured on the corresponding Niobium filter at T=4.2K is also displayed as a continuous curve in the same figure.

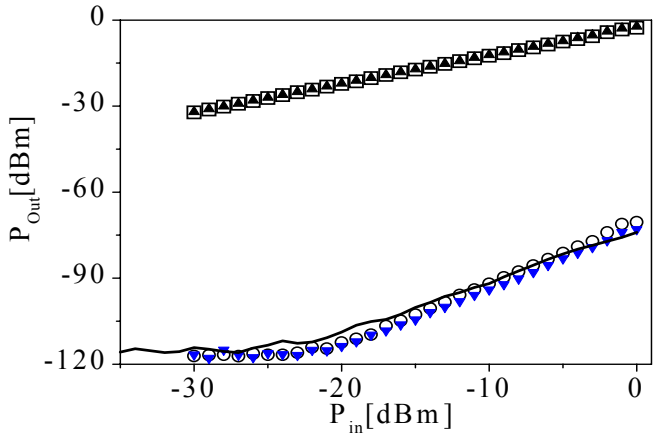

Fig.4.16 Fundamental tones (up-triangles and squares) and IMP output power (down triangles and circles) as a function of the input power for the YBCO star type filter at T=77K. The continuous line represents the IMP slope for the corresponding Niobium filter measured at T=4.2K

The close similarity of the slopes proves that in this case nonlinearity in the device response is independent on the superconducting film quality. This is not at odds with the results previously shown in fig.4.15, since the dominating source of non linearity in a superconducting device at low fields is the circuit inductance, which is related to the penetration depth. More precisely, due to the peaking of current distribution near the edges, it is mainly a small volume of material within a penetration depth that determine the insurgence and the initial increase of the intermodulation response. The observed quadratic regime is essentially what is expected, if one assumes that the inductance L of the superconducting device increases as the magnitude of the input current I circulating inside the resonator: $L=L_0+\alpha|I|$[86]. Indeed, nonlinearity of this form may be well explained by extrinsic factors, such as weak links, which are surely present at edges of both YBCO and Niobium planar structures, and may mask the difference in the filter response which shows up only at higher power. As far as the filter (1), Niobium and YBCO prototypes show very similar properties in terms of power handling, intermodulation product and insertion losses. The measured filter responses are reported in fig.4.17 and compared with simulations. In this case, a good agreement is found for both transmission

and reflection parameters, even if with a smaller than expected (10%) fractional bandwidth.

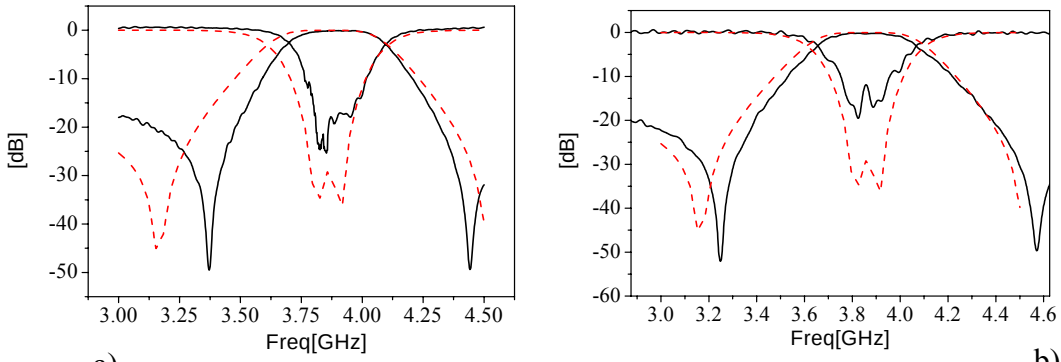

Fig.4.17 Comparison between simulated (dashed curves) and measured (continuous curves) response of a) Niobium and of b) YBCO cross type filter (1)

Insertion loss at $T/T_C=0.85$ is 0.17dB for the YBCO filter, decreasing at 0.09dB for $T/T_C \leq 0.5$. This is very similar to what measured for Niobium at 4.2K. Finally, no relevant effects of power degradation have been observed on the filter response up to $P_{in}=33$dBm, limited only by the experimental set-up. It is clear that in this case the better power handling of these filters is essentially due to the larger bandwidth [2].

4.2.2 Dual Stage Dual Mode filters design

In the realization of multi-pole filters based on dual mode resonators, it is necessary to couple the modes of different patches. In principle, this can be done simply by a capacitive gap which separates the two structures as sketched in fig.4.18, for a four pole filter based on the star type resonator. In this figure, we have also evidenced the presence of the four modes, by indicating the main direction of the corresponding current distributions. Intuitively, this solution assures the best possible miniaturization of the overall structure, but it is also

true that in this way, each mode of the first patch is also coupled to both modes of the other resonator.

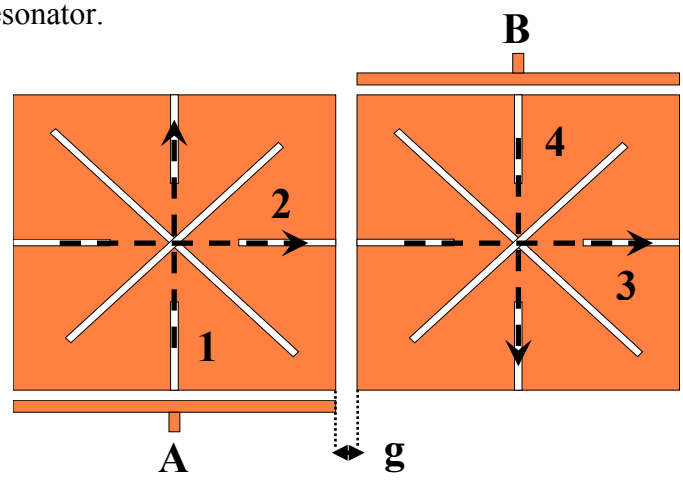

Fig.4.18 Possible layout of a four pole filter based on the star type resonator

Furthermore, the coupling strength is governed only by the gap g which results the only design parameter. In this condition, the control of the couplings is very complicated and for this reason, the coupling between the modes of different patches is usually obtained by external connections, at expense of higher dimensions of the final structure [87,80,81]. To this regard, we have considered the structure shown in fig.4.19, favoring the coupling between the mode 2 and 3 and reducing all the others which, at least in the Chebychev model, are undesired [88].

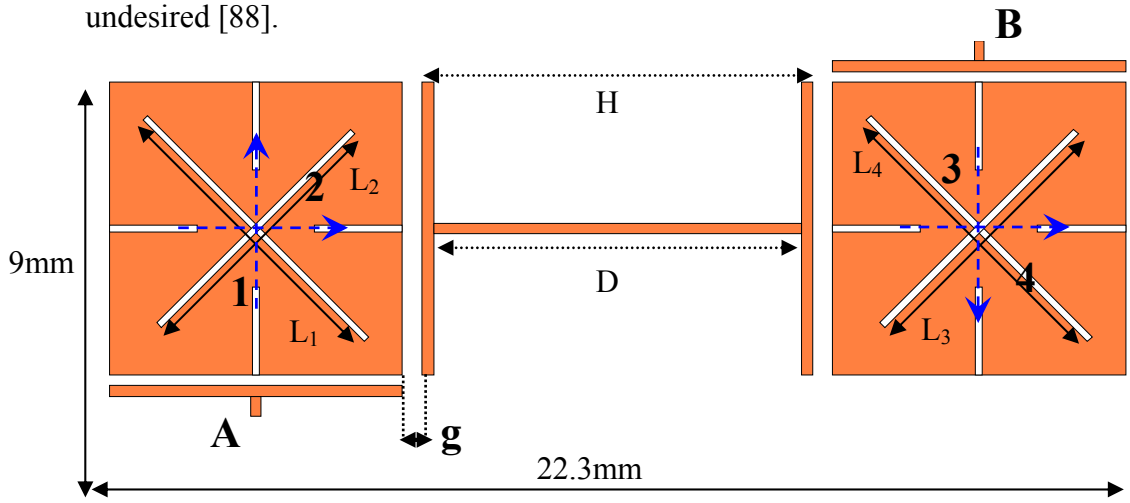

Fig.4.19 Dual mode dual stage (four pole) filter layout

In particular, the coupling k_{23} can be controlled either by the length *D* of the microstrip which connects the two stubs or by the capacitive gap g between the

patches and stubs. By using this layout, a 4 pole filter, with a center frequency of 3.25GHz and 1% fractional bandwidth, has been designed on $LaAlO_3$. The dimensions of the basic star type patches are unchanged with respect to the single stage filter above reported ($L=L_{slot}=3L_{cut}=6mm$). The coupling between the degenerate modes of the patches is achieved by $\Delta L=90\mu m$. In particular, L_1 and L_4 are $[L-(\Delta L/2)]$, while L_2 and L_3 are $[L+(\Delta L/2)]$. In our design, the gap g is kept fixed to 50μm, while the coupling k_{23} is studied as a function of the length D (fig.4.20a). As expected, the curve presents a periodical behavior directly related to the transmission properties of the connection microstrip. In our filter, D is fixed to 9mm and the overall dimensions are about $[22.3x10]mm^2$. In fig.4.20b, the simulated response (continuous curve), with a predicted IL of 0.4dB, is reported and compared with the ideal Chebychev response (dotted curve), evaluated by the lumped-element equivalent circuit.

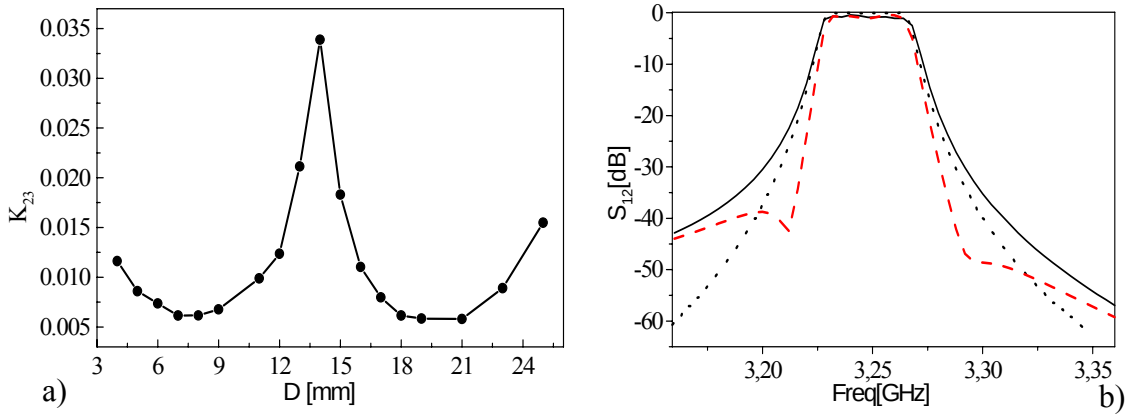

Fig.4.20 a) Coefficient coupling k_{23} as a function of D b) Simulated scattering parameters of the dual mode dual stage filter (continuous curve), compared with the alternative quasi elliptic response (dashed curve) and with the lumped equivalent circuit (dotted curve)

In this design, the large value of D makes k_{13}, k_{24} and k_{14} extra couplings very low. However, they are still present and can give rise to transmission zeroes which are not predicted by the Chebychev model. Indeed, a quasi elliptic response (dashed curve in fig.4.20b) has been obtained by inverting the length of the two slots in one of the two patches. Actually, this change modifies the phase of the residual extra coupling k_{14}, thus producing the presence of the

transmission zeroes. It is clear that this effect, undesired from a Chebychev point of view, can improve the filter performance in terms of selectivity. However, the presence of the transmission zeroes modifies slightly also the bandwidth of the initial design and this has to be carefully evaluated by the designers. The quasi elliptic version of this filter has been fabricated by using an YBCO double side commercial film. The response (solid curve) measured at 77K in liquid nitrogen, is reported in fig.4.21a and shows minimum insertion losses of about 0.9dB. Also in this case, a discrepancy of about 50MHz is found between the simulated and the measured f_0. As far as the bandwidth is concerned, the measurement is in good agreement with the simulation, while the ripple is higher than expected (about 1.5dB). The filter performances showed a certain dependence on the metallic box dimensions, with a special sensitivity to the height of the top side. Probably, this is due to the contribution that the metallic walls can give to the enhancement of the extra couplings with the consequent response distortion. Indeed, as shown in fig.4.21b, better performances of the filter have been obtained by using dielectric screws and by rearranging the overall dimensions of the metallic box. In particular, the minimum IL can be reduced to 0.7dB and the ripple to 0.9dB, whereas the center frequency is shifted downward of 20 MHz.

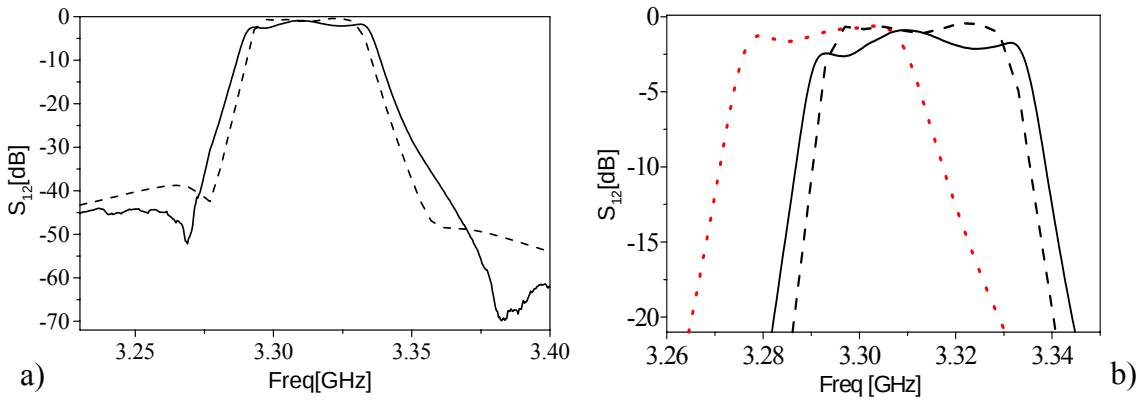

Fig.4.21 a) Comparison between measured (solid curve) and simulated response (dashed curve) of dual stage quasi elliptic filter b) An improved measured response (dotted curve) is reported

The wideband frequency response (1–5GHz) is plotted (solid curve) and compared with the simulation (dashed curve) in fig.4.22a. The out-of-band rejection is about 70dB, but undesired spurious modes are present at about 1.6GHz and 4.8GHz, with $|S_{12}|$ lower than 40dB. It is possible to demonstrate that these are simply the resonant frequencies of the central connecting structure, composed of the microstrip D and the two stubs.

In terms of both power degradation measurements and intermodulation products (IMP), the performances of the YBCO dual stage filter did not show appreciable differences compared with the single-stage version. Even in this case, the insertion losses become very critical (more than 2.5dB) close to 20dBm. In particular, fig.4.22b shows the IMP (scatter points) obtained with the standard two tone procedure. The data are compared with those obtained on the single-stage filter (solid and dashed curves, respectively), showing only a different noise floor.

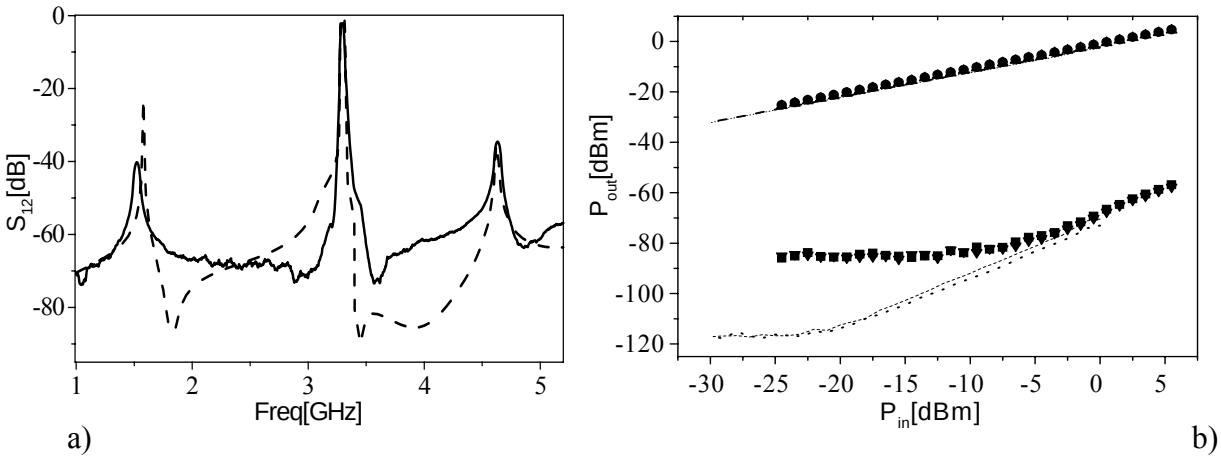

Fig.4.22 a) Comparison between measured at T=77K (continuous curve) and simulated (dashed curve) wideband transmission responses of dual mode dual stage filter b) Fundamental tones (up-triangles and square) and IMP products (down triangles and circles) at T=77K vs the input power. The continuous lines represent the measurement for the single stage filter.

4.3 Miniaturized Dual Mode filters based on mixed resonators

In our work, a further miniaturization improvement of the four pole filter has been obtained by combining the use of a star type dual mode resonator and two stepped impedance resonators. The layout of the new filter configuration is shown in fig.4.23 and represents clearly the direct development of the above analyzed filters [89].

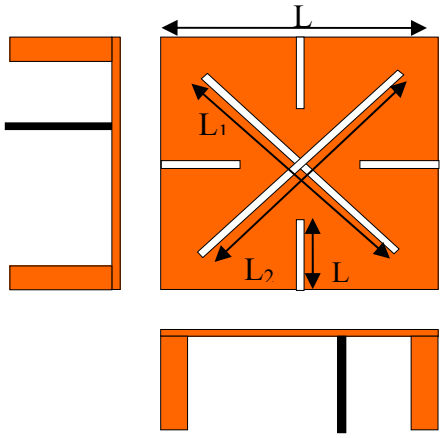

Fig.4.23 Four pole filter based on the combination of a dual mode star type resonator and two stepped impedance resonators

In particular, in comparison with the single stage filter, the dimensions of the feed line stubs have been rearranged in order to obtain two stepped impedance resonators with the same resonant frequency of the patch orthogonal modes. This topology is revealed to exhibit a very high degree of miniaturization, as it saves about the 50% of the area occupied by the dual mode dual stage configuration. In this case, the feed lines (black rectangular in fig.4.23) are simply 50Ohm lines tapped lines and, as discussed in the following, the necessary Q_{ext} is achieved by changing the distance between the tap point and the resonator midpoint. The proposed solution allows solving the problem to couple the modes of different patches and so all the difficulties related to the control of the couplings are attenuated. Furthermore, due to the presence of mixed resonators, the final filter response presents an improved out-of-band rejection, if compared with that of dual mode dual stage filter without the

presence of spurious modes. Even for this configuration, the peculiarities of the dual mode resonator have evidenced the possibility to realize quasi elliptic responses, without the necessity to introduce extra coupling structures. From this point of view, the new topology offers even a partial control of the transmission zeroes position, since different quasi elliptic responses with the same bandwidth can be obtained with the same layout, simply modifying the symmetry of feed line configuration.

According to the Chebychev model, which has been considered the starting point of our analysis, the related specifications (number of poles (N), centre frequency (f_0), bandwidth (BW) and maximum in-band ripple (r)) have been satisfied by the following steps:

a) fix the dimensions of each resonator in order to obtain the same resonance frequency
b) evaluate the required Q_{ext} as a function of the distance between the feed line tap point and the resonator mid point
c) evaluate the $k_{12}=k_{34}$ between the stepped and the patch resonator as a function of their distance and k_{23} between the two degenerate modes of the patch resonator, as a function of the difference ΔL between the lengths of the diagonal slots
d) for a desired response determine the geometrical parameters values in order to achieve the necessary Q_{ext} , $k_{12}=k_{34}$, k_{23}.

4.3.1 Stepped impedance resonators

In the proposed configuration, step (a) is certainly the crucial one, since resonators with different shapes are considered and the filter response can be strongly corrupted if the resonators do not exhibit the same resonant frequency f_0. Indeed, few MHz differences can produce significant in-band ripple distortions (some dB), which are unacceptable for the modern applications. To this regard, it is worth to mention that for a fixed mesh structure, commercial

simulators evaluate different resonators with different accuracy, resulting in an intrinsic limitation for the design. In order to overcome this problem, in our study the simulations have been carried out with the highest possible accuracy and the responses of different simulators have been compared. Fig.4.24 shows the typical layout of a stepped impedance resonator. It is a slight modification of the basic half wavelength resonator and its features have been extensively analyzed.

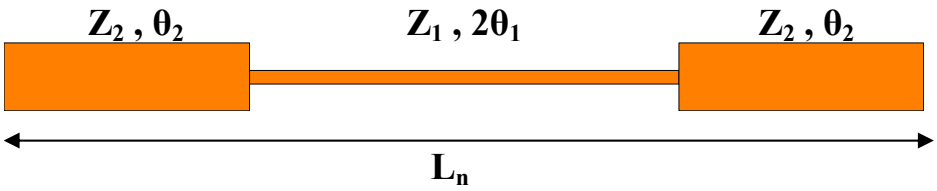

Fig.4.24 Stepped impedance resonator layout

By using the basic transmission line mode, it is easy to show that the resonance frequencies of the odd and even modes are respectively given by [75]:

$$\tan\theta_1 = \frac{Z_2}{Z_1}\cot\theta_2 \tag{4.1}$$

$$\text{and } \cot\theta_1 = -\frac{Z_2}{Z_1}\cot\theta_2 \tag{4.2}.$$

In particular, the fundamental resonance frequency f_0 is given by the lowest order solution of (4.1). At f_0, the resonator electric length $\theta_T = 2*(\theta_1 + \theta_2)$ results to be π ($L_n = \frac{\lambda_g}{2}$) if Z_2=Z_1 (uniform impedance resonator), but it is less than π if $Z_2 < Z_1$. This means that if L_n is kept fixed, the resonant frequency f_0 monotonically decreases if $\frac{Z_2}{Z_1}$ is reduced. This can be directly observed if we make the simplifying assumption that $\theta_1 = \theta_2$. Indeed, in this case, from (4.1) θ_T can be expressed by $\theta_T = 2arct\sqrt{\frac{Z_2}{Z_1}}$ and the miniaturization impact of the $\frac{Z_2}{Z_1}$ on θ_T is clear. Another important property of the stepped impedance resonators is that also the ratio between the higher mode resonance frequencies

and the fundamental one is a function of $\frac{Z_2}{Z_1}$. For example, considering the second harmonic f_1, it results that $\frac{f_1}{f_0}$ can be increased if $\frac{Z_2}{Z_1}$ is reduced and in particular if $\theta_1 = \theta_2$, we have $\frac{f_1}{f_0} = \frac{\pi}{2 * arct\sqrt{\frac{Z_2}{Z_1}}}$ [90]. Consequently, besides the miniaturization effect, the reduction of $\frac{Z_2}{Z_1}$ allows improving the out-of-band rejection of the stepped impedance resonators.

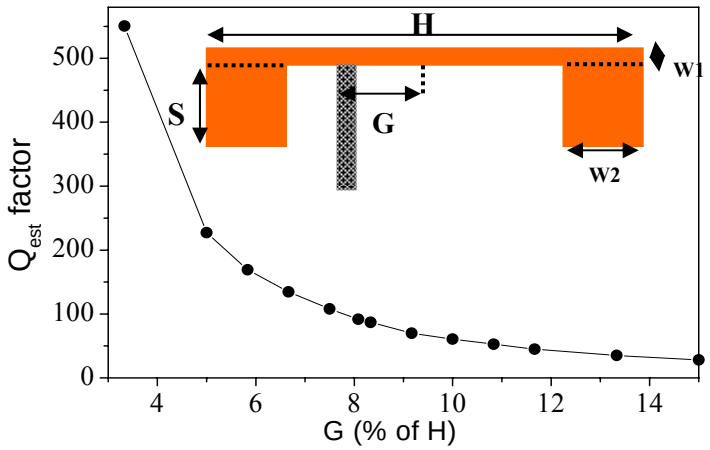

Fig.4.25 Q_{ext} factor as a function of the distance G between the tap point and the midpoint of the stepped resonator. G is expressed as a percentage of the patch side L. In the inset, the considered rearrangement of a stepped impedance resonator is shown

In our filter, according to the adopted rearrangement of the basic stepped impedance resonator shown in the inset in fig.4.25, we have that:

$$\theta_1 = \frac{2\pi}{\lambda}\left(\frac{H}{2} - \frac{w_2}{2}\right) \tag{4.3}$$

$$\text{and } \theta_2 = \frac{2\pi}{\lambda}\left(S + \frac{w_1}{2}\right) \tag{4.4},$$

where w_1 and w_2 are the microstrip widths, corresponding to the desired Z_1 and Z_2. For this configuration, S length is analytically evaluated by the equation (4.1), considering (4.3) and (4.4). Instead, H is taken equal to the patch side L.

However, during the simulation phase, an accurate optimization has to be carried out for S in order to obtain the same resonant frequency determined for the patch resonator, taking also into account the feed line effect. Finally, as presented in fig.4.25, Q_{ext} decreases when G (the distance between tap point and midpoint) is increased, as described also in the analytical model of the tapped feed lines [91]. Q_{ext} can easily range between 10 and 1000, supporting the realization of filters with fractional bandwidths from 10% to much less than 1%.

4.3.2 Four pole prototype filters

In the four pole filter design, the analysis of $k_{12}=k_{34}$ coupling between the stepped resonators and the orthogonal modes of the star type resonator is another delicate step, which needs particular attention. Even in this case, the coupling can be studied simply by varying the distance M in the layout sketched in fig.4.26a, thus obtaining the classic transmission responses with two peaks at the variable frequencies f_1 and f_2. The coupling has a magnetic nature and the placement at 90° of the feed lines is intuitively suggested by the surface current distribution on the stepped resonator.

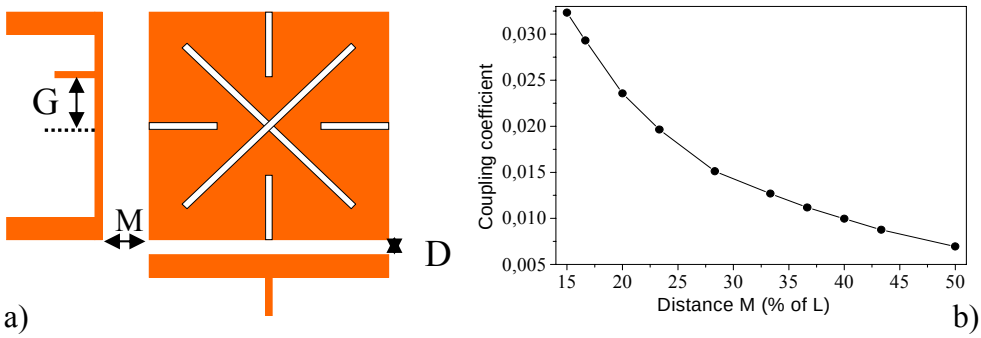

a) b)

Fig.4.26 a) Layout for the analysis of $k_{12}=k_{34}$ coupling b) Corresponding coupling curve as a function of the distance M

However, it is important to stress that, in order to evaluate this coupling by the simple graphical approach described in the chapter 1, it is necessary to assume

that the distance M does not affect the resonant frequencies of the two resonators, as generally occurs when M is relatively small and the couplings are consequently high. Indeed, in this case, a correct evaluation of the coupling has to take into account the difference between the resonant frequencies (asynchronously tuned coupled resonator circuit) and the corresponding formulas are quite more complex [92]. In our case, in the analyzed range of M, (for bandwidths up to 5%), the formula $k = \frac{2(f_2 - f_1)}{(f_2 + f_1)}$ is valid with a very good approximation (fig.4.26b). According to the abovementioned design principles, several prototype filters, operating in L, C and K band, have been designed both on $LaAlO_3$ and MgO substrates. First of all, in order to compare the dimensions of this topology with those previously described for the dual stage realization, we can analyze in details the design of a four-pole filter with f_0=3.3GHz and a 3% fractional bandwidth on $LaAlO_3$. With such specifications and selecting (N=4, rp=0.1dB), Q_{ext}=36.9, k_{12}=k_{34}=0.0249 and k_{23}=0.01973 are obtained [2]. According to these requirements, the geometrical parameters result to be: G=0.9 mm, ΔL=0.252μm and M=0.9 mm. The resulting overall dimensions are only [9.3x9.3]mm^2. In this way, the structure is highly miniaturized, yielding about 60% reduction of area occupation, if compared with the dual-mode dual-stage filter described above. Furthermore, as shown in fig.4.27a, even for this filter configuration, responses with and without transmission zeroes may be obtained without introducing direct cross-coupling structures but simply by inverting the positions of the two diagonal slots. More in detail, when the L_2 slot (fig.4.23) is equal to L+ΔL/2, two extra transmission zeros arise. Their physical origin will be discussed in the following section.

The wideband response in fig.4.27b confirms what stated before about the absence of the spurious modes. As shown, there is not a real second harmonic, since, due the characteristics of the stepped resonators, the second harmonics of the two types of resonator do not coincide. The miniaturization capabilities of this filter configuration have been also tested in L ad K band, designing devices on $LaAlO_3$ substrates of possible interest for terrestrial and satellite telecommunication systems.

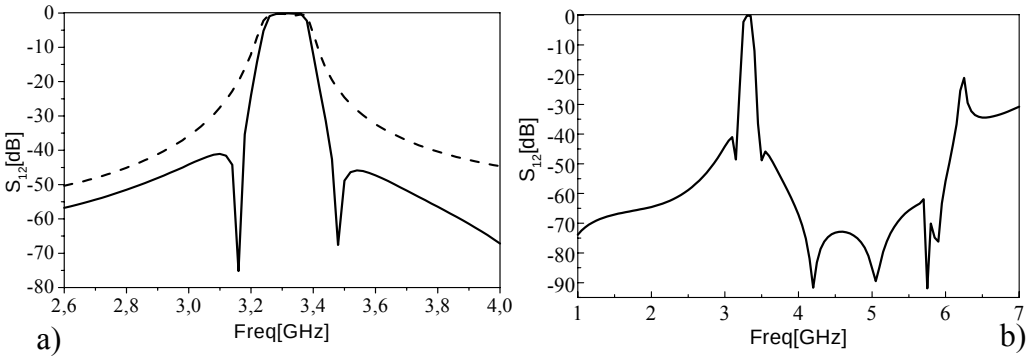

Fig.4.27 a) Quasi elliptic (continuous curve) and pseudo-Chebychev (dashed curve) response for a four pole filter with f_0=3.3GHz and BW=3%. b) Corresponding wideband response of the quasi elliptic filter.

In particular, a L band filter, with f_0=1.95GHz and a 3% fractional bandwidth, presents overall dimensions of only [14x14]mm^2. So, it results much more miniaturized if compared with the four pole filter recently developed by Pirelli Labs and Telecom Italia Lab (dimensions about [13.5x27]mm^2 on $LaAlO_3$, see chapter 2) to satisfy the needs of the up-link band of the terrestrial UMTS system [48]. To this regard, for the same application, fig.4.28 shows also a possible layout and the simulated response of an 8 pole filter, comprising two star patches and four stepped impedance resonators. The overall dimensions are about [19.5x29.3]mm^2 on $LaAlO_3$.

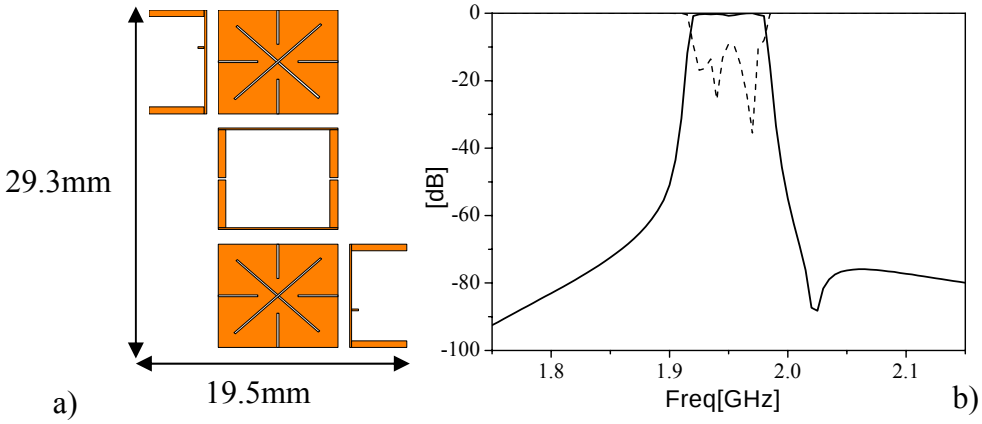

Fig.4.28 a) Layout and b) simulated response of an 8 pole filter, designed for UMTS up-link band and based on two star type and four stepped impedance resonators

Finally, the response of a filter operating at 11 GHz is reported in fig.4.29. At these frequencies, the resulting dimensions are only [3.5x 3.5]mm^2. However, it should be observed that at higher frequencies (f >20GHz), the above described design steps are not applicable, since some dimensions (the width of the feeding lines for instance) cannot be scaled with frequency, resulting in a considerable perturbation for the coupling investigation.

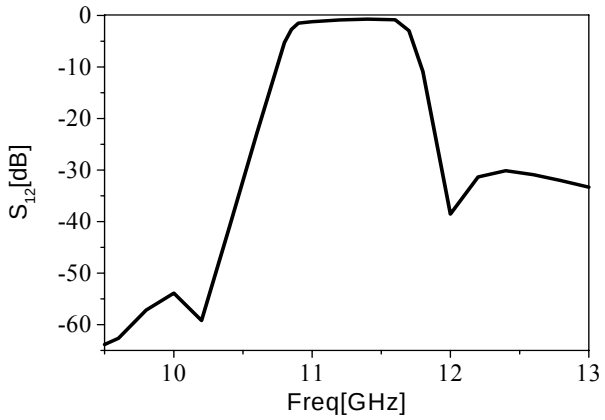

Fig.4.29 Simulated response for a four pole filter with f_0=11.25GHz and BW=6%

4.3.3 Transmission zeroes physical origin

Similarly to what reported for our resonators, the presence of transmission zeros in dual mode filters with no direct cross-coupling structures has been observed in many papers [93,94,95]. A physical explanation of this phenomenon can be given only by providing a more accurate equivalent circuit of a dual mode resonator, able to correctly reproduce the behavior of the feed lines. Indeed, as discussed in detail in [96,97] for a dual mode two pole filter, the 90° placement of the two feed lines creates a distortion of EM field distribution for each of the single mode configurations. Practically, the right angle arrangement of the feed lines breaks the structure symmetry and changes the current distribution of both modes, thus introducing a first contribution to their coupling. With reference to the equivalent circuit, this behavior can be modeled by considering a direct coupling between the two ports. In this sense,

from a theoretical pint of view, it was also recently confirmed that only a direct coupling between the feed ports can assure the presence of n zeros in a n-pole filter [98,73]. Keeping this model in mind, it is possible to demonstrate the possibility of introducing or not transmission zeros in $|S_{12}|$, according to the sign of the direct coupling between the two orthogonal modes. In fig.4.30a, we report the obtained responses for a two pole filter (f_o=3.25GHz and BW=1%) based on a star type resonator. As shown, it is possible to realize a response with (L_1>L_2, in fig.4.9) or without (L_1<L_2) transmission zeros, by simply changing the position of the diagonal slots, which in our configuration changes the sign of the direct coupling between the modes. This behavior can be reproduced adopting the circuital model in fig.4.30b, according to the sign of k_{SL}.

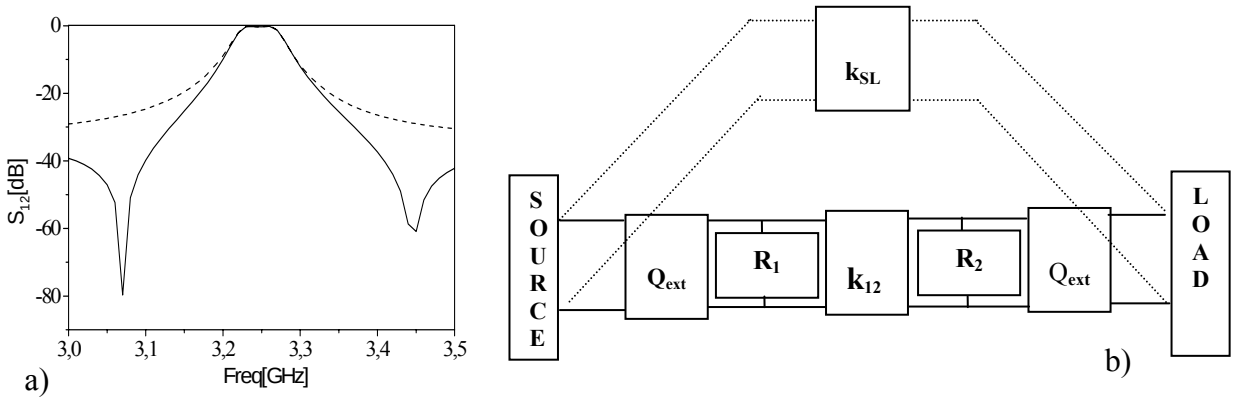

Fig.4.30 $|S_{12}|$responses with and without transmission zeroes obtained for a two pole filter based on a star type resonator b) Equivalent circuit reproducing the behavior of the dual mode filter

In particular, for the quasi elliptic response of our two pole filter, we have evaluated that this coupling is about k_{SL}=-0.007369 [99]. Besides, it is important to outline that the response without transmission zeroes is not a real Chebychev response as confirmed in [100]. Indeed in this case, the coupling k_{SL} is still present but with a positive sign. Consequently, it can be demonstrated that S_{12} has two zeroes located on the real axis of the complex s-plane, whereas the transmission zeroes for $|S_{12}|$ (quasi elliptic response) are

zeroes of S_{12}, located on the imaginary axis of the s-plane. The k_{SL} positive sign provides a final $|S_{12}|$ response with a poorer selectivity if compared with the ideal Chebychev model, where the transmission zeroes are theoretically located at infinity.

For our four pole filter configuration based on mixed resonators, the origin of the transmission zeroes can be explained by the same model adopted for a two pole filter considering as feeding structures the merge between the actual 50Ohm lines and the stepped resonators. In this case, the situation is complicated by the presence of four resonators and consequently an accurate model has to include equivalent couplings both between the two stepped resonators (k_{14} coupling) and between the stepped resonators and each of the two orthogonal modes of the patch (coupling $k_{12}=k_{34}$ and $k_{13}=k_{24}$). Only this complex model, with the introduction of all the coupling sources, gives the possibility to explain the existence of different quasi elliptic responses, with different number and position of transmission zeroes, depending on the feed line configuration. As example, fig.4.31b shows the three quasi elliptic responses obtained for an L band filter designed on MgO, with centre frequency f_0=2.1GHz and a 60MHz bandwidth (overall dimensions [19x19]mm^2).

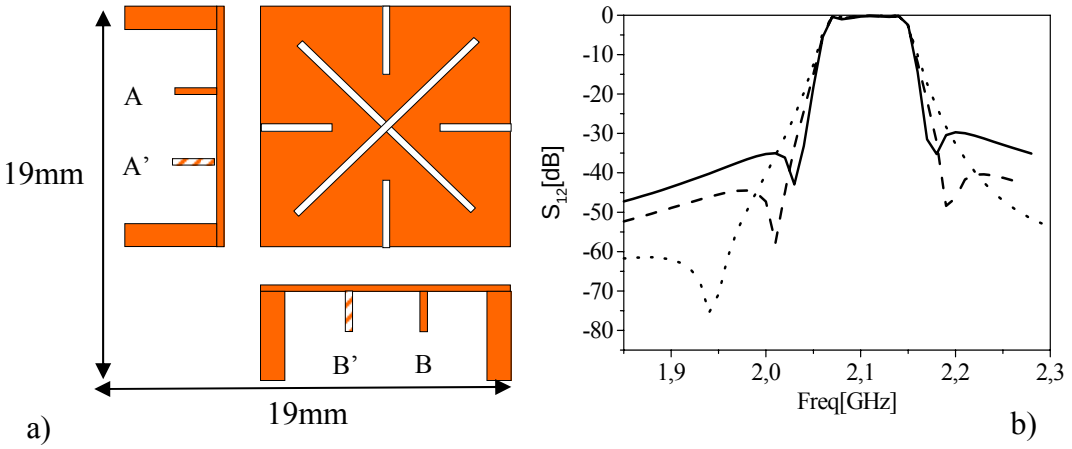

Fig.4.31 a) Three possible rearrangements (AB, A'B' and A'B= AB' for the feed lines b) Corresponding quasi elliptic responses: AB (dotted curve), A'B= AB' (dashed curve) and AB (continuous curve) [99]

The responses have been obtained by considering the three possible configurations AB, A'B' and AB'=A'B of the feeding lines shown in fig.4.31a. In these cases, without modifying the Q_{ext} factor and consequently the bandwidth, the presence and the position of the transmission zeros can be changed, resulting in different values of the skirt steepness.

The different configurations produce different values for the equivalent coupling k_{14} and $k_{13}=k_{24}$. In particular, in the AB case, it is possible to show that the coupling $k_{13}=k_{24}$ becomes predominant, thus resulting in a single transmission zero for $|S_{12}|$. This response can be reproduced using the equivalent circuit shown in fig.4.32; it should be noted that the position of the zero (left or right side) is determined by the sign of the coupling, related to the position of the diagonal slots.

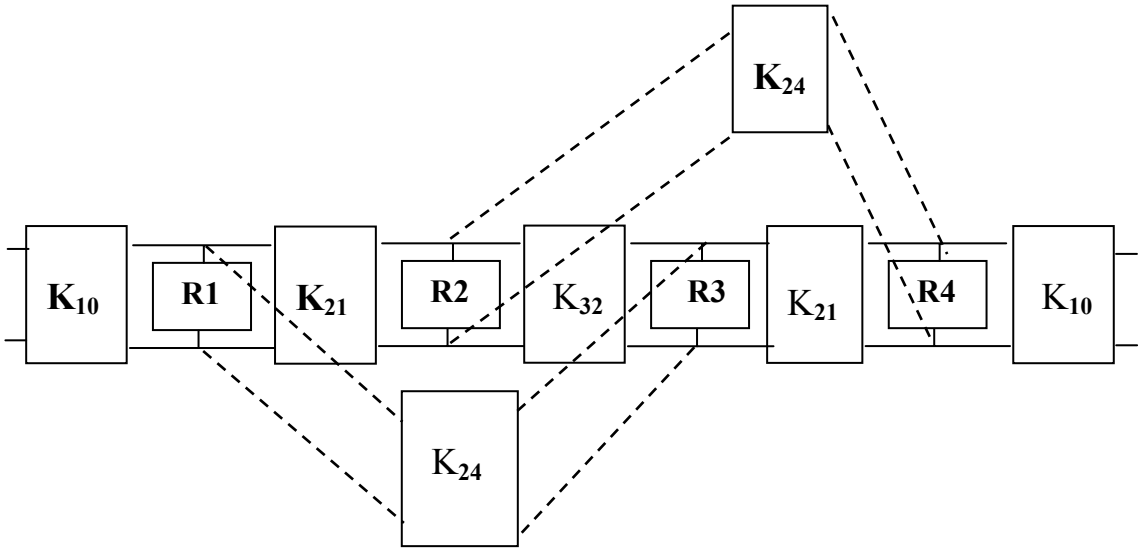

Fig.4.32 Equivalent circuit reproducing the AB behavior of our four pole filter

The AB response is compared with this ideal equivalent circuit (where $k_{13}=k_{24}= 0.00189$) in fig.4.33 and as shown, the agreement is very good. On the other hand, in the other two cases, the coupling k_{14} between the two stepped resonators forces the presence of two symmetrical zeroes and, according to what previously reported, it is clear that in the position A'B', a stronger coupling between the first and the last resonator is obtained, thus explaining

why the zeroes are closer to the useful pass-band. The position of the zeroes can be varied roughly by 1% of the central frequency.

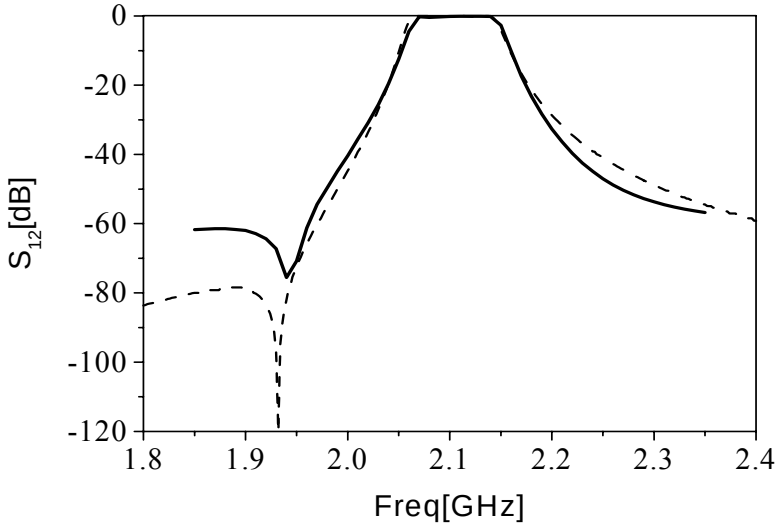

Fig.4.33 Comparison between the simulated response (continuous curve) and the equivalent lumped circuit (dashed line) for the AB configuration of L band filter on MgO substrate

Similar considerations can be repeated for other examples in C and X band both on $LaAlO_3$ or MgO substrates. It is clear that this phenomenon needs further investigations. In fact, it results very interesting for the filter designers since it seems to open the possibility to control the transmission zeroes of the dual mode structures at a level never obtained so far.

4.3.4 L band filter test

HTS four pole filters based on mixed resonators have been fabricated by commercial YBCO films, grown by co-evaporation technique on 0.5mm thick $LaAlO_3$ and MgO substrates.

In particular, in fig.4.34, the measured in-band and wideband responses of the L band filter discussed in the previous section, with AB feed line configuration, are reported and compared with simulations. In this case, the minimum

insertion losses (IL), measured at T=77K in a liquid nitrogen bath and with input power P_{in}= -10dBm, are in the range of 0.2 dB.

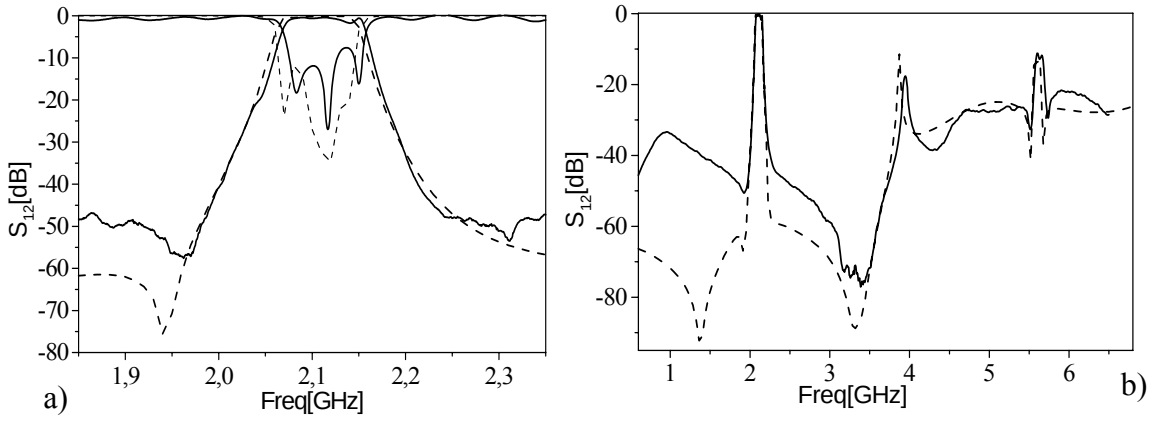

Fig.4.34 Comparison between the a) in-band and b) out-of-band simulated (dashed curves) and measured (continuous curves) responses at T=77K, for the L band HTS filter based on mixed resonators

The in-band ripple (0.8dB) is higher than that obtained in the simulation and it can be mainly related to the slightly different accuracy of the simulator (Ensemble 4.2) for the two shapes. However, it should be observed that the filter measurements have been carried out without using dielectric screws. A good agreement between simulation and measurement has been found in terms of center frequency, fractional bandwidth and out-of-band rejection in a wide frequency range, confirming the absence of spurious modes. Instead, the out-of-band rejection in the lower frequency range, around the band, results higher than predicted and this could be due to the copper box effect which is not taken into account in the simulation. The power handling measurements realized in liquid nitrogen by using a continuous wave signal, show only a slightly appreciable degradation of the response, as a function of the input power up to P_{in}=33dBm, with a breakdown field occurred at P_{in}=34dBm.

In order to better understand the nature of the input power dependence, we have investigated the current distribution of the filter at different frequencies. Fig.4.35 reports the simulated current distribution, normalized to the maximum, at different frequencies going from the lower to the upper edge band (f_0=2.07 – 2.09 – 2.22 – 2.13 – 2.15 – 2.16) GHz.

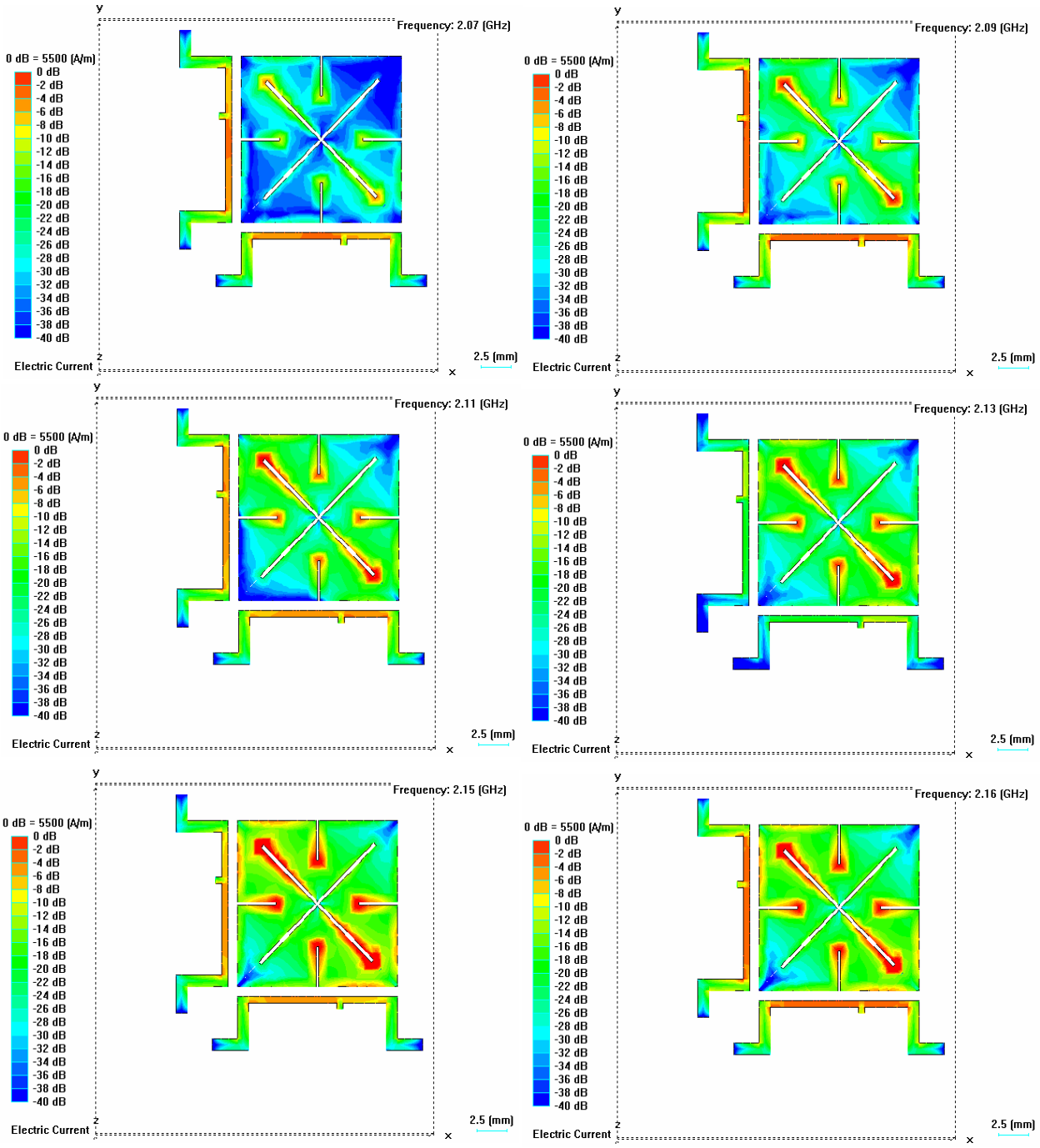

Fig.4.35 Current distribution on the four pole L band filter at freq= (2.07 – 2.09 – 2.22 – 2.13 – 2.15 – 2.16)GHz

It is interesting to observe that, as predicted by the theory (see chapter 1), the current tends to be maxima at band edges and in particular at upper one. Moreover the maximum of the current on dual mode patch, representing the

second and the third resonators, is in any case 6dB higher than the maximum values on the stepped impedance resonators, reached in the strongly inductive region of the tap point. Substantially, the use of a patch resonator allows improving the overall power handling filter, as also confirmed by the analysis of fig.4.36, where the current distribution at band edges is depicted for another L band four pole filter, based on $\lambda_g/2$ resonators in forward coupling configuration and with a similar bandwidth (about 3%). It is clear that now the surface regions with high current density are much larger.

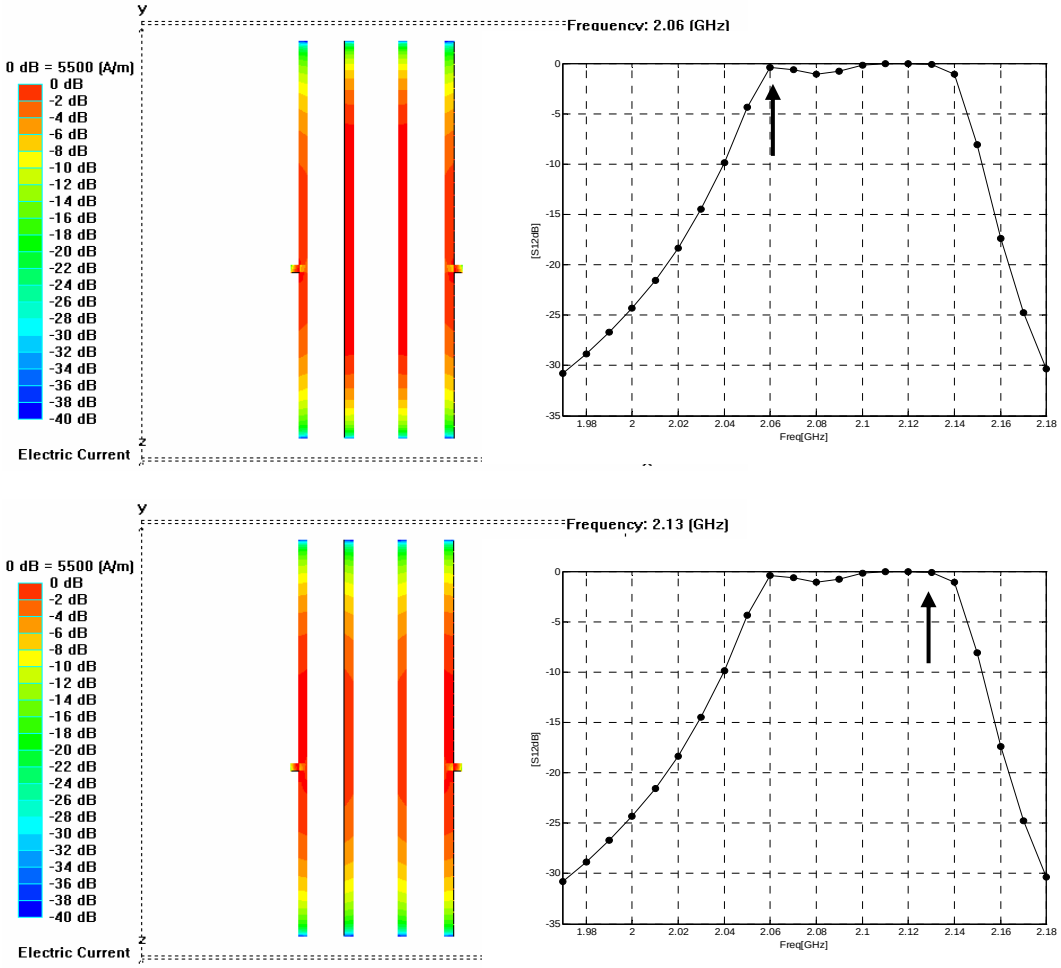

Fig.4.36 Current distribution of a four pole inter-digital filter obtained at band edges (freq=2.06 GHz and f_0=2.13 GHz)

Finally, the non linear behavior of the fabricated L band filter has been investigated in the breakdown region by the two tone technique. The resulting third order intermodulation (IM3 - $2f_2$-f_1) is plotted in fig.4.37 (circles) as a

function of single tone power (f_1) and are also compared with those observed on the microwave amplifier (squares) fixing the measurement resolution limit. It should be observed that the IMP introduced by the filter are low, resulting only 2-3dB higher than those due to the experimental set-up. It is worth to mention that the IMP power dependence has a slope ranging between 2.5 and 2.8, consistent with the slight degradation observed on the fundamental tones, while the IMP of the amplifier show the theoretical expected dependence with a slope n=3.

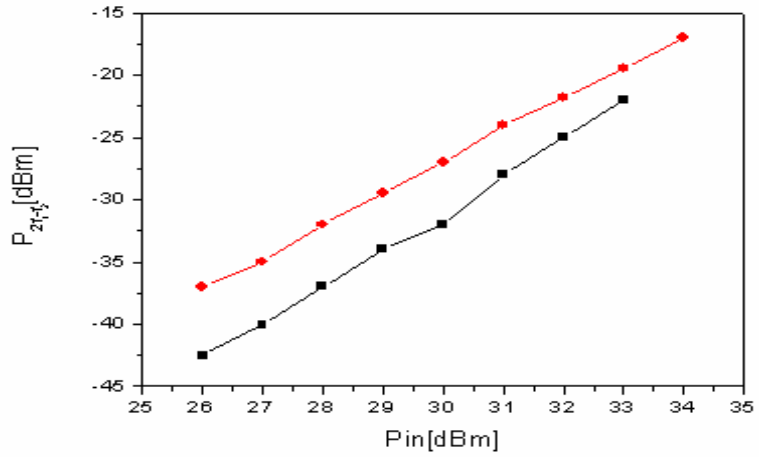

Fig.4.37 Third order intermodulation (IMP, $2f_2$-f_1) is plotted as a function of single tone power (f_1), measured on superconducting filter (circles) and compared with those obtained on the experimental set-up used (squares).

4.4 Integration with a LNA: design and experimental performances

As a preliminary step in the development of a new cryogenic front-end receiver of interest for UMTS applications, the L band four pole filter based on mixed resonators has been integrated with a cryogenic low noise amplifier, developed at University Tor-Vergata of Rome [101]. According to what extensively discussed in the chapter 2, the integration of a highly selective band pass filter and extremely low-noise amplifier provides a two-fold performance

enhancement: significant improvement in receiver sensitivity and substantial reduction in the effects of out-of-band interference.

In our work, the LNA has been assembled with the superconducting filter in a single copper package (fig.4.38), exhibiting a total space occupation of only [40x25]mm^2. The absence of external connections (SMA) between the filter and LNA should assure a further improvement in the reduction of the noise figure, if compared with other realizations based on commercial LNA.

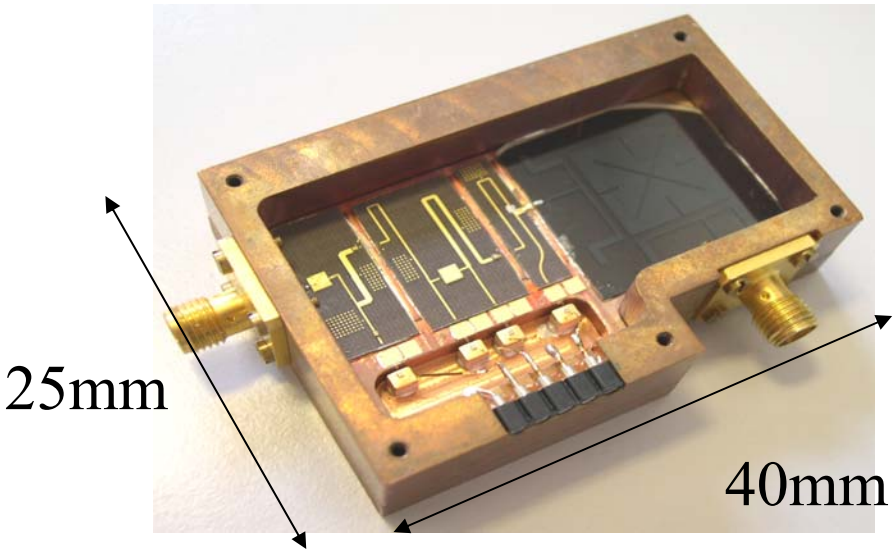

Fig.4.38 Photo of the filter integrated with the LNA

The built LNA, sketched in fig.4.39, is a two stage amplifier based on the pseudo-morphic low noise GaAs HEMT NE321000, manufactured by NEC.

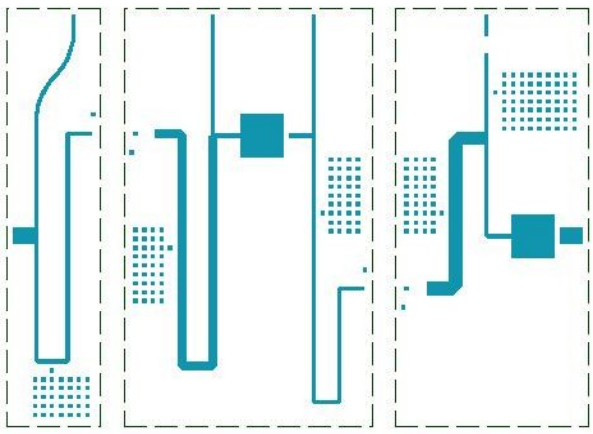

Fig.4.39 Layout of the realized dual stage LNA

The device exhibits a coplanar structure, a gate length equal to 0.2μm and a gate width equal to 160μm; chip sizes are 300μm square. The selected substrate for biasing and matching networks is the Taconic TLY-5, a soft woven dielectric laminate ($\varepsilon_r = 2.2$, $\tan\delta = 0.0009$ @10GHz).

Great care has been provided to ensure stable performances under all possible operating load conditions, therefore ensuring unconditional stability of the amplifying stages. The circuit topology adopted both to stabilize the FET and to get good trade-off between noise performances, gain as well as input and output return loss, is shown in fig.4.40.

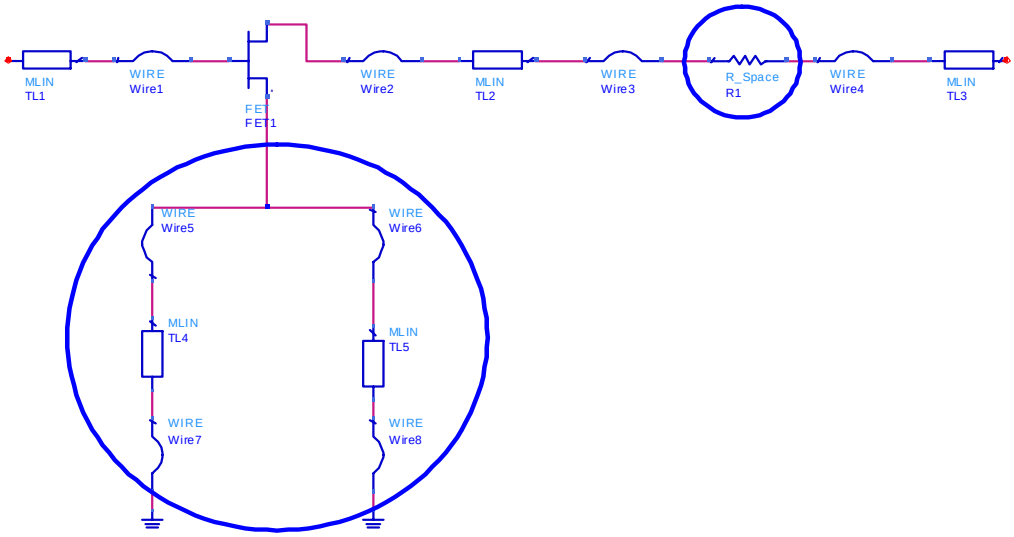

Fig.4.40 Source degenerative feedback and resistive drain loading

A source degenerative feedback has been used and the device output has been loaded with a series resistor: the latter mainly affects the circuit stability [102], while the source feedback influences both the stability, improving in-band performances, as well as the optimum loads for noise and matching, achieving a compromise between them. Amplifier stability was achieved for each frequency point, except for frequencies lower than 1.5GHz with this circuital solution. In order to stabilize the resulting amplifier also in the low frequency range, resistive biasing networks were employed, which are shunted to ground by DC filtering capacitors and essentially load the circuit at lower frequencies and stabilize it without the introduction of in-band noise contributions.

Stability was accomplished with the drain resistor with minor amount of additional DC power consumption (5mW per stage), whereas it practically has not any effect on the resulting noise figure, increased by 0.05dB (at 300K) only as a consequence of the high gain of the selected HEMT. The source inductance value has been selected in order to obtain a good compromise between noise performances, input and output return losses, rather than for the in-band stability requirement. A special care on the matching network topology has been taken into account in order to minimize losses and the associated thermal noise. The NE321000 needs 2 V of drain to source voltage and 10mA of drain current to get excellent noise performance; the DC power dissipation of the entire two stage LNA amounts to 52mW: 40mW due to the FETs biasing, and 12mW due to the dissipation in the biasing and stabilization components.

At a moment, a first set of experimental measurements on the overall device has been realized at 77K in liquid nitrogen. The scattering parameters are reported in fig.4.41. Both the measured center frequency and bandwidth are in good agreement with the simulation. The in-band gain is approximately 30dB (fig.4.41a), slightly higher than predicted (about 28dB), with an in-band ripple of about 1dB.

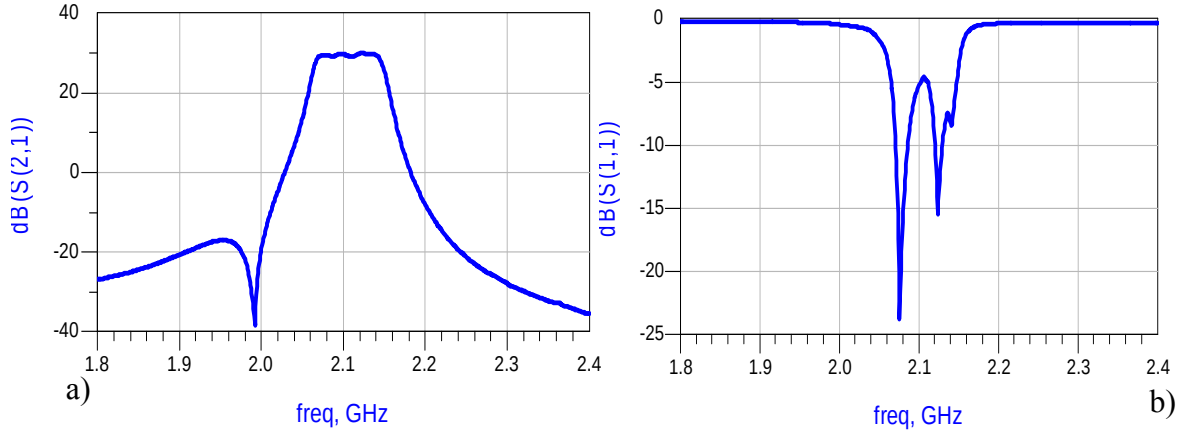

Fig.4.41 Filter/LNA experimental a) transmission and b) reflection response at T=77K, in liquid Nitrogen

Measured input matching (S_{11}) of the packaged is remarkably lower than the expected value (5dB instead of 10dB) and probably it is related to the input

connector, that has not been properly soldered, as evidenced once the system was heated up again to 300K.

Noise measurements were performed utilizing a commercial noise-figure meter (HP 8970 system) in conjunction with a calibrated diode noise source. This is the standard method used to measure room-temperature transistor amplifiers, and it works very well with DUTs that have an input noise temperature between the *off* and *on* noise temperatures presented by the diode noise source, i.e. between 300K and nx10^3K. Obviously this is not the case, so some uncertainties on the measure are to be considered. The measured in-band noise figure at T=77K reveals a value between 0.47 and 0.8 dB (fig.4.42), being higher than simulated one (about 0.3dB). This discrepancy can be explained appealing to the measurement uncertainties and to the assembly problems revealed by the input connector. Moreover, a more reliable testing of the noise figure has to be realized in a cryo-generator system, in order to avoid all the possible noise sources related to the liquid nitrogen presence, which can make difficult a good estimation of the device real performances.

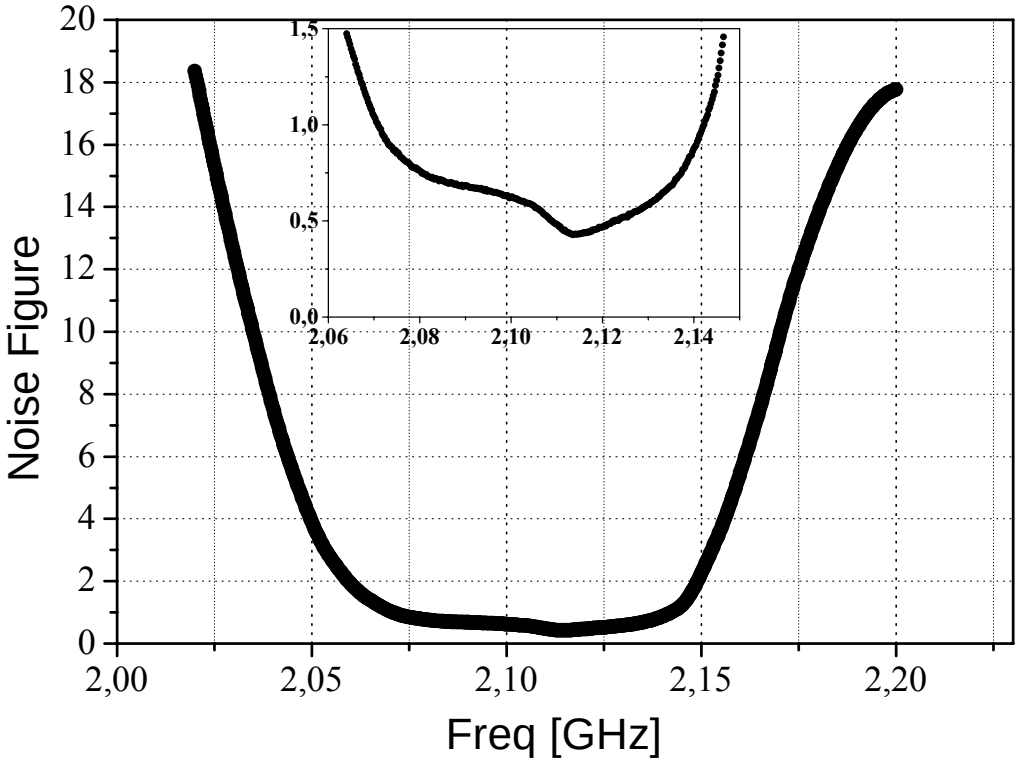

Fig.4.42 Measured noise figure at T=77K in liquid nitrogen

Conclusions

HTS filters and related integrated systems represent an emerging and innovative class of devices, able to face the technological challenge of modern telecommunication systems, requiring high performances and microwave equipment miniaturization. Sensitivity and selectivity of these devices have demonstrated to be unique and can play a decisive role to address the interference problems which are today getting more and more stringent, due to the phenomenal expansion of the telecommunication world. These features well explain the interest of many research and industrial groups for this new technology, where many efforts have been carried out in the last years to design miniaturized filters able to reduce the costs, to relax the cryogenic burden and to favor at the same time the integration with low noise amplifier in the fabrication of front-end receivers. The miniaturization of HTS planar filters is the subject of this thesis work, where new geometries have been investigated to fabricate highly compact devices, with both Chebychev and quasi elliptic responses, for telecommunication applications. In particular, prototype filters based on HTS (High Temperature Superconductors) films have been designed for mobile communications, with particular attention to the new UMTS application in L-band for which a miniaturized dual mode filter has been assembled with a LNA amplifier and tested in terms of noise figure, for satellite systems operating both in C and Ku bands and finally for radio astronomy receivers in UHF band.

The first part of this work, carried out in collaboration with the Universitat Politecnica de Catalunya of Barcelona (Spain), deals with the fabrication of filters based on fractal curves with space filling capabilities. In particular, the miniaturization performances and the quality factors of Koch-Minkowski and Hilbert resonators have been investigated as a function of the fractal iteration level. Thanks to their better space filling capabilities, Hilbert resonators present more compact size. As a reference point, at f_0=1.95GHz, the dimensions on MgO substrates of a Hilbert resonator are [3.6x3.6]mm^2, with a measured Q_0 of about $2.7*10^3$ at 77K. This value is similar to those reported in recent papers

for other compact resonators and no degradation of the frequency response was observed at circulating power levels up to 20W (P_{in} about 0dB). By using Hilbert resonators, a four pole quasi elliptic filter with f_0 close to 2.45GHz and a four pole Chebychev filter with f_0=1.9GHz have been fabricated on two commercial [10x10]mm^2 double sided YBCO films on MgO. The measured response at T=77K and P_{in}=0dBm of the former shows minimum insertion losses of about 0.2dB and a maximum in-band ripple response of about 0.6dB. The dimensions of the latter are only [8.2x7.93]mm^2, occupying about the 20% of the superconducting area occupied by a HTS filter developed recently by Pirelli Labs and Telecom Italia Lab for the same application. The insertion losses are 0.1dB as minimum value and the ripple is only 0.2 dB as maximum value. The filter performances have been tested up to P_{in}=10dBm and no response degradation was observed. In this case, the out-of-band rejection value is lower than simulated one, being limited to about 40dB around f_0, due to the effect of the metallic box, whose reduced dimensions have not been considered in the simulations. The packaging optimization as well as the use of tuning dielectric screws can be considered two fundamental issues to develop filters with a higher number of poles as future perspective. In conclusion, these filters can be particularly suitable to design L-band filters for receiving channels of future mobile communication systems, whereas 8-10 pole filters with quasi elliptic response can be fabricated in about [20x20]mm^2 areas, with Q_0 factor close to $3*10^4$ and power handling between 0 and 10dBm. To this regard, it is worth to remember that at present, in the most of modern BTS, the employed filters are based on coaxial TEM resonators with Q well below 10^4 at about 2GHz. Furthermore, in the next generations of mobile communication systems, based on more flexible software radio architectures, the digital conversion should be realized directly on RF signal, such that the requirements on the resolution, sampling rate, linearity and dynamic range of all devices will be more and more stringent. In this sense, the minimization of interference degradations on the useful signal is more and more essential. To this end, the aforementioned potentialities of the HTS filters, with their high selectivity, could be fully exploited in new “adaptive RF filtering” schemes, where the

tunability or switchability of the filter allows a frequency selective control of amplification, with the introduction also of possible zero amplification regions. The fabrication of tunable HTS filters seems to be one of the next frontiers in this research field, with performances unattainable by other technologies.

In the second part of this work, in the attempt to fabricate filters with a good trade-off between miniaturization and power handling, a new dual mode square patch resonator has been investigated. The application of surface (diagonal and transverse) cuts can reduce the resonant frequency without modifying the external dimensions and equivalent miniaturization close to 75% of the occupied area can be obtained, in comparison to a traditional square patch. Besides, the resulting current meandering implies also the reduction of the housing losses, which can be a consistent loss contribution for the superconducting dual mode resonators. At the same time, a good power handling is still preserved thanks to the widely spread current distribution. To this regard, power tests on two (single stage) and four pole (dual stage) YBCO filters show power handling higher than 2W (33dBm) and close to 0.1W (20Bm), for bandwidths of 10% and 0.1%, respectively.

The Dual Mode configuration has been developed by introducing a new four pole filter where the miniaturized patch resonator is combined with two stepped impedance resonators. This topology is revealed to exhibit very interesting features:

- a very high degree of miniaturization, as it saves about the 50% of the area occupied by the dual mode dual stage configuration
- an improved out-of-band rejection if compared with that of dual mode dual stage filter without the presence of spurious modes
- the possibility, by exploiting the peculiar characteristics of the dual mode resonators, to obtain more selective responses with transmission zeroes close to the band edges without extra coupling structures. In our configuration, the position of the zeroes is partially controllable by using different rearrangements of the tapped feed lines.

According to this new structure, YBCO filters in L, C and Ku bands have been fabricated both on $LaAlO_3$ and MgO substrates. In particular, an L band filter

for satellite UMTS (f0=2.1GHz – BW=60MHz) has been designed on MgO with resulting overall dimensions of [19x19]mm^2. In this case, the minimum measured insertion losses (IL), are at T=77K in the range of 0.2 dB, while the response is not degraded for input power up to Pin=33dBm, with a breakdown field occurring at P_{in}=34dBm. Besides for the receiving communication channels, this filter configuration could be interesting in future even for transmission applications of modern Code Division Multiple Access (CDMA) systems whereas, in order to avoid interference problems, related to the fact that more subscribers are utilizing the same frequency channel simultaneously, the transmitted power should be relevantly reduced if compared with the GSM system.

As a first step in the development of a cryogenic front-end receiver, the above described L band filter has been also integrated with a cryogenic low noise amplifier. In our work, the dual stage LNA developed at University Tor-Vergata of Rome has been assembled with the superconducting filter in a single copper package without the necessity of external connections (SMA). The overall device exhibits a total space occupation of only [40x25]mm^2. The first experimental measurements realized in liquid nitrogen show an in-band gain of approximately 30dB, slightly higher than predicted (about 28dB) and a high ripple (about 1dB) which limits the minimum returned loss to about 5dB. As far as the noise figure is concerned, measurements show a value of about 0.47dB, while a value of NF under 0.3dB is predicted from simulations. Improved performances are expected from the optimization of the experimental set-up.

ACKNOWLEDGMENT

First of all, I would like to thank my supervisor **Dr. Antonio Cassinese** for his very helpful ideas and long discussions concerning this thesis and **Prof. Ruggero Vaglio**, who gave me the possibility to work on an innovative and interesting field. I thank **Prof. Joan O'Callaghan**, **Dr. Carlos Collado** and **Dr. Jordi Mateu Mateu** for their support to my work during the exchange visit at Universitat Politecnica de Catalunya (UPC) and for their courtesy.

Also many thanks to **Prof. Antonello Andreone** (University of Naples "Federico II") for the stimulating discussions and to **Dr. Renata Mele, Dr. Vincenzo Boffa,** and **Dr. Fabrizio Ricci** (Pirelli Labs) to provide the experimental data of the field trials carried out by Pirelli Labs.

A special thank to **Prof. Matteo Cirillo** and **Dr. Roberto Russo** (University of Tor-Vergata, Rome) for the fabrication of the chrome masks, and to **Prof. Ernesto Limiti** and to **Dr. Walter Ciccognani** (University of Tor-Vergata, Rome) for the design of LNA amplifier integrated with the superconducting filter and for the related experimental tests.

I would like also acknowledge the extensive technical work provided by **Antonio Maggio**, **Stefano Marrazzo** (University of Naples) and **Luis Enrique Romero** (UPC) in the fabrication and mounting of all the tested devices. Finally, my best of thanks to my student friends from Dipartimento Scienze Fisiche of University of Naples – INFM Coherentia and to my Phd colleagues, **Dr. Antigone Marino** and **Dr. Gianni Mettivier**, who kept my moral high and provided good company.

References

[1] J.S. Hong and M.J. Lancaster, *Microstrip filters for RF/microwave applications,* John Wiley & Sons, 2001.

[2] G. Matthaei, L. Young and E.M.T. Jones, *Microwave Filters Impedance- Matching Networks and Coupling Structures,* Norwood, MA, 1980.

[3] H.J. Chaloupka, *Microwave applications of High Temperature Superconductors*, in Applications of Superconductivity, NATO ASO Series, pp.295-389, 2000.

[4] M.J. Lancaster, *Passive Microwave Device Applications of High Temperature Superconductors*, Cambridge University Press, Cambridge, 1997.

[5] R. E. Collin, *Foundations for Microwave Engineering*, McGraw – Hill 1992

[6] A.E.Atia, A.E. Williams and R.W.Newcomb, "*Narrow band multicoupled cavità synthesis",,* IEEE CAS-21, pp. 649-655, Sept 1974.

[7] R.J. Cameron, "*General coupling matrix synthesis methods for Chebychev filtering functions"*, IEEE Tans. On Microwave Theory and Techniques, vol. **47**, pp.433-442, April 1999.

[8] I. Bahal, B. Barthia, *Microwave solid circuit design*, John Wiley & Sons Ltd., 1992.

[9] J.S. Hong and M.J. Lancaster, *"Design of Highly Selective Microstrip Bandpass Filters with a Single Pair of Attenuation Poles at Finite Frequencies",* IEEE Trans. On Microwave Theory and Techniques, Vol. **48**, pp.1098-1107, July 2000.

[10] T. Itoh, *Numerical techiques for microwave and millimeter wave passive structures*, John Wiley & Sons, LTd 1989.

[11] M.Sagawa, K. Takahashi and M. Makimoto, *"Miniaturized Hairpin resonator filters and Their Application to Receiver Fornt end MIC's",* IEEE Trans. On Microwave Theory and Techniques, vol. **37**, pp.1991-1997, Dec 1989.

[12] T.D.A. Glocker and S.I. Shah, *Handbook of Thin Film Process Technology,* IOP PUBLISHING*,* Philadelphia, 1995.

[13] M. Tinkham, *Introduction to superconductiviy*, Mc-Graw and Hill, International Editions, 1996.

[14] R. Mansour, B. Jolley, Shen Ye, F. T. Thomson and Van Dokas, "*On The Power Handling Capability Of High Temperature Superconductive Filters",* IEEE Tans. On Microwave theory and techniques, vol. **44**, pp.1322-1238, July 1996.

[15] M. Klauda, T.Kässer, B.Mayer, C. Neumann, F. Schnell, B. Aminov,A. Baumfalk, H. Chaloupka*,* S. Kolesov, H. Piel, N. Klein, S. Schornstein and M. Bareiss , "*Superconductors and Cryogenics for Future Communication Systems",* IEEE Trans. On Microwave Theory and Techniques, Vol. **48**, pp.1227-1239, July 2000.

[16] H. Chaloupka, M. Jeck, B. Gurzinski and S. Kolesov, *"Superconducting Planar disk resonators and filters with high power handling capability,* ELECTRONICS LETTES, No.**18**, pp.1735-1737, 29th August 1996.

[17] A. Baumfalk, H.J. Chaloupka, S. Kolesov, M. Klauda and C. Neumann, *"HTS Power Filters for Output Multiplexers in Satellite Communications",*IEEE Trans. On Appl. Supercondictivity, Vol. **9**, pp.2857-2861, June 1989.

[18] M. Reppel, *Novel Hts Microstrip Resonator Configurations for Microwave Band pass Filter*, PHD Thesis, Wuppertal 2000.

[19] S. Remillard, H.R. Yi. and A. Abdelmonem, *"Three- Tone Intermodulation Distortion generated by uperconducting Bandpass Filters",* IEEE Trans. On Applied Superconductivity, Vol. **13**, pp.3797-3802, Sept. 2003.

[20] J. M. Pony, K. Carrol and E. Cukauskas, "*Ultra compact microwave filters using kinetic inductance microstrip",* IEEE Trans. On Magntics, Vol.**27**, pp.2696-2699, 1991.

[21] K. Carrol, J. M. Pond, and E. Cukauskas, "*Superconducting kinetic inductance microwave filters",* IEEE Trans. On Applied superconductivity, Vol. **3**, pp.8-16, 1993.

[22] M. Reppel and J.C. Mage, *"Superconducting Microstrip Bandpass Filter on $LaAlO_3$ With High Out-Of-Band Rejection",* IEEE Microwave and Guided letters, Vol. **10,** pp. 180-182, May 2000.

[23] Jia-Sheng Hong, M.J. Lancaster, D. Jedamzik and R.B. Greed, "*On the Development of Superconducting Microstrip Filters for Mobile Communications Applications"*, IEEE Trans On Microwave Theory and Techniques , Vol. **47**, pp. 1656-1663, Sept. 1999.

[24] F. Huang, *"Ultra-compact superconducting narrow band filters using single and twin spiral resonators",* IEEE Trans On Microwave Theory and Techniques, Vol. **51**, pp. 487-491, Feb.2003.

[25] J.S. Kwak, J.H. Lee, J.P. Hong, S.K. Han, W.S.Kim and K.R. Char, *"Narrow Pass-band High –Temperature Superconducting Filters Of Highly Compact Sizes for Personal Communication Service Applications",* IEEE Trans. On Applied Superconductivity, Vol. **13**, pp- 17-19, March 2003.

[26] G.L. Matthaei, *"Narrow Band, Fixed Tuned And Tunable Bandpass Filters With Zig-Zag Hairpin Comb Resonators",* IEEE Trans. On Microwave Theory and Techniques, Vol. **51**, pp 1214/1219, April 2003.

[27] H..J. Chaloupka and S. Kolesov, *Design of Lumped Element 2D RF Devices, in Microwave Superconductivity*, NATO ASO Series, 2001, pp.205-238.

[28] G. Tsuzuki, S. Ye and S. Berkowitz, "*Ultra-Selective 22-Pole 10-Transmission Zero Superconducting Bandpass Filter Surpasses 50-Pole Chebyshev Filter",* IEEE Trans. On Microwave Theory and Techniques, Vol. **50**, pp 2924-2929, Dec. 2002.

[29] C.K. Ong, L. Chen, J. Lu, C. Y. Tan, and B. T. G. Tan, "*High-Temperature Superconducting Bandpass Spiral Filter"*, IEEE Microwave and Guided Letters. Vol. **9,** pp. 407-409, Oct. 1999.

[30] C.Y. Tan, Linfeng Chen, Jian Lu, X. S. Rao, and C. K. Ong, *"Cross-Coupled Dual-Spiral High-Temperature Superconducting Filter"* IEEE Microwave and Wireless Components Letters, Vol. **13**, pp.247-249, June 2003.

[31] J. Zhou, M.J. Lancaster and F. Huang, *"Superconducting microstrip filters using compact resonators with double-spiral inductors and interdigital capacitors",* IEEE MTT-S, Int. Microwave Symp. Dig. 2003, TH1-D3.

[32] H. R. Yi, S.K. Remillard and A. Abdelmonem, *"A Novel Ultra-Compact Resonator for Superconducting Thin-Film Filters",* IEEE Trans. On Microwave Theory and Techniques, Vol. **51**, pp. 2290/2296, Dec 2003.

[33] www.**umts-forum**.org

[34] www.**suptech**.com,"*The Effect of Out-of-Band Interference on Base Station Receiver Performance"*, from Technical Library.

[35] S.C. Bundy, *"Quantifying the benefits of enhanced filter selectivity*", IEEE Microwave Mag, Vol. **4**, pp. 48–59, June 2003.

[36] www.**suptech**.com

[37] D.G Smith and V.K. Jain, "*Superconducting filters for wireless communication: A reappraisal",* IEEE Trans on Applied Superconductivity Vol. **9**, pp.4010 4013, June 1999.

[38] B.A. Willemsen, *HTS Wireless Applications*, in Microwave Superconductivity, NATO ASO Series, 2001, pp.387-416.

[39] R. CONLON, *"Superconductors do more with less"*, Wireless System Design- July August 2003.

[40] R.D. Lithgow and J.M. Peters, "*Electromagnetic resonant filter comprising cylindrically curved split ring resonators*", U.S. Patent 6616540°, 1997.

[41] S. K. Remillard, *"Thick Film HTS Filters Revealed*", presentation in HTSHFF04, 26-29 MAY 2004, Bengur (Spain).

[42] G.Tsuzuki, M. Suzuki and N. Sakakibara, *"Superconducting Filter for IMT-2000 Band*", IEEE Trans on Microwane Theory and Tech., Vol. **48**, pp. 2519-2525, Dec. 2000.

[43] S.Y. Lee and B. Oh, "*Recent progress in Microwaev HTS Technologies in Korea and Japan",* Journal of Superconductivity, Vol. **16**, pp.823-831, Oct. 2003.

[44] J.S. Hong, M.J. Lancaster, D. Jedamzik, R. B. Greed and J. C. Mage, *"On The Performance of HTS Microstip Quasi Elliptic Function Filters For Mobile Communications Application",* IEEE Trans On Microwave Theory and Techniques, Vol. **48**, pp.1240-1246July, 2000.

[45] H.J. Chaloupka, *"Advanced concepts for high-performance HTS filters",* presentation at HTSHFF02, Cape Cod, June 9-12, 2002.

[46] A. Cassinese and A.Andreone, *"Final test on front end cryogenic receiver",* in Final ACTA of "Progetto Sud : Filtri Superconduttivi per telecomunicazioni", Naples 2000.

[47] G. Bertin, B. Piovano, L.Accatino, G.Dai, R.Tebano, F.Ricci, *paper presented*, IEEE MTT-S, Int. Microwave Symp. Dig. 2004.

[48] R. Mele, "*A High Temperature Superconducting Front-End Receiver",* presentation at "SATT- Superconduttività ad Alta Temperatura di Transizione" Conference, 21-23 April 2004 Rome.

[49] M. Nisenoff, J.C. Ritter, G. Price and S.A. Wolf, "*The High Temperature Superconductivity Space Experiment: HTSSE I – Components and HTSEE II- Subsystems and Avanced Device",* IEEE Trans on Applied Superconductivity, Vol.**3**, pp.2885-2890, March 1993.

[50] M. Nisenoff amd W.J. Meyers, *"On Orbit Status of the High Temperature Superocoductivity Space Experiment",* IEEE Trans. on Applied Superconductivity, Vol. **11**, pp.799-805, March 2001.

[51] R.R. Mansour, S. Ye, B. Jolley, G. Thomson, S. F. Peik,T. Romano,W.-Cheung Tang, C. M. Kudsia, T. Nast, B. Williams, D. Frank, D. Enlow, G. Silverman, J. Soroga, C. Wilker, J. Warner, S. Khanna, G. Seguin and G. Brassard*,"A 60-Channel Superconductive Input Multiplexer Integrated with Pulse-Tube Cryocoolers",* IEEE Trans On Microwave Theory and Techniques, Vol. **48**, pp.1171-1180, July 2000.

[52] R. Mansour, S. Ye, S. F. Peik, V. Dokas and B. Fitzpatrick, "*Quasi Dual Mode resonators"*, IEEE Trans On Microwave Theory and Techniques, Vol. **48**, pp-2476-2481, Dec. 2000.

[53] S. Schorstein, I.S. Ghosh and N.Klein, "*High Temperature superconductor shielded high power dual mode filter for applications in satellite communications"*, IEEE MTT-S, Int Microwave Symp. Dig. 1998, TH2A-4.

[54] H.R. Yi and N. Klein, *"High-Q Cryogenic Dielectric Resonator Filters for C-band and Ku Band freqeuncies"*, IEEE Trans On Applied Superconductivity, Vol. **11**, pp.489-492, March 2001.

[55] G. Zhang, *"Superconducting Bandpass Filter with Quasi-elliptic Characteristic at 408MHz",* presentation in HTSHFF04, 26-29 MAY 2004, Bengur (Spain).

[56] Y.Li and M.J. Lancaster, *"Fifteen pole Superconducting filter for radio Astronomy"*, IEEE MTT-S, Int. Microwave Symp. Dig. 2001.

[57] Y.Li and M.J. Lancaster, F. Huang and N. Rodds "*Superconducting Microstrip Wide Band Filter for Radio Astronomy*", IEEE MTT-S Int Microwave Symp. Dig. 2003.

[58] J. Zhou, *"HTS Narrow Band Filters at UHF Band for Radio Astronomy Applications",* presentation in HTSHFF04, 26-29 MAY 2004, Bengur (Spain).

[59] B. B. Mandelbrot, *The fractal geometry of nature*, New York, W. H. Freeman, 1983.

[60] H.O. Peitgen, H. Jurgens and D. Saupe, *Chaos and fractals: New frontiers of science*, Springer-Verlag, New York, 1992.

[61] D. L. Jaggard, *On fractal electrodynamics*, in *Recent advances in electromagnetic theory*, H. N. Kriticos and D. L. Jaggard, Eds New York, 1990.

[62] J. M. O'Callaghan, C. Puente, N. Duffo, C. Collado, E. Rozan, *Fractal and Space-Filling Transmission Lines, Resonators, Filters and Passive Network Elements,* Patent-WO0154221 (Fractus S.A.).

[63] S.R. Best,"*A Comparison of The Performance Properties Of The Hilbert Curve Fractal And Meander Line Monopole Antennas",* Microwave and Optical technology letters, Vol. **35**, pp. 258/262, Nov. 2002.

[64] J. Anguera, C. Puente, E. Martinez and E. Rozan, "*The Fractal Hilbert Monopole: A Two-Dimensional Wire"*, Microwave and Optical technology letters, Vol. **36**, pp.102/104, 20 Jan. 2003.

[65] K. J. Vinoy, K.A. Jose, V.K. Varadan, and V.V. Varadan, *" Hilbert Curve Fractal Antenna: A Small Reconant Antenna For Vhf/Uhf Applications"*, Microwave and Optical Technology Letters, Vol. **29**, pp.215-219, 20 May 2001.

[66] J.M. Gonzalez-Arbesú, S. Blanch, J. Romeu, *"The Hilbert curve as a small self-resonant monopole from a practical point of view",* Microwave and Optical Technology Letters, Vol. **39**, pp.45-49, 5 Oct 2003.

[67] J.P Gianvittorio,Y. Rahmat-Samii, *"Fractal loop elements in phased array antennas: reduced mutual coupling and tighter packing",* Proceedings IEEE International Conference on Phased Array Systems and Technology, pp.315 – 318, 21-25 May 2000.

[68] J.P. Gianvittorio and Y. Rahmat-Samii, *"Fractal loop elements in phased arrays for wireless communication: design, analysis, and measuremen",* IEEE-APS Conference on Antennas and Propagation for Wireless Communications, pp.129 – 132, 6-8 Nov. 2000.

[69] C.P. Baliarda, J. Romeu and, A. Cardama, *"The Koch monopole: a small fractal antenna"*, IEEE Trans. Antennas Propagation, Vol. **48**, 2000.

[70] J.P. Gianvittorio and Y. Rahmat-Samii, *"Fractal antennas: a novel antenna miniaturization technique and applications",* IEEE Antennas Propag. Mag. Vol. **44**, pp**.** 20–36, 2002.

[71] K.S.K. Yeo and M.J. Lancaster, *"The design of microstrip six-pole quasi-elliptic filter with linear phase response using extracted-pole technique",* IEEE Trans. On Microwave Theory and Techniques, Vol. **49**, pp. 321-327, Feb 2001.

[72] A. Prigiobbo, M. Barra, A. Cassinese, M. Cirillo, F.Marafioti, R Russo and R Vaglio, "*Superconducting resonators for telecommunication application based on fractal layout",* Supercond. Sci. Technol. Vol. **17** pp. 427–431, 2004).

[73] S. Amari and J. Bornemann "*Maximum number of finite transmission zeros of coupled resonator filters with source/load multi-resonator coupling and a given topology*" in Proc, Asia Pacific Microwave Conf, pp.1175-1177, Sidney 2000.

[74] M. Barra, C. Collado, J. Mateu and J.M. O'Callaghan, *"Hilbert fractal curves for HTS miniaturized filters",* accepted to be published in IEEE MTT-S Int. Microwave Symp. Dig. 2004.

[75] S.Y. Lee and C. M. Tsai, "*New cross-coupled filter design using improved hairpin resonators"*, IEEE Trans On Microwave Theory and Techniques, Vol. **48**, pp. 2482-2490, Dec. 2000.

[76] I. Wolff, "*Microstrip band pass filter using degenerate mode of a microstrip ring resonator"*, Electronic letters 25, April 1972.

[77] A. Flores, C. Collado, C. Sans, J. O'Callaghan, R Pous and J. Fontcuberta, *"Full Wave Modeling of HTS Dual Mode Patch Filters and Staggered Couplet Line Filters"* IEEE Trans. On Applied Superconductivity, Vol. **7**, pp.2351-2354, June 1997.

[78] K. Setsune and A. Enokiara, *"Elliptic disc filters of high Tc superconducting films for power handling capability over 100W",* IEEE Tans. On Microwave Theory and techniques, Vol. **48**, pp.1256-11264, July 2002.

[79] F. Rouchad, V. Madrangeas, M. Auborg, P.Guillon, B. Theron and M. Maigna, *"New classes of microstrip resonators for HTS microwave filters applications"*, IEEE MTT-S Int Microwave Symp. Dig. 1998, WEIF-64.

[80] K.F. Raihn, G. L. Hey- Shipton "*Folded Dual-Mode HTS microstrip band pass filter"* IEEE MTT-S Int Microwave Symp. Dig. 2002, pp. 1959-1962.

[81] Z.M. Hejazi, P.S. Excell and Z. Jiang, "*Compact Dual-Mode Filters for HTS Satellite Communications Systems"*, IEEE Trans. Microw. And Guided Wave letters,. Vol. **48**, pp.275-277, August. 1998.

[82] L. Zhu, P. M. Wecowski, and K, Wu, *"New planar Dual-Mode filter using cross-slotted patch resonator for simultaneous size and loss reduction",* IEEE Trans. Microw. Theory and Techn., Vol. **47**, pp. 650-654, May 1999.

[83] A. Cassinese, A. Androne, M.Barra, C. Granata, P.Orgiani, F. Palomba, G.Panariello, G.Pica and F. Schettino,*"Dual Mode Superconducting Planar Filters based on Slotted Square Resonators",* IEEE Trans. On Applied Superconductivity, Vol. **11**, p.473-476, March 2001.

[84] A. Cassinese, A. Andreone, F. Palomba, G. Pica, G. Panariello, *"Dual mode cross-slotted filters realized with superconducting films",* Appl. Phys. Lett. Vol. **77**, pp. 4407-4409, Dec. 2000.

[85] R. Monaco, A. Andreone and F. Palomba, "*Intermodulation measurements in Nb superconducting microstrip resonator",* J. Appl. Phys, Vol. 88, pp. 2898-2902, (2000).

[86] B.A. Willesem, K.E. Kihlstrom and T. Dahm *"Unusual power pendence of two tone intermodulation in high Tc superconducting microwave resonators"* Appl. Phys. Lett. Vo. **74**, pp. 753-756, 1999.

[87] J.A. Curtis; S.J. Fiedziuszko, *"Miniature dual mode microstrip filters"*, IEEE MTT-S Int.Microwave Symposium Digest 1991, pp.443 – 446.

[88] M.Barra, A.Cassinese, M.Cirillo, G.Panariello, R.Russo and R.Vaglio, *"Superconducting Dual Mode Dual Stage Cross-Slotted Filters*," Microwave and Optical Technology Letters, Vol.**33**, pp.389-392, Jun 2002.

[89] M. Barra, A. Cassinese and A. Prigiobbo, "*Superconducting filters based on mixed resonators",* Supercond. Sci. Technol. Vol. **16**, pp. 407–411, Jan. 2003.

[90] M. Makimoto and S. Yamashita *"Bandpass Filters using Parallel Coupled Stripline Stepped Impedance Resonators",* IEEE Trans. On Microwave Theory and Techniques, Vol. **28**, pp.1413-1417, Dec 1980.

[91] J.S. Wong, "*Microstrip Tapped-Line Filters Design"*, IEEE Trans. On Microwave Theory and Techniques, Vol. **27**, pp. 44/50, Jan 1979.

[92] J.F. Liang, K. A. Zaki, and A. E. Atia, "*Mixed modes dielectric resonators filters*," IEEE Trans. Microwave Theory Tech, Vol. **42**, pp.2449–2454, Dec. 2002.

[93] L.H. Hsieh and K. Chang, *"Compact dual mode elliptic function bandpass filter using a single ring resonator with one coupling gap",* Electronics Letters, Vol. **36**, pp 1626-1627, 14 Sept 2000.

[94] L.H. Hsieh and K. Chang, *"Dual mode Quasi- elliptic- function bandpass filter using ring resonators with enhanced coupling tuning stubs",* IEEE Tans. On Microwave theory and techniques, Vol. **50**, pp. 1340-1345, May 2002.

[95] A. Görür, *"Description of coupling between degenerate modes of a dual-mode microstrip loop resonator using a novel perturbation arrangement and its dula-mode bandpass filter applications"* IEEE Trans. Microwave Theory Tech., Vol. **52**, pp. 671–677, Feb. 2004.

[96] K.A. Zaki, C. Chen and A.E. Atia, *"A circuit model of probes in dual mode cavities",* IEEE Trans. On Microwave theory and Techniques, Vol. **36**, pp 1740-1746, Dec.1988.

[97] I. Awai, A. C. Kundu, and T. Yamashita, *"Equivalent-Circuit Representation and Explanation of Attenuation Poles of a Dual-Mode Dielectric-Resonator Bandpass Filter",* IEEE Trans. On Microwave theory and tachniques, Vol. **46**, pp.2159-2163, Dec 1998.

[98] S. Amari, U Rosenberg and J. Bornemann, *"Adaptive synthesis and design of resonator filter with source/load multiresonator coupling",* IEEE Tans. On Microwave Theory and Techniques, Vol. **50**, pp.1969-1977, Aug. 2002.

[99] A. Cassinese, M. Barra, W. Ciccognani, M. Cirillo, M. De Dominicis, E. Limiti, A. Prigiobbo, R Russo, and R.Vaglio *Miniaturized Superconducting Filter realized by Using Dual-Mode and Stepped Resonators* IEEE Trans. Microw. Theory and Techn., Vol. **52**, pp. 97-104, Jan 2004.

[100] S. Amari, *Comments on "*"*Description of coupling between degenerate modes of a dual-mode microstrip loop resonator using a novel perturbation arrangement and its dula-mode bandpass filter applications",* IEEE Trans. Microw. Theory and Techn. Vol. **52**, pp. 2190-2192, Sept. 2004.

[101] A. Cassinese, M. Barra, W. Ciccognani, , M. De Dominicis, E. Limiti, A. Prigiobbo, and R.Vaglio, "*Miniaturized Superconducting filter realized by using dual mode and stepped resonators integrated with a LNA".* Proceedings EUCAS 2003.

[102] Gorge D. Vendelin, Anthony M. Pavio, Ulrich L.Rohde, *Microwave Circuit Design*, WILEY INTERSCIENCE.